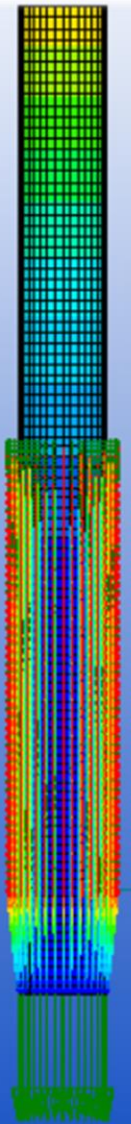


# Optimizing the Vibrodrill system

An investigation in progress



FEMAP®





# Optimizing the Vibrodrill system

## An investigation in progress

Development of an effective pile-soil reaction model to research the optimization of vibratory driving of monopile foundation piles with the GBM Vibrodrill system.

By

S.T. van Nieuwenhuizen Ing.

in partial fulfilment of the requirements for the degree of

### **Master of Science**

in Offshore and Dredging Engineering at the Delft University of Technology,  
to be defended publicly on Friday the 22<sup>nd</sup> of November, 2019 at 14:30 AM.

Thesis committee:

Prof. Dr. A.V. Metrikine,

Dr.ir. A. Tsouvalas

Ir. B.J.M. Arntz

Dr.ir. J. de Oliveira Barbosa

TU Delft

TU Delft

GBM Works

TU Delft





## i. Abstract

---

As the offshore wind industry grows, the demand for larger wind turbines and foundations increases. The most common foundation type for a wind turbine is a monopile which is currently installed by large hydraulic hammers. This installation method generates a lot of underwater noise which may harm marine life. To solve this problem and its unwanted consequences, GBM aims to implement a new silent installation technique. By applying fluidization, jetting and by inducing vibrations by harmonically exciting the bottom of the pile, both the dynamic tip resistance and the shaft resistance are reduced so that the monopile can penetrate the soil. These techniques are aimed to produce less harmful underwater noise than conventional hammering.

Little is known about the penetration performance of a pile which is harmonically excited at the bottom. This thesis aims to provide more insight on the penetration performance when exciting a pile at the tip.

A literature study is performed on existing pile penetration models. From this study it is concluded that, currently, there are no available penetration models capable of describing the penetration performance of the pile when exciting the system at the bottom with varying harmonic excitations. Therefore, the aim of this thesis is to develop a new penetration model. The purpose of this model is to describe the penetration performance at different harmonic force parameters. The developed model is based on finite elements by using the FEMAP software.

The pile is represented by shell elements. The interaction between the pile and the soil is modeled using multiple spring-damper-slider elements which are spread along the pile surface. The slider elements allow the relative motion between the pile and the surrounding soil. The different soil-structure interaction elements are uncoupled and the sliding resistance is assumed linearly elastic, perfectly plastic. Energy radiation due to elastic waves is captured by simple dashpot elements.

The developed model is used to analyze the effect of certain parameters on the penetration of the pile. This is done by changing the amplitude, the frequency or the direction of the harmonic force for a specific set of soil parameters. For each variation, the model calculates the pile displacement at a certain depth from which the penetration speed is determined. This penetration speed is then compared to the other results to determine the effect of each chosen parameter. Also, the location of excitation is analyzed. The model is used to analyze a pile which is excited from the top or at the bottom.

From the results it is concluded that an increase in the amplitude and the frequency of the excitation has a positive effect on the penetration speed. The dependence of the direction of the vibration on the pile penetration is complex. Therefore, a clear correlation between the two could not be obtained within the time framework of this research. Finally, it is concluded that exciting the pile from the top results in a faster penetration speed compared to a pile which is excited at the bottom.

This research provides a first step towards understanding of the Vibro-drill system performance. As this is an investigation which is still in progress there are some recommendations for further research on this topic. One important recommendation is to improve the soil reaction in the model to a coupled system where it is now uncoupled. Furthermore field tests can be performed providing more knowledge on the effects of the soil and to validate the model.

## ii. Preface

---

The research that is the subject of this thesis was undertaken with a view to obtaining a Master degree in Offshore and Dredging Engineering at the Technical University of Delft. Conducting this study has been a long and sometimes challenging journey into often uncharted areas. It could never have been done without the advice, help and support of other people. To them I am immensely grateful.

I would like to thank my committee members that supervised my work on this thesis, consisting of Prof. Dr. A.V. Metrikine, Dr.Ir. A. Tsouvalas and Ir. B.J.M. Arntz.

Also a special thanks to Dr.ir. J. de Oliveira Barbosa who's door to his office was always open. Whenever I was stuck, needed some feedback or just needed someone to help me reflect on ideas, I felt welcome to walk through his door.

I would like to acknowledge Ir. B. Arntz of GBM Works for his guidance trough each stage of the process. For challenging and pushing me. He gave me invaluable advice. His day-to-day availability for bouncing off ideas was of great help to me.

Thank you to Leo, Sanne, Ben, basically the whole GBM team for not only being my colleagues but for being my friends as well. I have learned so much and I will always cherish my memories at GBM.

I thank my girlfriend for her patience and for sticking with me during the long months of researching, writing and re-writing even when I retreated to long days with my computer.

Finally, I also want to express the deepest appreciation to my family for their encouragement, understanding and unconditional love during my long time a student even during hard times they always kept believing in me. Without them I could not have finished this master and for that I am forever thankful.

Sven van Nieuwenhuizen

Delft, November 2019

# Table of contents

---

i.	Abstract.....	4
ii.	Preface .....	5
	Table of contents.....	6
1	Introduction .....	8
1.1	Introduction to the Vibrodrill .....	9
1.2	Function of the Vibrodrill system .....	10
1.3	Mechanical principles.....	10
1.4	Problem statement.....	12
2	Objective and scope.....	14
2.1	Initial Objective of thesis .....	14
2.2	Revised Objective of Thesis .....	14
2.3	<i>Outside of the Scope</i> .....	15
3	Vibratory installation theoretical background .....	16
3.1	Soil Resistance (to axial pile capacity and displacement in Static Soil) .....	16
3.2	Dynamic Soil Behavior in Vibratory Driving.....	17
3.3	Fluidization soil .....	19
3.4	Pile Dynamics.....	19
3.5	Dynamic Pile-Soil interface (Pile Dynamics and Soil Dynamics) .....	19
3.6	Determine Factors of influence on penetration performance .....	20
4	State of art on penetration models .....	22
4.1	Existing models of vibratory driving .....	23
4.1.4	Momentum-conservation models.....	24
4.2	Numerical models.....	28
4.3	Conclusion .....	31
5	Modelling approach (proposed model) .....	32
5.1	Modelling of the Pile .....	32
5.2	Modelling of the Pile-soil interaction .....	33
5.3	Modelling of the Forcing .....	34
5.4	<i>Effective pressure</i> .....	34
5.5	$\mu_z$ & $\mu_y$ .....	34
5.6	<i>Kradial</i> ( $K_x$ ) .....	35
5.7	<i>CRadial</i> ( $C_x$ ).....	35
5.8	<i>Ktangential</i> ( $K_y$ & $K_z$ ) .....	35
5.9	<i>Ctangential</i> ( $C_y$ & $C_z$ ).....	35

5.10	Assumed effects .....	35
6	Determining Input Values .....	36
6.1	Pile values .....	36
6.2	Soil values .....	36
6.3	Force excitation values .....	45
7	Model application & results.....	49
7.1	Hypotheses .....	49
7.2	Approach & Results .....	50
7.3	Frequency sensitivity 2.0 .....	55
7.4	Analysis of the motion.....	57
8	Conclusions .....	59
9	Recommendations .....	61
	Bibliography .....	63
ii.	List of Figures .....	66
iii.	List of Tables .....	67
iv.	List of Definitions .....	68
	Appendices.....	69
A1:	Implementation of the 1D effective model .....	69
A2:	Damping value determination .....	75
A3:	Appendix P-Y method parameters.....	76
A4:	Using FEMAP .....	77
A5:	Plate model .....	81
A:6	OD vs FEM sawtooth .....	85
A7:	Output values.....	86

# 1 Introduction

In 2017 Global energy demand increased by 2.1% and Renewables saw the highest growth rate of any energy source, meeting a quarter of global energy demand growth (OECD & IEA, 2018). Wind power accounted for the largest share of overall renewables growth, at 36% (OECD & IEA, 2018). Bloomberg New Energy Finance (BNEF) even states it expects the global offshore wind market to grow at a 19% compound annual growth rate between 2017 and 2025, reaching cumulative capacity of 71 gigawatts in 2025, almost doubling in size by 2020(BNEF, 2017).

Many Offshore wind farms are planned to be constructed in the near future. Besides the fact that there are more wind farms being constructed also the sizes of wind turbines are increasing and hereby the monopile size that need to be installed will be larger. To install these large diameter monopiles, currently hydraulic hammers are still used for “piling”. However, as the size of the installed monopiles increase, the suitability of using this conventional method diminishes.

The installation process is currently suboptimal, with high Sound Exposure Levels (SEL) causing permanent hearing loss to marine mammals (Kastelein, 2014) and regulations leading to operational downtime. Besides the additional cost caused by the downtime, the piles also suffer from high fatigue damage which require expensive over dimensioning of the monopile foundation.

Considering wind energy being the largest growing energy source in the world, the current methods are not at all optimum for the future needs. There are certainly opportunities associated with the optimization of monopile installation: Firstly, the costs of the installation of offshore wind turbines needs to be reduced. Secondly the installation process should be optimized and less harmful for the direct environment. At GBM WORKS these opportunities were noted which led to developing a possible solution: The Vibrodrill. (Figure 1)

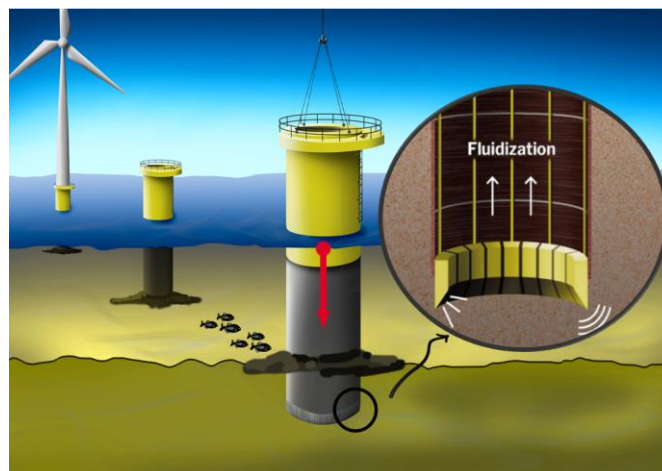


Figure 1 Vibrodrill concept

## 1.1 Introduction to the Vibrodrill

The Vibro-drill is an improved installation method for offshore foundation piles where a set of vibrating and water jetting elements are installed at the bottom of the monopile. Using a hydraulic motor which rotates an eccentric mass, a vibration is induced. These vibrating elements are rigidly connected to the pile and induce a vibration in the pile reducing the soil resistance along the inner and outer part of the shaft (and at the tip). To simultaneously reduce the tip resistance, water is jetted downwards at the tip of the pile.

A third advantage is that water is injected on the inner part of the pile, fluidizing the soil and reducing its resistance on the inside of the pile. The combination of these techniques results in a temporary reduction of the pile-soil resistance. This allows the monopile to penetrate the soil to a target depth under its own weight. No further hammering is required, potentially reducing noise levels and fatigue damage.

This idea has led to winning the Philips innovation award 2017 and to a feasibility study that has been performed on a conical prototype version:

*The noise levels during the experiments were significantly lower than the noise levels for conventional piling (B Arntz, 2018). The experiments performed by Arntz (2018) show that it is possible to penetrate the prototype pile to its full penetration of 4.5 meters into the soil. Penetration rates were found between 1 and 5 cm/s depending on the properties of the applied oscillations and soil conditions. To determine the feasibility of reaching penetration depths that are similar to those of offshore foundation piles, i.e. 30 to 40 meters with larger diameter monopiles, additional experiments are required (B Arntz, 2018).*

## 1.2 Function of the Vibrodrill system

The main goal of the Vibrodrill system is to silently install a monopile to a certain target depth. Unlike conventional systems where the focus lies on applying a force at the top of the monopile the Vibrodrill system is focused more on reducing the soil resistance on the total system. The idea is that by reducing the soil resistance on the system, penetration occurs under the monopiles own weight.

The soil resistance reduction taking place is divided into 3 parts; On the Inside shaft of the pile, - Outside shaft of the pile and at the tip.

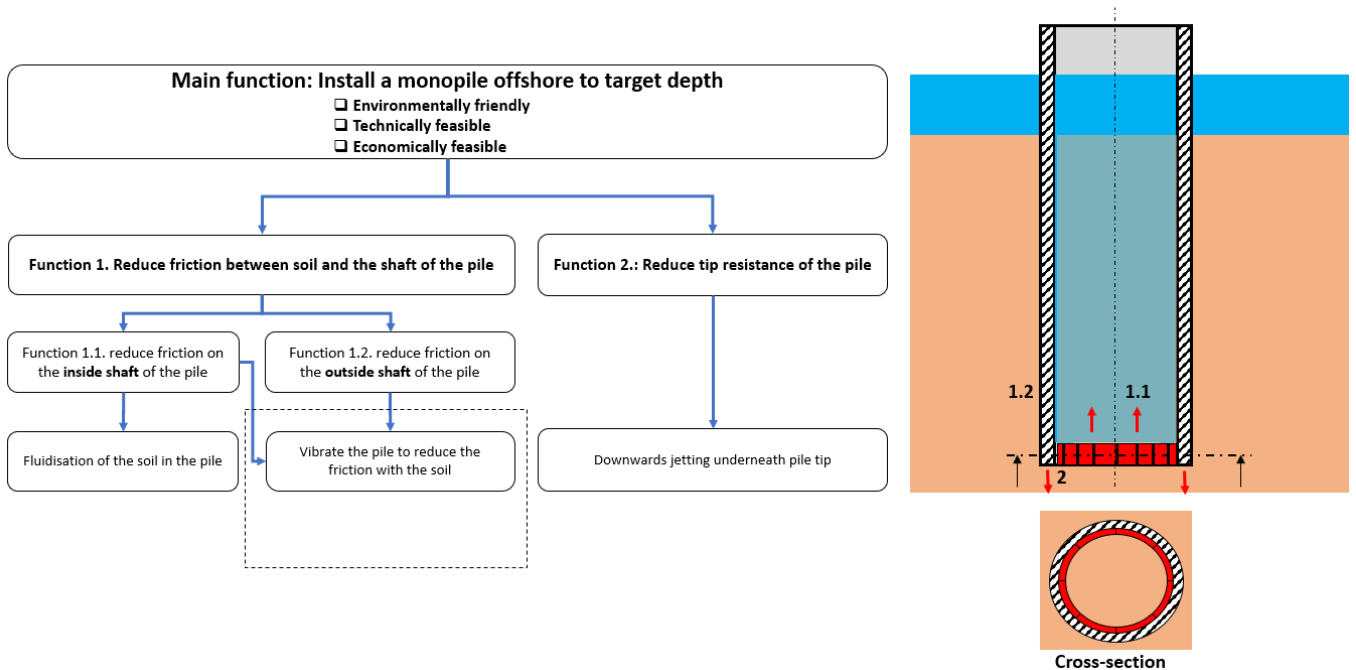


Figure 2 Functions of the Vibrodrill system

## 1.3 Mechanical principles

To model dynamic soil resistance reduction properly, the mechanical principles of the Vibrodrill system on how the friction reduction is achieved need to be understood. In this chapter, a description of the different mechanical principles is described.

### 1.3.1 Downward Jetting

To reduce the tip resistance, jetting is applied. The great advantage in jetting is its ability to modify the characteristics of the soil. The effect of fluid jetting at very high speeds is that it can break up the structure and mix the soil, partially replacing it with consolidating fluid. Due to the jetting, liquefaction occurs. *“Liquefaction is a decrease in the shear resistance of the soil, after reaching the condition of fluidity. The total loss of resistance is reached when the water pressure filling the void becomes equal to the confining pressure”* (Spagnoli, 2014)

### 1.3.2 Fluidization

To reduce the inner shaft resistance, water is injected into the inside of the pile. It is considered that soil is fluidized due this water injection. Due to the fluidization, the shaft friction along the inside of the pile is reduced.

### 1.3.3 Vibrations

Using a hydraulic motor, which rotates an eccentric mass, vibrations are induced in the system. The vibrations that are created reduce the frictional resistance in the system in two ways: first, due to vibration, the characteristics of the soil can change (a further elaboration of the soil characteristics in vibratory driving is described in chapter 3); second, when the amplitude of the cyclic forcing exceeds the static frictional resistance along the shaft, the system will start sliding and enter the dynamic frictional resistance regime. Since static friction exceeds the kinetic (sliding) friction (T. W. Lambe & R.W. Whitman, 1969) this could also be considered as a friction reduction.

*The shear force required to initiate sliding between two surfaces is often greater than the force required to maintain the motion.* (T. W. Lambe & R.W. Whitman, 1969)

Like in conventional hammering systems and vibratory driving systems, the goal is to make the pile penetrate the soil. In the former systems, a downward forcing is applied to overcome the resistances. In the Vibrodrill system, to optimize the efficiency of the penetration, the frequency in which the system acts is planned to be close to an eigenfrequency of the system. The idea is that this will induce resonance in the system which can greatly amplify the response of the pile soil system. Due to the resulting larger downward force amplitudes, the critical force to initiate sliding will be reached sooner and the sliding distance will be greater.

For sheet piling, Massarsch stated the following: *“At resonance, the sheet pile oscillates in phase with the surrounding soil, i.e. the relative displacement between pile and soil is very small. Static friction exists along the pile-soil interface, which enhances the transfer of vibration energy to the soil. This effect is beneficial during vibratory compaction but reduces penetration speed and can cause vibration problems during pile or sheet pile installation.”* This acknowledges the fact that the importance lies in the relative displacement. (Massarsch, Fellenius, & Bodare, 2017)

The functions of the Vibrodrill system summarized:

1. *Downward Jetting (reducing tip resistance)*
2. *Fluidizing inside of the pile, by Injecting water (reducing friction on the inside shaft of the pile)*
3. *Vibrations by rotating an eccentric mass. (generates a downward force and decreases resistance)*

## 1.4 Problem statement

Since the prototype has been proven feasible, the challenge to make it a full scale project arises. The prototype for the feasibility study had one conical flipper installed. Since then, a next step in the development was made in the design to get to a full scale product. This design consists of attaching multiple “triangular prism shaped” flippers to the bottom of to the pile.

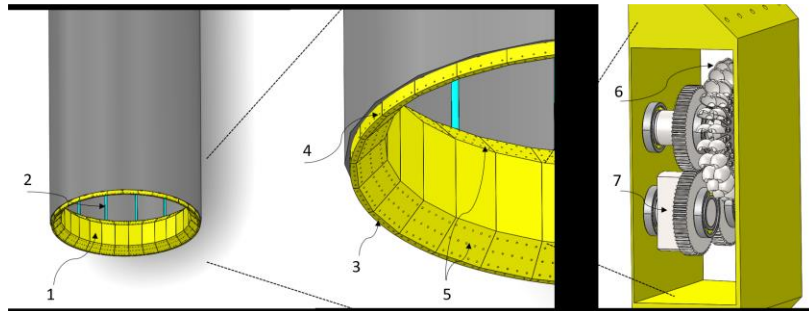


Figure 3 New improved mechanics of the vibrodrill system

The problem with the flipper concept was that there was a great unknown on how the different moving flippers will interact with each other when all connected to the same structure. When connecting multiple flippers to the same structure, the flippers will not only affect the ground it is in but also they will affect the structure vibrations. These vibrations will, in turn affect the other moving flippers. The different flippers would need to synchronize in order for the total exciting force to be in phase.

During the course of this thesis, to account for the problem of the harmonic forces not being in phase, the design has changed from these uncoupled flippers that were attached to the end of a plate, to a system where all the different eccentric masses are coupled and rotate in phase (Figure 3). This ensures that the harmonic forcing is in phase as this is believed to be more efficient for driving.

With these design changes the problems also change, the basis however stays the same. GBM needs more knowledge and information on how to optimally install a monopile using the Vibrodrill system. This is an investigation in progress. The model that is planned to be developed will be used to determine further design choices and to investigate what the optimum forcing mechanism is to penetrate the soil. Unlike initially determined, the soil-interaction will need to be a part of the scope.



## 2 Objective and scope

---

### 2.1 Initial Objective of thesis

The initial aim of this thesis was to research the dynamic properties of the Vibrodrill system and create a model in which the flipper interactions caused by hydraulically induced vibrations through the plate could be predicted. The idea was to gain knowledge on the performance of the system and to use this for further optimization.

The initial aim of the Thesis was to build and validate a model that can predict vibrations of a plate and multiple Vibrodrill flippers in free air. The interaction with soil was not in the initial scope.

As described in the previous section during the course of this thesis the design was changed and the benefit for the company in this objective was lost. A choice was made to change the objective and the scope of the thesis. For the purpose of keeping flow in this report and not side tracking too much, this will not be elaborated here further. A summary of the work done for this initial objective can be found in Appendix A5: Plate model.

### 2.2 Revised Objective of Thesis

For the revised objective the scope is focused on the vibrations of the pile to reduce the friction with the soil (Figure 2). The resistance reduction due to fluidizations and the jetting process will be left outside the scope of this thesis.

A main interest in this thesis is how different variables affect the system on penetration performance on the shaft resistance. Due to the unknown factors of the effects of jetting and fluidization which will require their own full research in this thesis the focus will be limited to the shaft resistance. As described in section 1.3.1, jetting will reduce the tip resistance. For this thesis it will be assumed the tip resistance will be reduced to zero.

The objective of this Thesis is therefore:

***Optimize the Vibrodrill by determining factors of influence on shaft resistance and their relative contribution to the penetration performance.***

- 1. Identify factors of influence with respect to forcing with a generic pile-soil model.*
- 2. Identify relative differences in influence factors on the penetration speed.*

For an optimum method of silently installing a monopile, a model will be developed to gain more insight on the installation process. As a result of this thesis, more insight will be gained into the subjects that are needed to validate the usage of vibratory driving using the Vibrodrill. The main interest lies in gaining more insight on how to (optimally) apply a force to install a monopile in soil with the specific technique described earlier.

### 2.3 *Outside of the Scope*

In this early phase of development, there will be no results from physical tests against which validation could be done. Research will be done on existing models and software packages; these models will be compared in order to select the most appropriate software to model the dynamical system under investigation. The problem for this thesis is considered to be a mathematical exercise.

Since the driving mechanisms are still in development, and this development will depend on the outcome of this thesis, the applied vibrations will be a harmonic force input and not a power input which drives the rotating eccentric mass. The desired harmonic force input will be useful in further developing the driving mechanism and the power needed.

- No simulation of rotating eccentric masses but a harmonic force input (in phase) is considered

As also described in the previous section, the following statements also apply to this research:

- Tip resistance is assumed to be zero (Only Shaft resistance is considered )
- No determination of the effectiveness of tip resistance reduction due to jetting
- No determination of the effectiveness on resistance reduction due to fluidization

### 3 Vibratory installation theoretical background

During monopile installation, the pile encounters shaft and tip resistance by the soil. The Vibro-drill machine developed by GBM Works aims to reduce this resistance by means of three mechanisms. Firstly the machine induces vibrations, the goal of inducing these vibrations is to influence the soil which reduces the resistance to improve the penetration performance. Secondly, downward waterjets at the bottom of the pile aim to reduce the tip resistance. Lastly, the fluidization of the soil inside the pile aims to reduce shaft resistance and thus enhance pile penetration. The pile dynamics and the soil-pile interaction have an overall influence on the behavior of the system. The physical working mechanisms of the Vibro-drill are explained in this chapter.

#### 3.1 Soil Resistance (to axial pile capacity and displacement in Static Soil)

In the case of installing a monopile using the Vibrodrill method, a temporary reduction of friction between the soil and the pile shaft is desired. To explain the principles of what happens physically in the soil during vibratory driving the case where a pile is statically located in the soil is first described.

The unit skin resistance  $q_s$  between the pile and the surrounding soil is calculated by multiplying the friction factor,  $\mu$ , between the pile and soil by the horizontal effective stress ( $\sigma'_h$ ) (Wrana, 2016)

$$q_s(z) = \mu\sigma'_h = \mu(z)K'(z)\sigma'_v(z) = \beta(z)\sigma'_v(z)$$

The horizontal effective stress is customarily expressed as a proportion of the vertical effective stress by the coefficient of lateral earth pressure  $K$ . In turn, the friction coefficient and the coefficient of earth pressure are described in one  $\beta$  value. This is called the  $\beta$  method which are further elaborated in the research done by Wrana (2016).

The vertical effective stress ( $\sigma'_v$ ) in the soil is calculated from two parameters, total vertical stress ( $\sigma_v$ ) and pore water pressure ( $u$ ) according to:

$$\sigma'_v = \sigma_v - u \quad (1)$$

In the simple static situation the effective stress and pore pressure are respectively described with:

$$\sigma_v = H_{soil}\gamma_{soil}; u = H_w\gamma_w$$

where:

$$H_{soil} = \text{the thickness of overlying layer (Depth of the location)} [m]$$

$$\gamma_{soil} = \text{unit weight of the soil} \left[ \frac{N}{m^3} \right]$$

$$H_w = \text{depth below water table} [m]$$

$$\gamma_w = \text{unit weight of water} \left[ \frac{N}{m^3} \right]$$

The coefficient of lateral earth pressure,  $K$ , is defined as the ratio of the horizontal effective stress,  $\sigma'_h$ , to the vertical effective stress,  $\sigma'_v$ . According to Verruijt (Verruijt, 1987), the coefficient of lateral earth pressure in elastic materials under water is defined by:

$$K' = \frac{\nu}{1 - \nu}$$

When the Poisson's ratio  $\nu = 0.5$ ,  $K$  would be 1 and the horizontal effective stress would be equal to the vertical effective stress. When  $\nu < 0.5$ , it implies that the horizontal effective stress is lower than the vertical effective stress, and thus the unit skin resistance is lower.

Multiple determinations for  $K$  and  $\beta$  for the static case have been made and are described in Wrana (2016).

### 3.2 Dynamic Soil Behavior in Vibratory Driving

When introducing a dynamic force in the pile, the soil particles in contact with the pile will also start to move and will be forced outwards, which in turn move the rest of the particles outwards. Massarch (Massarch, 2002) states that during vibratory driving the following mechanism takes place

*“vertically oscillating force creates – due to shaft friction – a horizontally oscillating force. As this horizontal force is directed away from the pile shaft, it reduces the shear resistance with each downward movement. This phenomenon is believed to be the main reason for enhanced pile penetration in coarse-grained soil.”*

Which is illustrated in Figure 4 to Figure 6.

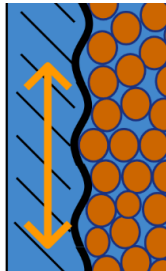


Figure 6 movement of the pile

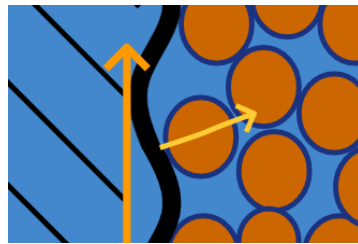


Figure 5 outward movement of soil

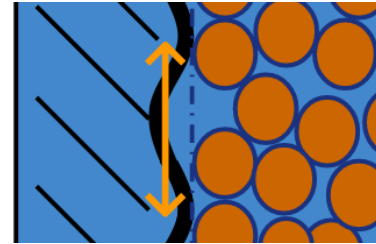


Figure 4 Soil in motion

If the frequency of the vibration is low, the soil has time to settle back into place. But if the frequency is high enough the soil is considered to not have enough time so settle back and is thus constantly being forced outwards and keeping the soil in motion (Figure 4).

These phenomena are frequency dependent but also amplitude dependent. If the amplitude of the vibrations is too low the principle does not work and the soil will still stay “attached” to the pile. If the amplitude and/or frequency of the movement of the pile increases, the soil particles will have less contact/grip with the pile shaft. In this case, the movement will surpass the “threshold of motion” and go from static friction to kinetic friction. Kinetic friction has a lower friction coefficient between the pile shaft and the soil, this will be elaborated in a later section.

It is generally recognized that vibratory driving is most efficient in coarse-grained (frictional) soil and less efficient in fine-grained (cohesive) soil. Besides the earlier described reaction of a coarse grained soil, a more recent research (Massarsch et al., 2017) states the following: *“In fine-grained (cohesive) soils, shaft resistance decreases due to strain and the number of vibration cycles (remoulding) occurring when the relative displacement between the pile and the soil exceeds about 5–10 mm. The magnitude of the eccentric moment of the vibrator is therefore important for the vibratory driving of piles in cohesive soils as it determines the relative displacement between pile and soil, see eq. 2.”* In eq. 2 it can be seen that Massarch describes the displacement amplitude independent of frequency.

$$s = \frac{M_e}{m_t} \quad (2)$$

$s$  = Displacement amplitude [m]

$M_e$  = eccentric moment [kgm]

$m_t$  = total mass of the system [kg]

Massarch describes the importance of the amplitude and introduces a difference between soils types. Besides the a decrease in resistance by a reduction in friction  $\mu$ , there is also a reduction in the effective pressure  $\sigma'_h$  due to the induced vibrations (this is further elaborated in the chapter “liquefaction of soil”).

### 3.2.1 Initially dense and loose soils

In this study, it is considered that the soil is saturated with water, with a degree of saturation of  $S = \frac{V_w}{V_v} = 1$

Another important soil property is the void ratio ( $e$ ). The void ratio is the ratio of the volume of voids ( $V_v$ ) to the volume of soil solids ( $V_s$ ):  $e = \frac{V_v}{V_s}$  (the void ratio of loose soils is higher than that of dense soils). When considering an initially loose soil (with a relative high void ratio) which is forced to move, the total volume and thereby the void ratio will go down (with an increase of strain). This is called compression or compaction.

Due to this compression the water that was initially in the voids is forced outwards resulting in a rise of pore pressure. Due to equation (1), a rise of pore pressure will result in a decrease of the total effective stress which in turn reduces the friction between the soil and the plate.

When an initially dense soil (with a relatively low void ratio) is also forced to move the total volume and thereby the void ratio is forced up. This is called dilatation. The increase in void ratio results in a “suction effect” reducing the pore pressure which due to equation (1) increases the effective stress and thus the unit skin resistance of the pile. Both (initially dense and initially loose) soils in shear strain tend towards a “Critical Specific Volume” (figure 9). The difference between the initial soil volume and the specific volume determines the compression or dilatation magnitude.

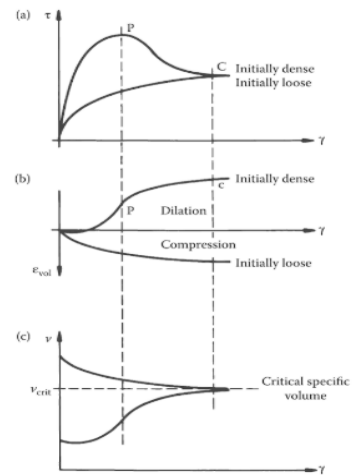


Figure 7 Soil Mechanics: Concepts and Applications (Powrie, 1997)

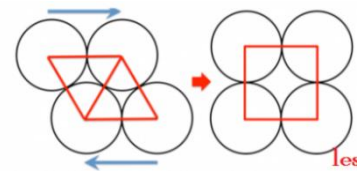


Figure 8 Dilatation (Shahraini, 2019)

### 3.2.2 Liquefaction of the soil

In dynamically loaded soil, i.e. sand, liquefaction is a very important phenomenon to consider. Liquefaction is defined as the characteristic transformation of soils from a solid to a liquid state due to an increase of pore pressure and a reduction of effective stress as described in equation (1). Saturated cohesionless soils are most affected by this phenomenon. Under relative high frequency loading, the pore water will not have enough time to drain outwards. Therefore this loading condition is called “the undrained loading condition”. Cohesionless soil (considered the density is not above critical) has a tendency to densify, especially when subjected to cyclic loading. Excess pore pressure occurs when the pores are saturated and cannot drain sufficiently. The excess pore water pressure can result in a severe reduction of the effective stress. A reduction in effective stress in turn could result in a desired reduction in friction between the soil and the pile. However, after some time, the pore pressure is dissipated and the soil is densified to the critical state.

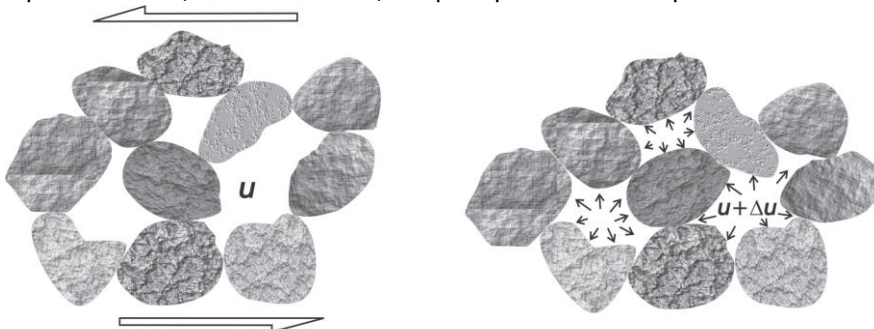


Figure 9 changes in the soil skeleton caused by cyclic loading results in excess pore-water pressure (Lenart, 2018)

Static liquefaction or flow failure is the fast increase in pore-water pressure followed by a sudden loss of strength after the peak value of the deviator stress is reached, until a residual/steady-state strength is reached. Flow liquefaction appears when the residual strength of the soil is smaller than the static shear stress required for the equilibrium of a soil mass. The liquefied stress state, in that case, is represented by the initial effective confining pressure, decreased by the excess pore pressure. (Lenart, 2008)

### 3.3 Fluidization soil

Apart from vibrations, a main function of the Vibrodrill is to fluidize the soil inside the pile by injecting water inside the pile which is a confined space. This mechanism aims to decrease the friction of the soil on the inner shaft. In this process, a granular and static soil is changed to a fluid and dynamic soil. This happens by letting a liquid (or a gas) flow through the soil causing the medium to become a more fluid state than the initial soil state.

When the medium behaves more like a fluid and the shear resistance is reduced due to the buildup of water overpressure, the skin friction reduces between this medium and the inner side of the pile in comparison to a dense solid state. In clays, fluidization will not be possible due to the cohesive and impermeable characteristics of this soil. In such a case the Vibrodrill will “cut” through the soil by jetting and the shaft friction reduction will happen due to a creation of a lubrication layer between the pile shaft and the soil by the injected water.

### 3.4 Pile Dynamics

When introducing a force to a pile, a wave will propagate through the pile in all directions with a speed that is dependent on the pile material. The main material characteristics that are of importance in determining the dynamics are the density  $\rho$ , Poissons ratio  $\nu$ , and the Youngs or Shear modulus,  $E$  or  $G$ , respectively. In dynamics of a plate or a pile, two types of waves are considered: pressure waves (P-waves) and shear waves (S-waves). The difference between these waves is

shown in Figure 10. The speed of a pressure wave is described by  $c_{solid} = \sqrt{\frac{E}{\rho}}$ . In shear waves, the Young’s modulus  $E$  is replaced by the shear modulus  $G = \frac{E}{2(1+\nu)}$

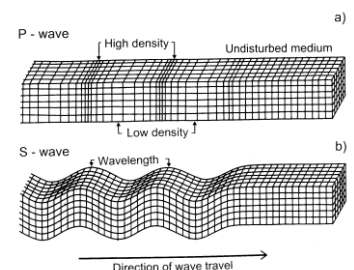


Figure 10 difference in waves (Zheng., 2015)

These pressure and shear waves cause a movement or vibration in the material. If no further forcing is applied to the material, the propagating wave will fade out due to material damping. If a harmonic force is applied, as with the Vibrodrill, the material will keep on vibrating due to new propagating waves. If the period of the harmonic excitation is the same (or close to) the duration of the wave propagation along the length of the material, the first natural frequency of the system is reached and the system is in resonance. When exciting a system at its natural frequency a small applied force can produce a large vibrational response. In a free-free rod this natural frequency is  $\omega_n = \frac{n\pi c}{l}$  where  $c = \sqrt{\frac{E}{\rho}}$  for longitudinal vibrations and  $c = \sqrt{\frac{G}{\rho}}$  for torsional vibrations.

### 3.5 Dynamic Pile-Soil interface (Pile Dynamics and Soil Dynamics)

As described, the type of soil determines the effect of vibration on the pile. Considering that soil properties can vary over depth, the effect of the soil to the system will also vary with depth. It can be assumed that the soil has a changing effect on the system and thereby also the natural frequency changes. This is due to the fact that the pile is “clamped” in the soil in varying depths and with varying soil characteristics over depth.

If the soil would be rigidly connected to the pile, the system frequency would be relatively easy to calculate. But since the soil is also dynamic and constantly moving, the pile-soil interface is considered very complex and at this time impossible to accurately model. Estimations have to be made about the true pile soil interaction. A main factor for this thesis is the shaft resistance where an important parameter is the resulting friction. To estimate the resulting friction in Vibrodriving research has been done by Viking (2002). He reported that the friction coefficient was reduced depending on the displacement amplitude and frequency applied. This is confirmed by Heerema, who carried out vibratory direct shear tests on both cohesive and non-cohesive soil samples (Edward P. Heerema, 1979).

### 3.6 Determine Factors of influence on penetration performance

The main question in this thesis is : *to determine the weighted factors of influence on shaft resistance and their relative contribution to the penetration performance.*

In penetration performance penetration speed and potential target depth are considered. To model this we first need to identify all the factors of influence on the potential penetration speed and potential target depth. The factors are divided into 3 sections; The pile, the forcing and the soil.

#### 3.6.1 Pile

Logically the pile dimensions and characteristics are of great influence to the system and the penetration performance. The dimensions; length, diameter and wall thickness in combination with the material properties determine the weight of the pile. In combination with the material properties wherefrom The E-modulus and damping are derived, the influence of the dynamic performance of the pile is captured.

#### 3.6.2 Forcing

Considering that the forcing is created by eccentric rotating masses, the frequency, amplitude and direction of the forces can be varied. It might also be interesting to vary the location of the applied forcing along the length of the pile. It is expected that the forcing has significant influence on the system. The matter of sensitivity of these factors is a question that will be touched upon in this thesis.

#### 3.6.3 Soil

The soil is the medium in which the penetration of the pile takes place. The characteristics of the soil logically has a great influence in the penetration performance. Site selection can be done to specify ideal soil for penetration. The soil at the location of where installation takes place has a certain initial state. Statically at rest with a given soil characteristics which are further elaborated here to define the factors of influence.

##### 3.6.3.1 Classification of soils

In geotechnical engineering, soils are typically classified on the engineering properties. Classification systems have been developed to easily transfer field observations to basic predictions of the soil properties and behavior. The unified soil classification system (USCS) (Figure 12) and the European soil classification system are considered most common. Mainly these classification systems classify the soils by grain size (apart from amount of organic matter in the soil).

FINE-GRAINED SOILS (50% or more of material is smaller than No. 200 sieve size.)		
<b>SILTS AND CLAYS</b> Liquid limit less than 50%	ML	Inorganic silts and very fine sands, rock flour, silty of clayey fine sands or clayey silts with slight plasticity
	CL	Inorganic clays of low to medium plasticity, gravelly clays, sandy clays, silty clays, lean clays
	OL	Organic silts and organic silty clays of low plasticity
<b>SILTS AND CLAYS</b> Liquid limit 50% or greater	MH	Inorganic silts, micaceous or diatomaceous fine sandy or silty soils, elastic silts
	CH	Inorganic clays of high plasticity, fat clays
	OH	Organic clays of medium to high plasticity, organic silts
<b>HIGHLY ORGANIC SOILS</b>	PT	Peat and other highly organic soils

Figure 11 USCS fine grained soils (ASTM D-2487-98)

COARSE-GRAINED SOILS (more than 50% of material is larger than No. 200 sieve size.)		
Clean Gravels (Less than 5% fines)		
<b>GRAVELS</b> More than 50% of coarse fraction larger than No. 4 sieve size	GW	Well-graded gravels, gravel-sand mixtures, little or no fines
	GP	Poorly-graded gravels, gravel-sand mixtures, little or no fines
Gravels with fines (More than 12% fines)		
	GM	Silty gravels, gravel-sand-silt mixtures
	GC	Clayey gravels, gravel-sand-clay mixtures
Clean Sands (Less than 5% fines)		
<b>SANDS</b> 50% or more of coarse fraction smaller than No. 4 sieve size	SW	Well-graded sands, gravelly sands, little or no fines
	SP	Poorly graded sands, gravelly sands, little or no fines
Sands with fines (More than 12% fines)		
	SM	Silty sands, sand-silt mixtures
	SC	Clayey sands, sand-clay mixtures

Figure 12 USCS Course grained soils (ASTM D-2487-98)

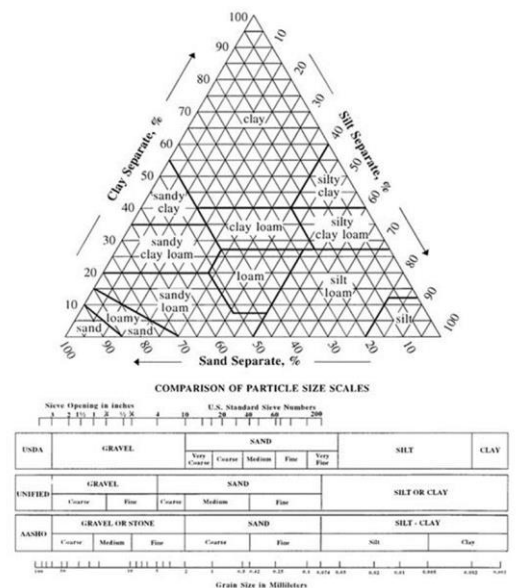


Figure 13 USDA Classification system (Barman, 2019)

### 3.6.3.2 Factors of influence of the soil to penetration performance

The type of soil determines the resistance of the soil and thereby an effect on the penetration speed and target depth. A certain soil can consist of different materials (like calcareous or silica sands) and can be described by the percentages of different particle sizes that are present within the soil (Figure 14). The particle size is of great importance as with a bigger particle size the void ratio is larger and the soil is considered to be more loose. The initial state of the density greatly influences the soil characteristics when the forcing and thus dynamics come into play. Soil type and density are main contributors to side friction (shaft resistance) in piles (Noorany, 1985).

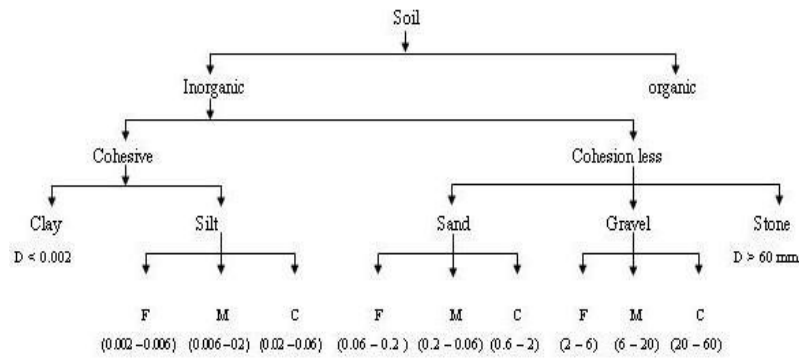


Figure 14 soil classification in particle size

In general coarse grained soils like sands and gravels are treated as drained materials. Because the permeability is high and therefore water can flow through the large void spaces. These coarse grained soil types consisting of larger particles is in general more cohesionless. Fine grained soils like silts and clays have a low permeability so there is no direct route for water to flow freely. This is considered undrained. These soil types are in general more cohesive. The factor of cohesion has a direct influence on the soil shear strength. This factor is of importance as the soil shear strength of the soil can influence the system in terms of dynamics. The percentage of water that is present in the soil or saturation level is of great importance to the soil characteristics. Furthermore, the fluidized soil will turn into a soil-water mixture which has severely different characteristics in comparison to a non-fluidized static soil.

The embedded depth has an influence on the total dynamic system. Also, the further the pile is embedded into the soil the more pressure and thus effective stress is acting on the pile. As described in “soil behavior in vibratory driving” a higher effective stress generates a higher friction which results in a lower penetration performance.

Pile	Forcing	Soil
<ul style="list-style-type: none"> <li>•Pile length</li> <li>•Pile Diameter</li> <li>•Pile wall thickness</li> <li>•Material</li> </ul>	<ul style="list-style-type: none"> <li>•Amplitude</li> <li>•Frequency</li> <li>•Direction</li> <li>•Location(along length)</li> </ul>	<ul style="list-style-type: none"> <li>•Soil Characteristics:</li> <li>•Soil type(material)</li> <li>•Particle size (density)</li> <li>•Cohesive/ cohesionless</li> <li>•Drained/undrained</li> <li>•Initial state (dense or loose)</li> <li>•Saturated/ unsaturated</li> <li>•Fluidized/non fluidized soil</li> <li>•Imbedded depth (pile soil interaction)</li> <li>•Pressure (hydro&amp;soil)</li> </ul>

Table 1 factors of influence summarized (non-accounted factors of influence on friction between soil and steel : Surface Roughness, Rate of deformation (Suba Rao))

## 4 State of art on penetration models

---

In this section research has been done on existing penetration models and a conclusion is drawn on the usability of the researched models.

As concluded in section 3.6, soil is a major factor of effect on the pile driveability. The model should be able to describe the physical characteristics of the soil. Determining the characteristics of the soil over the depth is usually performed statically by CPT. Ideally, the model should relate to the soil characteristics during installation and since vibratory driving can be considered dynamic other methods and models might need to be used. The model should ideally be able to simulate the soil phenomena that can occur during the vibratory driving of the system. As described, major factors are the pile-soil interactions, fluidization and liquefaction phenomenon of the soil. Since these occur due to the vibratory driving of the system and due to water injection they also need to be accurately modelled.

Likewise, the pile characteristics and the forcing characteristics as described in the factors of influence need to be an input to the model. In this thesis a goal is to determine the factors of influence on shaft resistance and its relative contribution to the penetration performance. To reach this goal the model would ideally need to quantify the penetration performance.

Quantifying the penetration performance can be viewed from different angles. In conventional hammering techniques the performance can be quantified by distance penetrated per blow (Harpoth, 2017). For the vibratory driving of sheet piles Viking (2002) uses the term “vibro-driveability”; The rate of penetration, or penetration speed which is normally given in mm/s.

Interests for research could be to investigate the total duration of reaching target depth, the maximum achievable target depth, determining the required energy needed to reach target depth and a variation on the conventional penetration distance per blow: Penetration distance per rotating eccentric mass cycle (at a certain depth). In this research the focus will be on the vibro-driveability; the penetration speed versus depth during vibratory driving.

## 4.1 Existing models of vibratory driving

To obtain the desired functionality of the model, a short investigation into the existing models on vibratory driving is performed. In this section the background theory of pile driving models is described and, in particular, the existing vibratory drive-ability models from literature research. This is done to research the usability of existing models for this thesis as described in chapter 2 (note that the tip resistance will not be accounted for). The existing modelling approaches can be categorized into different parts: parametric, force balance, energy balance, momentum conservation, integration of the laws of motion and numerical modelling. These are described in different segments in this chapter.

### 4.1.1 Parametric models

This approach is based on very early predictive methods that were based on observations and simple expressions. These models have been reviewed by Rodger and Littlejohn (1980) and will not be reviewed in this section. An important statement to consider is that these early models were approaching the soil response as linear-viscous or linear-elastoplastic. Experience gathered shows that viscosity, elasticity and plasticity are better considered non-linear. (Rodger & Littlejohn, 1980)

### 4.1.2 Force-balance models

The force balance model predicts if a vibration force, including the surcharge force that is induced, is able to overcome an estimated soil resistance. One of the flaws of these models is the incapability to estimate the penetration rate; it only shows the magnitude of the driving force and compares this with the resistance force.

Jonker proposed the “beta formula” in 1987 and introduced soil resistance to vibratory driving (SRV). Here the resistance factors of the static bearing capacity are multiplied by empirical reduction factors  $\beta$ . This beta factor estimates the reduction of resistance due to dynamic effects on the outside and inside shaft friction and the pile toe. The beta factors depend on soil type, consistency, density and driving conditions and resulting the level of excess porewater pressure during driving. (Jonker, 1987)

$$Fv + Fi + Fs > SRV = \beta_0Rs_0 + \beta_iRsi + \beta_tRt \text{ (jonker 1987)}$$

*Fv* is the maximum vertical force generated by the vibrator,

*Fi* is the inertial forces of dynamic mass,

*Fs* is the constant surcharge force,

*Rs0* is the soil friction outside pile shaft,

*Rsi* is the soil friction inside the pile shaft,

*Rt* is the empirical pile toe resistance

Type of soil	Value of $\beta$
Round coarse sand	0.10
Soft loam/marl; soft loess; stiff cliff	0.12
Round, medium sand; round gravel	0.15
Fine angular gravel; angular loam; angular loess	0.18
Round fine sand	0.20
Angular sand; coarse gravel	0.25
Angular/dry fine sand	0.35
Marl; stiff/very stiff clay	0.40

Figure 15 Values of the empirical factors of shaft resistance(Viking, 2002)

A second and less elaborated approach is the Tünkers method, presented by Warrington (1989):

$$F_v = \sigma * A_s$$

Where:  $F_v$  is the force generated by a vibro-driver [kN],

$\sigma$  is the soil resistance [kPa] according to the Warrington table for different soil types

$A_s$  is the shaft area of soil [m<sup>2</sup>].

This formula is only applicable when the displacement amplitude is less than 2.38 mm (Warrington, 1989).

SPT value (blows/30) [cm]		Soil resistance ( $\sigma$ ) [kPa]
cohesion less soil	cohesive soil	
0-5	0-2	9.86
5-10	2-5	11.87
10-20	5-10	12.83
20-30	10-20	14.84
30-40	20-30	15.80
40+	30+	16.76

Figure 16 Values of soil resistance (After Warrington 1989)

The force balance models are deemed to be of little use in this thesis since they only indicate a forcing balance and will therefore not be able to produce a penetration speed. However, they would be able to determine if the pile is able to overcome the soil resistance and penetrate at a certain depth while being vibrated into the ground.

The determination of the beta factors, which are then used to determine the SRV, is achieved at a frequency of 20-30 Hz. For insight in the frequencies, considering that if for the Vibrodrill resonance is desired in a 80 meter pile in longitudinal direction, the frequency would need to be 32,3 Hz respectively. Exciting at higher modes or shorter piles require an even higher frequency. Jonker stated that all beta values may be different for driving and extraction conditions (Jonker, 1987). Since the Vibrodrill will excite at a higher frequency the beta values will probably not be applicable in the model that is to be made.

#### 4.1.3 Energy-balance models:

The energy balance models describe the driveability by determining the energy that is applied and the energy that is consumed by the system. The calculations are estimated with a contributing empirical loss factor. This so called beta factor can be calculated using the Davisson's formula which was developed to predict the bearing capacity of Bodine resonant driven piles. In addition to this, Schmid (1969) suggested a formula for the steady state penetration for this method. In contrary to earlier discussed models, the energy-balance method is able to estimate the penetration speed.

The Davisson's formula was based on resonant driving which the Vibrodrill also intends to do. However, in the case of the Vibrodrill system there are jets fitted to the pile toe. This is not taken account in the calculations of the energy balance method. Considering this, the beta factors that were used in the Energy-balance method will be presumed unsuitable.

#### 4.1.4 Momentum-conservation models

Over the time duration of one cycle of vibration the soils resistance impulse is balanced with the total weight of the system. This method is based on the dynamic resistance force developed at the pile toe. However it does not take jetting into account and is therefore deemed less interesting. For further interest in this method, the reader is referred to the research done by Schmid (1969).

Momentum based methods may produce a penetration speed very similar to that of the integration of law of notation of a rigid body (Holeyman, 2000). Another downside of using this model for this research is that the resonance of the system in which the Vibrodrill system would ideally operate might interfere with this approximation.

#### 4.1.5 Integration of the laws of motion models

The integration model is the most up to date method of the described methods. It predicts the drivability integrating the equilibrium conditions of the system at all times. The pile is considered as a rigid body with one degree of freedom. In doing so, Newton's second law can be applied. This results in the following equations.

$$F_0 + F_v + F_m - R_s - R_t = a m_{dyn}$$

$F_0$  is the static surcharge force,  
 $F_v$  the unbalanced force,  
 $F_m$  the static force of the dynamic masses,  
 $R_s$  the dynamic soil resistance along the shaft,  
 $R_t$  the dynamic soil resistance at the toe,  
 $a$  the acceleration of the driven element  
 $m_{dyn}$  the sum of all masses that vibrate.

This formula can be used to determine the penetration speed. The dynamic resistance forces at the pile toe, inner and outer shaft are each modelled differently. The difference in these dynamic soil resistance forces depends on the geotechnical parameters.

Using this principle several models have been further developed. Main models to consider are the the Karlsruhe model (Dierssen, 1994) the viper model (Berghe, 2001) and the Vibdrive model (Holeyman, 1993) which was later refined by Vanden Berghe and Holeyman in 1997.

**The Karlsruhe model** (Dierssen, 1994) presents the dynamic toe resistance during slow vibratory motion. Because that in this thesis the interest is focused on shaft resistance and at a relatively higher frequencies, this model is considered not useful and will not be further elaborated.

**The Vibdrive model** was initially developed by Holeyman (Holeyman, 1996) based on CPT results. It is considered to be of much interest for this thesis. This semi empirical model which is based on sheet piling takes the earlier described phenomena, fluidization (due to cyclic motion of particles) and liquefaction (due to induces pore pressure build-up), into account. These phenomena both alter the initial shear strength characteristics of the soil. It predicts the magnitude of this soil shear-strength reduction (the penetrative resistance) during vibratory driving.

The dynamic shaft resistance ( $R_s$ ) is also modelled by a step function, where the direction of the shaft resistance is always in the opposite direction to the movement:

$$R_s = \text{sgn}(v)X \int_0^z \tau_d dz \quad ; \quad \text{sgn}(v) = \begin{bmatrix} 1 \text{ if } v > 0 \\ 0 \text{ if } v = 0 \\ -1 \text{ if } v < 0 \end{bmatrix}$$

$R_s$  = dynamic shaft resistance [kN],

$X$  = perimeter of the sheet pile [m],

$\tau_d$  = maximum shear stress at the shaft of the sheet pile [kPa],

$v$  = velocity of the vibratory-driven sheet-pile, and

$z$  = penetration depth of the sheet-pile toe [m].

The driving unit resistance is a function of the liquified soil resistance as shown in the following formula:

$$\tau_d = (1 - e^{-\alpha})\tau_l + \tau_s * e^{-\alpha}$$

Where:

$q_d$  = driving unit resistance at the toe [kPa]

$q_l$  = liquidied soil resistance at the toe [kPa]

$q_s$  = static toe resistance profile [kPa]

$\alpha$  = accereration ratio ( $a/g$ ) [-]

$q_d$  = driving unit resistance at the toe [kPa]

$q_l$  = liquidied soil resistance at the toe [kPa]

$q_s$  = static shaft resistance profile [kPa]

In turn the liquified soil resistance is determined by the static shaft resistance profile the friction ratio and an empirical liquefaction factor which expresses the loss of resistance. this will be lower for saturated and loose sands.

$$\tau_l = \tau_s \left[ (1 - \Psi)e^{-\frac{1}{R_f}} + \Psi \right]$$

Where:

$\Psi$  = emperical liquifaction factor, set between  $4 < (1/\Psi) < 10$ , [-]

$R_f$  = friction ratio ( $f_s/q_s * 100$ ) taken from the CPT results [%]

$\tau_l$  = liquidied soil resistance along the shaft [kPa]

$\tau_s$  = static shaft resistance profile [kPa]

**The Vipere model** (Vibratory PENetration RESistance) is a semi numerical model and the most recent of these models. It was developed by Vanden Berghe(2001). The Vipere model is used to study the penetration speed at varying depths during vibratory driving and to predicted the variation of soil resistance over time. Viking (2002) researched the vibro-driveability of sheet piles in non-cohesive soils. He compared results from the field studies with the latter two vibro-driveability models, Vibdrive and Vipere. A more elaborated description of these models and the application of Vipere and Vibdrive model can be found in Viking (2002). The fact that a shaft friction reduction due to vibratory driving has been taken into account by means of CPT data in the Vibdrive model is of great interest to this thesis. The dynamic shaft resistance as described in this method could be taken into account in the further development of the Vibrodrill model.

4.1.6 Wave-Equation models (in longitudinal one dimensional models):

in the 1950s, E.A. Smith developed the wave equation analysis to analyze the behavior of driving foundation piles numerically. This is done by predicting the pile capacity versus blow count and pile driving stress. In this model the pile hammer is represented mathematically. The pile is represented as a series of masses and springs. This is all done in a 1D analysis as can be seen in Figure 17. The soil response for each pile segment is modelled as viscoelastic-plastic.

The basis for the procedure that Smith developed is the Classical one dimensional wave equation that was formulated by Jean-Baptiste le Rond d'Alembert in 1717:

$$\frac{\partial u^2}{\partial t^2} = c^2 \frac{\partial u^2}{\partial x^2}$$

Where  $c$  = velocity of propagation (of longitudinal strain wave along a bar =  $\sqrt{\frac{E}{\rho}}$ )  
 $x$  = direction of longitudinal axis  
 $u$ =displacement of bar cross section in  $x$  direction

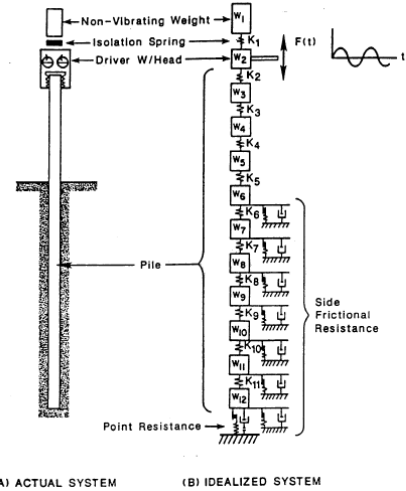


Figure 17 Discription of principle behind the modified one dimensional model (gardner, 1987)

Since the 60's this method of analysis has been improved by for example including residual stress. The model proposed by Smith (1960) is commonly accepted in industry, however, it presents a number of limitations. Software has been developed which is commercially available, such as TNOWAVE, AllWave-PDP and GRLWEAP.

GRLWEAP (Pile Dynamics) is a top excited wave equation based software with vertical 1D model of multiple mass springs inputs: soil properties quake, damping and resistance values.

Allwave VDP (allnamics) is a 1D model of multiple mass springs which is also excited at the top. Like the Pile Driving Predictions for impacts hammers (PDP), simulations can be made for piles installed by means of a vibratory hammer. Comparable to the results with PDP, one can study the efficiency of a vibratory hammer, maximum reachable penetration or refusal level, the maximum stresses and the amount of fatigue. Using the AllWave-VDP software and a large database of predicted and monitored results, leads to reliable prediction results. (Allnamics Pile Testing Experts, 2019)

The advantage of All Wave-VDP is that they have a large database of predicted and monitored results. Since all these measurements have been done on vibrodriven piles which were excited at the top this data would

most probably be different compared to vibrodriven piles excited from the bottom in combination with water injection which is of interest here.

The fact that the wave equation models do consider the dynamics of the pile is considered to be an advantage. Holeyman (2000) stated that this method should not produce penetration speeds significantly different from those obtained from a rigid body analysis, provided the vibrator speed is lower than the resonant frequency of the pile. Exceptions to this general case include the Bodine resonant driver, which aim to operate at the resonant frequency, and very long piles longer than 50m(Holeyman, 2000)(Vanden Berghe & Holeyman, 2014). In the case for GBM the excitation would be near the resonant frequency and for long piles. The result of using the wave equation or any other method that includes the pile dynamics is considered to do have a significantly different outcome and would thus be considered more useful for this research.

## 4.2 Numerical models

To estimate the (vibro-)driveability of piles and sheetpiles, numerical models and mainly finite element models have been developed. A main issue with these finite element models is the pile-soil interaction. In this chapter a description of various numerical models and the assumed applicability is given.

### 4.2.1 Finite Element Modelling

Finite Element Method (FEM) is a widely used numerical method in which complex problems in areas such as solid mechanics, dynamics and structural analysis can be performed (Qi, 2006). It is a numerical technique that can solve problems which are described by partial differential equations (Nikishkov, 2004). The name finite element comes from the fact that the area of interest is imitated by numerous finite elements which represent the actual physical model to solve the problem. Hereby a continuous problem is transformed into a discrete system of finite elements. This method has an advantage over analytical methods with complex boundary problems.

### 4.2.2 Existing Numerical Models

As described above, the most difficult part in modelling a vibratory driving system is the modelling of the soil. Prior research using FEM analysis has been done to estimate the soil reaction (and possible ground vibrations). To get a better understand the modelling procedures and a few papers are summarized.

The first type of FEM model can be considered the one from Holeyman & Legrand (1994), where they developed a one-dimensional radial discrete model. In their model, the pile was considered as a rigid body, which is surrounded by a semi-infinite medium. The research was focused on a non-linear analysis on the vertical shear waves that propagate due to vibrating a cylindrical pile. In this research (Holeyman & Legrand, 1994) it was concluded that, when modelling vibratory penetration in numerical analysis, the decreasing soil resistance in the near-field of the pile is an important factor.

Ramshaw et al. (2000) developed a finite element-infinite element method or FE-IEM. This research was focused on groundwaves in soil in vibrodriven rigid piles and impact hammered pile. The modelling was built using Abaqus software. In this software they developed an axisymmetric model with elastic material(Ramshaw, 2000). At first the pile was rigidly oscillated and after that the sinusoidal wave distribution into the soil was determined. The peak particle velocity (PPV) of the measured and computed vibrodriven pile showed a good agreement(Ramshaw, et al.,2000).

Mahutka & Grabe (2006) also worked with the software package Abaqus, and developed a non-linear axisymmetric finite element analysis. With an adaptive mesh they managed to simulate the pile driving process penetrating down in granular soil. To calculate the pile-soil interaction they used a Coulomb friction method. By means of using the constitutive equations of hypo plasticity the non-linear and inelastic behavior of the granular soil was calculated (Grabe, 2006). For the vibration velocity the variation in extreme values was higher in the numerical calculations than the field measured values within a range of 5-10%. Mahutka & Grabe (2006) also performed a parametric study where they concluded that an increase in driving frequency decreases the velocity amplitude.

Henke & Grabe (2009) performed research on Numerical modelling of pile installation in which they stated the following: *“Pile installation leads to significant changes in the main state variables of the surrounding soil depending on the cross-section of the driven piles and the installation method”*. They describe that Mainly, the void ratio distribution and the stress state around the driven piles are influenced, and that the influence on the surrounding soil in pile driving has not been fully investigated yet. As described before Henke & Grabe (2009) state that, to investigate mechanisms occurring during (vibratory) pile driving. *Numerical methods like Finite-Element-Method are helpful tools. With these methods, changes in void ratio and stress state around the driven piles can be described.* (Henke & Grabe, 2009)

Henke & Grabe Used Abaqus software to investigate the main factors which influence the additional loading on structures if a pile is driven next to it. The formulation they used was based on the master–slave principle which was implemented in ABAQUS without contact elements. For the contact a friction coefficient of  $\tan \delta = \frac{1}{3} \varphi'$  was used in the Coulomb friction model for all analyses performed. (Henke en Grabe 2008)

Lo, et al. (2012) simulated the vibratory driving of a pile using Scaled Boundary Finite Element Method (SBFEM). The focus was on ground surface vibrations. The near-field (pile-soil) was modelled by FEM and far-field (unbounded soil) was modelled SBFEM. They assumed the soil to be linear elastic. Using time domain analysis the model simulated the vibratory driving from a predetermined imbedded pile depth. They conclude that vibration amplitude do not get affected in a significant way by the different subsoil properties even if the penetration depth is varied. They also concluded that the soil stiffness affect the surface vibration. An amplification of the wave amplitude was noticed, when penetrating a softer layer between two stiffer layers. (Lo, Ni, Huang, & Lehmann, 2012)

Ekanayake, et al. 2013 did their research on the Influence zone around a closed-ended pile during vibratory driving, to investigate the effect of wave propagation on the surrounding ground. A FEM-model is used to investigate the effect of vibratory and resonant vibratory pile driving in cohesive soil. An elastic-perfectly plastic soil model with an adaptive mesh was used. They used this model to simulated a pile driving to a depth of 4 m using a time domain approach in Abaqus software. While penetrating the pile was assumed as a rigid body. In this research a friction coefficient, to account for the pile-soil interaction, was set at 0,2.. Ekanayake, et al. (2013) concluded that varying the amplitude, vibrator frequency or penetration depth, does not change the influence zone for the vibratory pile driving (affected zone due to vibrations and the pile). However when looking at resonant pile driving, an increase was seen in the influence zone at higher frequencies. For the depth or amplitude no significant change were seen. The soil rigidity has an influence on PPV at both the resonant and vibratory driving. An improved agreement with the field measurements was seen when a 2% damping was added to the model. (Ekanayake et al. 2013).

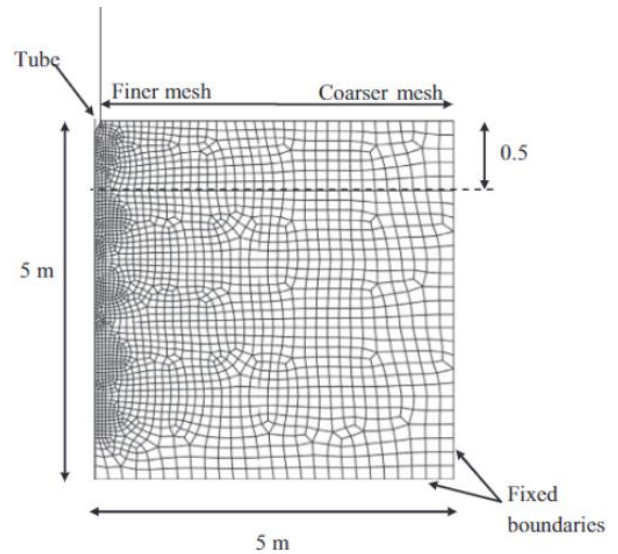


Figure 18 axisymmetric model for pile jacking (Ekanayake et al. 2013)

Olsson (2014) developed two 3D-FEM models to research the Dynamic Response Study on Optimal Piling Depth with respect to Ground Vibrations. Both of the models are linear elastic using a frequency and a time domain approach. A material damping is applied in the models and they are computed for one depth at the time. A good agreement with studies by Robertson (1966) and Kuo and Hunt (2013) were found. Olsson (2014) concluded that over a frequency of 4 Hz, piles shorter than 20 m seem to excite Rayleigh waves, and piles longer than 20 m do not excite Rayleigh waves.

Other interesting studies, which are not elaborated here further, to recommend are: A. Holeyman (2014) who researched Axial Non-linear Dynamic Soil-Pile Interaction. The research on Simplified simulation of the installation of vibro-piles in water saturated soil by Grandas-Tavera, C. E. (2019) and Simulation of pile driving by 3-dimensional Finite-Element analysis by Henke & Grabe (2006).

### 4.3 Conclusion

A challenge in this thesis is to include and accurately consider resonance and dynamics in multiple dimensions in vibratory driving of a pile. This is especially difficult when considering the soil interaction as accurately as possible. As Holeyman (2000) stated: “A critical parameter to assess in order to produce reasonable prediction in vibro-driving is the soil resistance to vibratory driving. That is unfortunately where pertinent information and recent consistent experimental data is cruelly missing”

The behavior of the pile will be greatly affected by the surrounding soil. In particular the shear modulus, the soil near the pile within the pile-soil interaction is considered to behave non-linearly and thus difficult to model. This interaction between the soil and the pile is considered to be a major uncertainty in FEM modelling (Masoumi & Degrande, 2008).

The existing models are not considered directly suitable for this thesis. The models researched have been designed to be loaded from the top. Considering that for the Vibrodrill, the vibration will be induced from the bottom with a fluidized inner part of the pile, it is assumed that the semi-empirical data for direct solutions will not be directly applicable. Most of the described models are one dimensional in longitudinal direction which means leaving out the torsional vibrations and torsional flexibility of the pile. These factors are also considered necessary to study in the Vibrodrill method. The models described are mostly suitable for smaller diameter piles. For this thesis large diameter (8m) piles are considered.

For this research an interest lies in the penetration performance when harmonically exciting the pile from the bottom in torsional direction, the only downward force in this case would be due to the weight of the pile. The ability to test this and compare it with longitudinally excited scenario was not found in existing models.

Masoumi (2006) and Whenham (2011) both conclude that the assuming linear behavior of the space considered to be a “fairly good” compromise for research on the vibratory driving of piles and sheet piles. Considering the fact that the modelling of the soil and pile soil interactions are not completely reliable in any non-empirical dynamical analysis. A very accurate solution will be unlikely due to the complexity of the pile soil interaction. For this thesis, the relative factor of influence to drive the pile with the Vibro-drill is of biggest interest. Computation time is also a factor since it is desired to compare many different simulations in this thesis. DEM and FEM models with large space of soil in general have a long computation time and are deemed not to be suitable in their state of complexity.

The purpose of this thesis is not to have an as accurate model as possible simulation of the soil, but to investigate the relative differences on the penetration speed of the factors of influence. The main focus is on the SSI, not the soil space. This considered, together with the fact that the interest lies in vibratory driving in all directions, the decision was made to develop a numerical model in FEM with linearly assumed soil stiffness.

## 5 Modelling approach (proposed model)

As concluded in the previous chapter, the decision was made to use FEM analysis with a linear approximation of the soil reactions. FEM is a widely used method and is accepted by DNV-GL, which is a well-known certifying body for the offshore industry.

To model the penetration performance, the pile will be considered partially embedded into the soil. Along the depth the horizontal effective pressure increases. This pressure is perpendicular to the inside and the outside of the pile. Depth also has an increase in radial stiffness. The model needs to be able to slide in longitudinal direction with having a certain frictional resistance to vibratory driving. The determination of the values will be done in later chapter.

### 5.1 Modelling of the Pile

To accurately implement the resonance phenomena of the “thin walled” pile, the pile will not be modelled as a rigid body but will consist of a cylinder representing the pile made of shell elements. The implementation of shell elements is done due to the fact that the pile is thin walled. Material characteristics can be implemented in any FEM software chosen to ensure the proper pile dynamics is implemented.

The decision to use a flexible pile instead of a rigid body lies in the fact that the flexibility of the pile is thought to be of influence to the penetration speed. The effect it has on the penetration is assumed to be positive since the inertial effect of the dynamic mass of the pile can contribute to the downward motion, especially when resonance occurs.

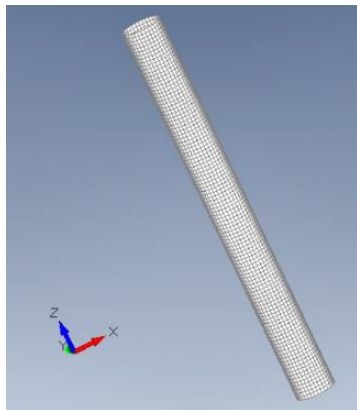


Figure 19 Model of the pile without soil

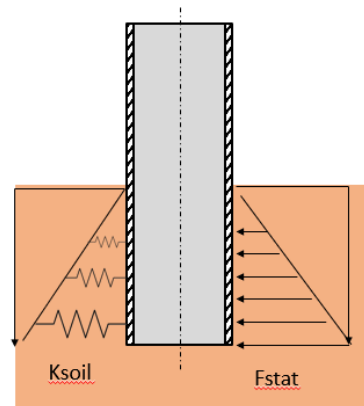


Figure 20 Pile in soil with depth dependent force and soil stiffness

## 5.2 Modelling of the Pile-soil interaction

As described, the pile will be modeled as shell elements containing multiple nodes here described as node(i,j). To model the interaction between the pile and the soil ( as shown in Figure 21) a lot of assumptions and simplifications are made. In this chapter, the modelling of the pile-soil interaction is explained and the assumptions compared to reality are described per input value.

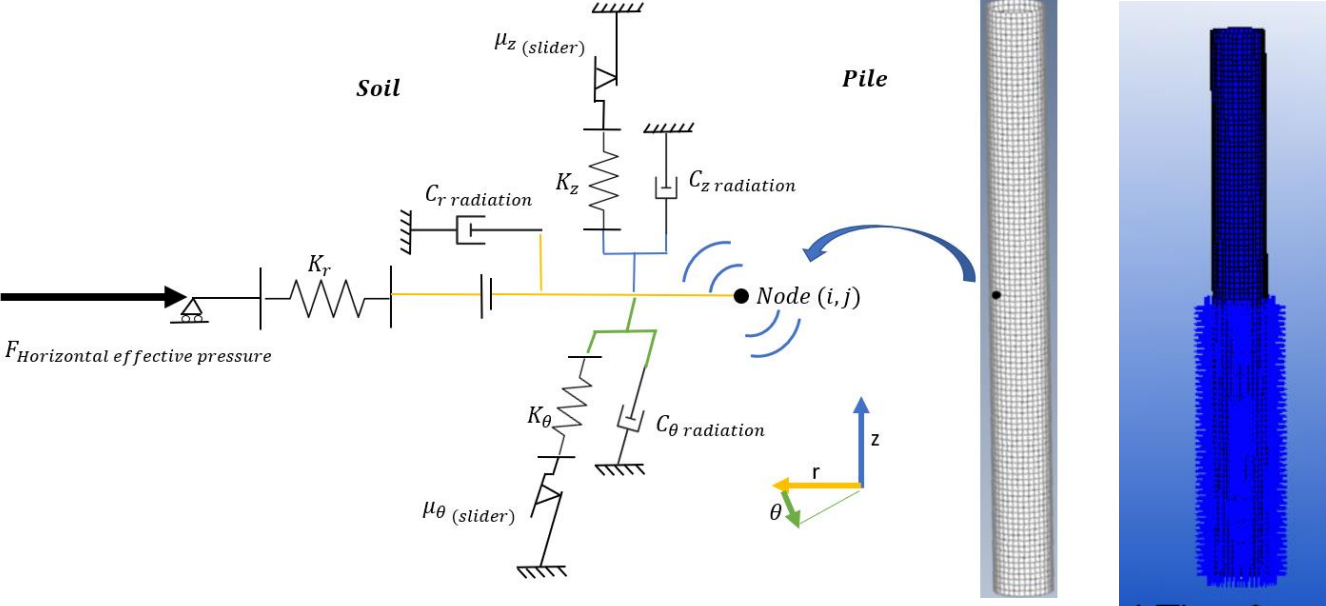


Figure 21 Schematic view of the proposed model

ELEMENT	MODELS	SOIL ANALOGY
<b>NODE (I,J)</b>	Surface of the pile	Contact area with the soil
$F_{\sigma'_h}$	Force due to Horizontal effective pressure	Effective pressure on the pile
$\mu_{\theta\&z}$	Frictional resistance to vibratory driving in $\theta$ & z direction	Resistance of the soil in plastic deformation
$K_r$	stiffness in radial direction	Small strain soil stiffness
$K_{\theta\&z}$	stiffness in shear	Small strain shear stiffness
$C_r$	Damping ratio in radial direction	Radiation and material damping in x direction;
$C_\theta\&C_z$	Damping in transverse direction	Radiation and material damping in $\theta$ &z transverse (shear) direction;

Table 2 Model element description

To model for the horizontal effective soil pressure acting on the pile, the pressure (depending on the density of the soil and water and the depth) is calculated. This pressure is multiplied by the area that the node in question represents on the pile, resulting in a force per node.

For the soil interaction the decision was made to have a spring slider element and a damper to the ground that simulated the resistance to sliding and the damping in that direction. The sliding is necessary to determine the penetration displacement. These elements have been implemented into an uncoupled pile-soil interaction model. In the normal direction (w.r.t. the pile) a spring( $K_r$ ) and a damper ( $C_r$ ) system is implemented representing the soil stiffness and damping in radial direction. Also a gap element is introduced to account for the fact that if the soil is disconnected from the pile there is no friction considered. In the transverse plane (w.r.t. the pile;  $\theta$  &  $z$ ) also a Spring and a damper system is applied representing the friction and damping in their directions. Here also a friction sliding element is implemented with a predefined critical value  $\mu$  before sliding occurs. The attached spring is considered linear.

This part of the model could be considered as linear elastic perfectly plastic as the element will start sliding with a constant reaction force when the critical friction force is exceeded.

### 5.3 Modelling of the Forcing

The forcing as it will be modelled will represent an eccentric rotating mass. Here for the harmonic forcing that will be applied on the nodes will be harmonic in 2 perpendicular directions with a 90 degree phase shift, either longitudinal, torsional or torsional and longitudinal, depending on the orientation of the eccentric rotating mass. The individual harmonic forcing on each node are considered to be in phase with each other. The force will be exerted on the bottom or top nodes of the pile.

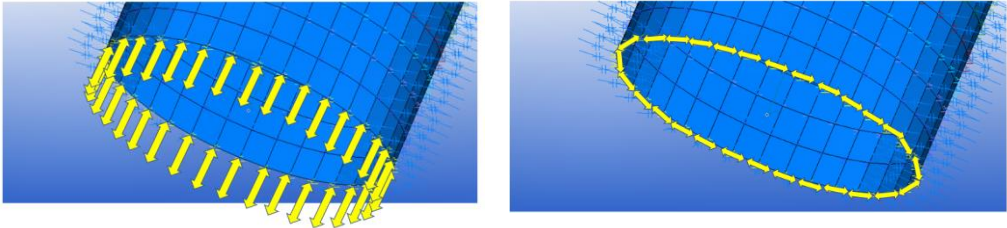


Figure 22 Visualization of applied axial and torsional forcing at the bottom of the pile

### 5.4 $F_{effective\ pressure}$

In reality the effective pressure in the soil [ $N/m^2$ ] acts in all directions. In this model, it is assumed that it can be represented as a force [ $N$ ] on a single node (representing the area). If the mesh size is taken too large this could create inaccurate results. In the current configuration the force due to the effective soil pressure is a function of depth and soil characteristics in the static situation. If dynamics would come into play the effective pressure could reduce considering liquefaction.(Viking, 2002) this would lead into a decrease of this force.

### 5.5 $\mu_z$ & $\mu_y$

The friction element (in combination with the  $F_{effective\ pressure}$ ) simulates the resistance to driving due to the friction between the soil and pile surface. In this model Coulomb friction is assumed. In this case the shear (between the pile and the soil) is linearly elastic before the critical Yield point which depends on  $\mu$  is reached and plasticity (sliding) occurs. In reality the soil elasticity is not perfectly linear. During the sliding phase perfect plasticity is assumed, in reality this will not be constant. The frictional resistance will have to be estimated during vibratory driving with one value while in reality this would be constantly fluctuating.

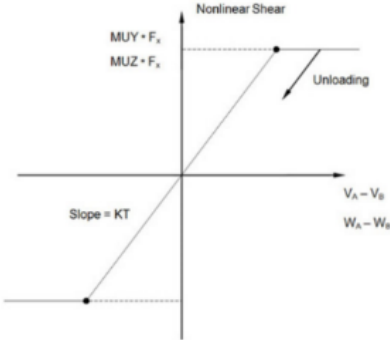


Figure 23 CGAP element (linear elastic perfect plastic) (MSC Nastran, 2012)

### 5.6 $K_{radial}$ ( $K_x$ )

$K_x$  defines the Soil stiffness of the soil in radial direction. In the model this is approximated as linear while in reality this is a nonlinear phenomenon. Next to the linearity approximation the different springs are also uncoupled ( or independent): The nearby soil will in reality have an influence on each other, here the different adjacent springs are independently determined. Also, because soil is defined with only one spring in radial direction, no reflected wave in the soil space is modelled.

### 5.7 $C_{Radial}$ ( $C_x$ )

$C_x$  defines the Damping of the soil in radial direction (Radiation damping). This is also approximated as linear and uncoupled while in reality this would be non-linear and coupled. The total damping in reality acts in all directions, here it is captured in one dimensional dampers (with one constant value).

### 5.8 $K_{tangential}$ ( $K_y$ & $K_z$ )

This element models the Stiffness of soil in shear during vibratory driving. Here a linearly elastic perfectly plastic system is assumed. In reality this is expected not to behave perfectly linear as it would be expected to behave more nonlinear. Likewise the plasticity is also expected not to be quantifiable by an exact constant value. In this model the stiffness is assumed linear.

### 5.9 $C_{tangential}$ ( $C_y$ & $C_z$ )

This element models the damping in shear direction during vibratory driving. The approximation of being able to describe the whole shear space in linear dampers in 2 directions is made.

### 5.10 Assumed effects

The assumptions made to generate the model can highly affect the outcome compared to reality. The interface between pile and soil is considered to be very complex. In the current model, is assumed the soil and pile are attached like described in this chapter. However, the soil in reality is non-homogeneous and made out of a lot of different sized particles with varying characteristics. Combining the uncertainties in soil parameters with dynamics creates very complex situations. The generalizations made are necessary to create a working model with the current knowledge and computing power.

## 6 Determining Input Values

In this section a description is given on how the values that will be used in the model are determined. It must be noted that the goal of the model is not to have an outcome which perfectly resembles reality but to compare what the reaction of the model will be when varying the determined input parameter. The values, that were assumed as accurate as possible for this model, are described in this section:

### 6.1 Pile values

For the values of the pile, in this research, an 80m pile with a L/D ratio of 10 made out of steel is used. Since the values are chosen dimensions and material properties, no further explanation is deemed necessary. The input values as will be used to describe the pile are described below:

#### Pile Characteristics:

Pile Length	$L_p = 80 [m]$
Pile Diameter	$D_p = 8[m]$
Wall Thickness	$t_p = 0,008 [m]$
Young's Modulus Steel:	$E_{steel} = 2,1 * 10^8 [Pa]$
Density Steel:	$\rho_{steel} = 7850 \left[ \frac{kg}{m^3} \right]$
Poisson ratio	$\nu_p = 0,3 [-]$
Critical Damping ratio	$\zeta_p = 0,02[-]$ (V. Adams and A. Askenazi, 1999)
Overall structural Damping coefficient	$G_c = 2 * \zeta_p = 0,04 [-]$ (Nastran, 2012)

### 6.2 Soil values

In this section an explanation is given on the determined input values that have been chosen for the predetermined soil characteristics. Even though the model will not accurately represent reality, accurate research on determining the values of the soil has been done to get an as accurate as possible approximation. In this thesis the assumed soil is fine saturated sand.

#### Soil Characteristics (fine saturated sand)

Density of seawater:	$\rho_w = 1.025 \left[ \frac{kg}{m^3} \right]$
Unit weight of sea water:	$\gamma_w = g * \rho = 9,81 * 1.025 = 10.055 \left[ \frac{N}{m^3} \right]$
Density of saturated sand:	$\rho_{sat} = 1.930 \left[ \frac{kg}{m^3} \right]$ (tpub, 2002)
Specific weight saturated sand :	$\gamma_{sat} = g * \rho_{sat} = 18.933 \left[ \frac{N}{m^3} \right]$ (Muni Budhu, 2015)
Poisons ratio of soil	$\nu = 0,4$ (Subramanian, 2016)
Shear Modulus soil	$G=90 [MPA]$ (Brennan, 2005)

As described in the section 5.2, the input values for the soil elements will need to be accurately determined for fine saturated sand. The elements for which the values will be determined in this chapter are shown in Table 3.

Element	Models	unit
$F_{\sigma'_h}$	The horizontal effective force (per surface area)	N
$\mu_z$	frictional resistance to vibratory driving in z	-
$\mu_y$	frictional resistance to vibratory driving in y	-
$K_r$	Soil stiffness in radial direction	N/m /m <sup>2</sup>
$K_\theta$	Soil stiffness in transverse direction	N/m /m <sup>2</sup>
$K_z$	Soil stiffness in transverse direction	N/m /m <sup>2</sup>
$C_r$	Soil Damping ratio in radial direction	Ns/m /m <sup>2</sup>
$C_\theta$	Soil Damping ratio in transverse direction	Ns/m /m <sup>2</sup>
$C_z$	Soil Damping ratio in transverse direction	Ns/m /m <sup>2</sup>

Table 3 Soil elements

### 6.2.1 Unit skin resistance

Firstly it is noted that the skin friction increases over the depth until a critical depth where it has been said to stay constant. However, Wrana's (2016) research shows that the skin friction is actually reducing at the critical depth (Randolph, Dolwin, & Beck, 1994) as can be seen in Figure 24. Wrana (2016) also states that it is assumed that the lowest critical depth is at 10D (D is the pile diameter or the width). Typically for the installation of a monopile this ratio will not be reached and thus a reduction of the unit skin resistance due to the critical depth is not taken into account in the model.

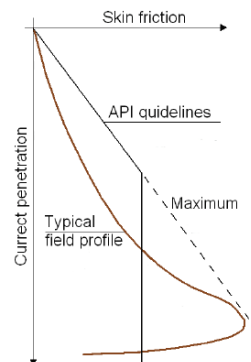


Figure 24 Variation of skin friction (Randolph & Beck 1994)

As described in section 0, to determine the unit skin resistance in statics (pile load capacity) the Beta method for cohesive and cohesionless soils can be used:

$$q_s(z) = \mu \sigma'_h = \mu(z) K'(z) \sigma'_v(z) = \beta(z) \sigma'_v(z) \quad (4)$$

Here it is described that a perpendicular force ( $\sigma'_h$ ) multiplied by a friction coefficient ( $\mu$ ) results in the skin friction of the pile (in vertical direction).

These calculations are designed for static situations and since in this thesis a dynamic situation is considered the question is if it is possible to approximate the values determined by these calculations.

## 6.2.2 Horizontal effective pressure ( $F_{\sigma'_h}$ ) & Friction coefficient ( $\mu$ )

To determine the Horizontal effective pressure, the vertical effective pressure is determined first. The vertical pressure ( $\sigma_v$  [pa]) is a function of the unit weight of saturated soil  $\gamma_{sat}$   $\left[\frac{kN}{m^3}\right]$ , the depth of the soil  $z_{soil}$  [m], the unit weight of water  $\gamma_w$   $\left[\frac{kN}{m^3}\right]$  and the depth of the water  $z_w$  [m].

$$\sigma_v(z) = \gamma_{sat} * z_{soil} + \gamma_w * z_w \quad (\text{Figure 25})$$

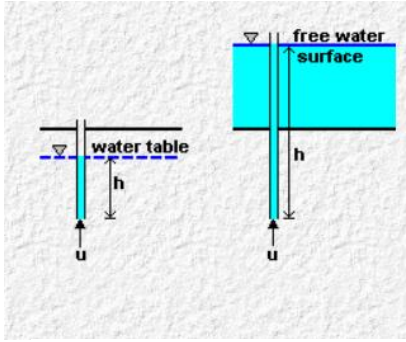


Figure 25 Pore water pressure (Prof. John Atkinson, 2019)

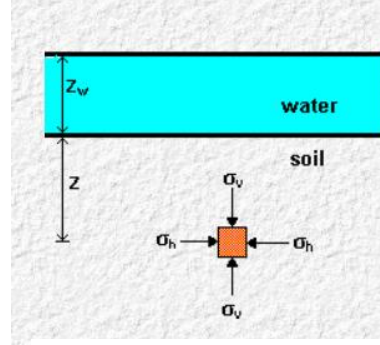


Figure 26 effective pressure (Prof. John Atkinson, 2019)

The pore water pressure;  $u$  [pa] is determined by the unit weight of water and the height of the water table from the location in question as can be seen in (Figure 26):

$$u = \gamma_w * h_w$$

To finally get to the vertical effective pressure Terzaghi's principle is used;

$$\sigma'_v(z) = \sigma_v - u$$

From Terzaghi's principle and the vertical effective pressure for our case can be calculated;

$$\sigma'_v(z) = \sigma - u = \gamma_{sat} * z_{soil} + \gamma_w(z_w - h_w)$$

$$z_w - h_w = -z_{soil}$$

$$\sigma'_v(z) = z_{soil}(\gamma_{sat} - \gamma_w)$$

$$\sigma'_v(z) = 8.88 * z \text{ [Kpa]}$$

According to NAVFAC DM 7.2 (1984)  $\beta = \mu(z)K(z) = \tan(\delta(z))K(z)$ . For steel piles the pile skin friction angle is  $\delta = 20^\circ$  and the Lateral earth pressure coefficient is  $K=0.4-0.9$  for driven and jetted piles under compression ( and 1.0-1.5 driven displacement piles). (Wrana, 2016) Assuming  $K=0.9$  and  $\delta = 20^\circ$   $\beta = \tan(20^\circ) * 0.9 \approx 0.3276$

$$q_s(z) = \beta * \sigma'_v(z) \approx 0.3276 * 8.88 * z \text{ [Kpa]}$$

$$q_s(z) = \mu * \sigma'_h(z) = \mu * K(z) * \sigma'_v(z) = \beta * \sigma'_v(z)$$

If  $K=0.9$

$$\sigma'_h(z) = K(z) * \sigma'_v(z) = 0.9 * 8.88 * z \text{ [Kpa]} = 7.99 * z$$

From these calculations the horizontal effective pressure is defined as well as the friction.

$$\mu = \tan(20^\circ) = 0.364$$

This frictional coefficient is also meant for a static situation. In a dynamic situation the frictional coefficient will be expected to go down due to liquefaction of the soil.

### 6.2.3 Vibrodriven unit skin resistance research

Since the values determined in the previous chapter are initially developed for static situations and the situation to study is dynamic, further investigation on the unit skin resistance in dynamic situations was desired. As described before, Viking (2002) researched the installation of sheet piles and determined “The driving unit resistance” as a function of the liquified soil resistance as shown in the following formula:

$$\tau_d = (1 - e^{-\alpha})\tau_l + \tau_s * e^{-\alpha}$$

Where:

- $q_d$  = driving unit resistance at the toe [kPa]
- $q_l$  = liquidied soil resistance at the toe [kPa]
- $q_s$  = static toe resistance profile [kPa]
- $\alpha$  = accereration ratio ( $a/g$ ) [-]
- $q_d$  = driving unit resistance at the toe [kPa]
- $q_l$  = liquidied soil resistance at the toe [kPa]
- $q_s$  = static shaft resistance profile [kPa]

The liquified soil resistance is determined by the static shaft resistance profile, the friction ratio and an empirical liquefaction factor which expresses the loss of resistance. This will be lower for saturated and loose sands.

$$\tau_l = \tau_s \left[ (1 - \Psi)e^{-\frac{1}{R_f}} + \Psi \right]$$

Where:

- $\Psi$  = emperical liquifaction factor, set between  $4 < (1/\Psi) < 10$ , [-]
- $R_f$  = friction ratio ( $f_s/q_s * 100$ ) taken from the CPT results [%]
- $\tau_l$  = liquidied soil resistance along the shaft [kPa]
- $\tau_s$  = static shaft resistance profile [kPa]

Considering as an upper bound, an empirical liquefaction factor of 0,25 and a friction ratio of 2% the driving unit resistance is reduced to 70,4% of the static shaft resistance. As a lower bound an empirical liquefaction factor of 0,1 and a friction ratio of 1% the driving unit resistance is even reduced to 43,1% of the static shaft friction. These values are considering  $\alpha > 5$  (Figure 27) .

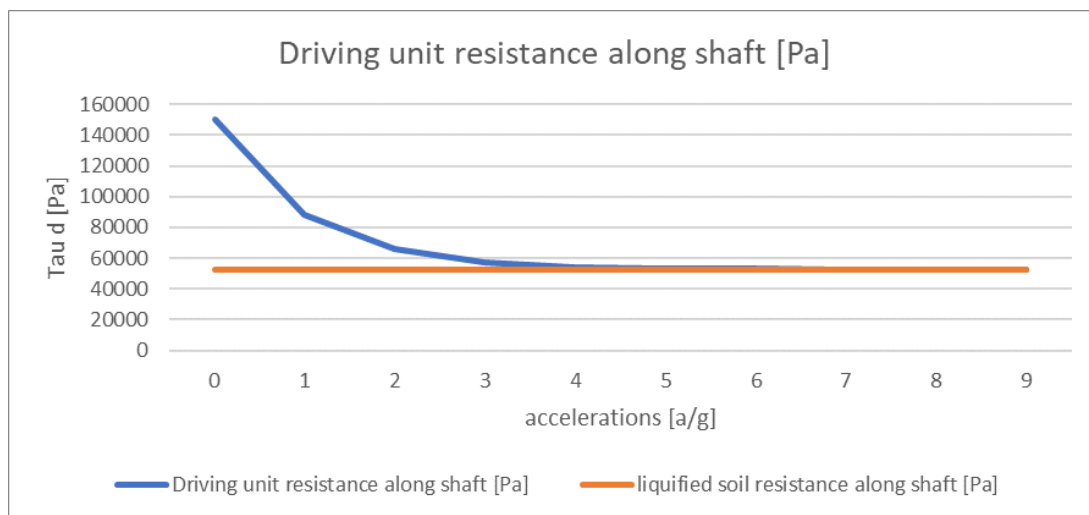


Figure 27 Driving unit resistance reduction

Considering the lack of validation especially on piles and the uncertainties of using the empirical factors determined for a sheetpiles in a cylindrical pile it has been decided not to consider this reduction in further calculations. The friction coefficient determined for the static case  $\mu = 0,364$  shall be used and will be assumed to be a conservative case.

### 6.2.4 Determining Soil Stiffness (Kx, Ky, Kz)

In this section, a description of two methods of determining the Soil stiffness parameters is given. First the conventional p-y method and secondly a more recent method used by Versteijlen and Barbosa (2018).

#### 6.2.4.1 P-y Method

The P-y method used to analyze the resistance to lateral loads on deep foundations like monopiles.

$$p = k * y \text{ (API P-y method)}$$

where p is the actual lateral resistance per unit length of the pile (Figure 28). k is the non-linear spring stiffness defined by the p-y curve which is a representation of non-linearity in soil stiffness.

The p-y curve was meant for slender piles. By using the p-y method using a 1m diameter pile the nonlinear resistance (per unit depth) is acquired (values used are shown in appendix A3).

To get a value of a linear spring the resistance is divided by a certain deflection. In the case at hand a small strain stiffness needs to be determined and thus need to define the initial tangent modulus.

The initial tangent modulus is estimated by determining the lateral resistance P (which varies over depth) for a small deformation of 0.01m and dividing this by the set deformation. (Brennan, 2005)

$$E(d) = \frac{p}{y} \left[ \frac{\frac{kN}{m^2}}{m} \right] \text{ (Johnson, Parsons, Dapp, & Brown, 2006)}$$

By applying this formula at a very small deflection the initially nonlinear spring stiffness over the deflection is now considered as a linear small strain spring stiffness. (Figure 30)

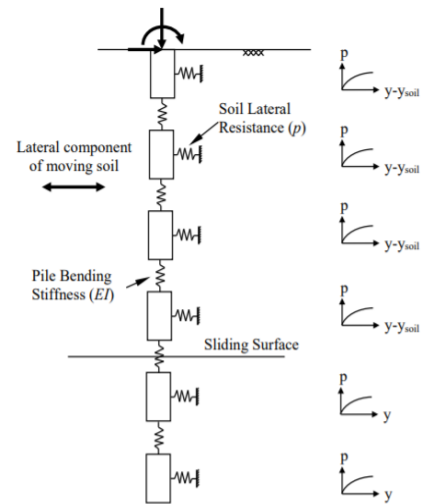


Figure 28 Laterally Loaded Pile Theory (Rocscience, 2018)

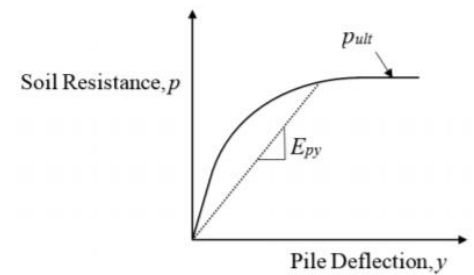


Figure 29 Generic p-y curve defining soil reaction modulus (Rocscience, 2018)

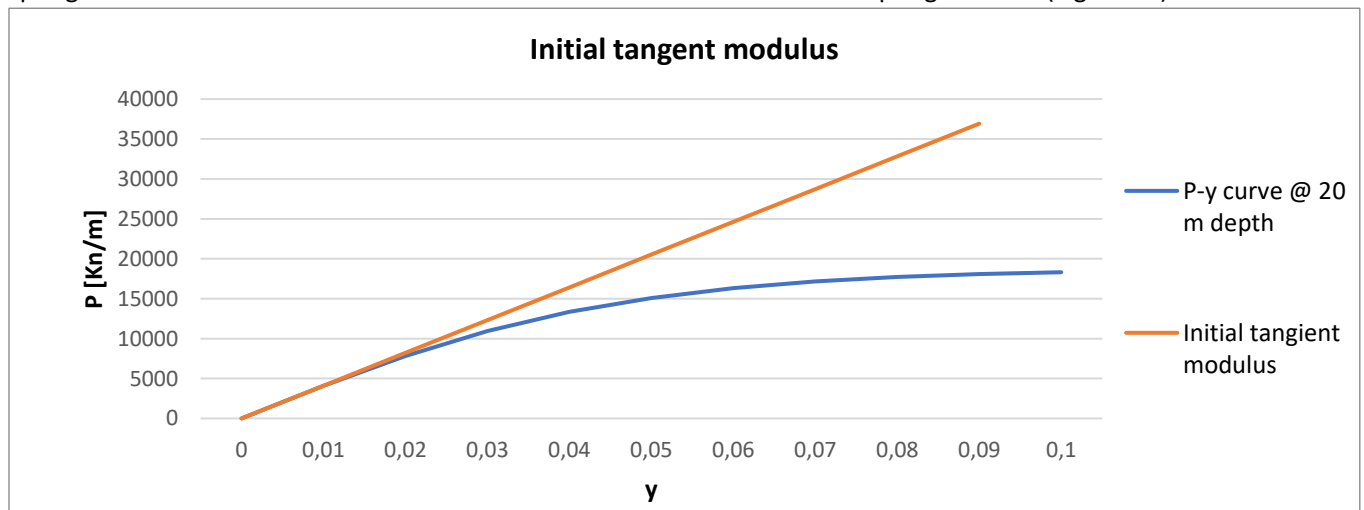


Figure 30 Initial tangent modulus

At 20 meters depth the initial tangent modulus in our case is 410.000 [Kn/m/m]. This is still considering per meter length of a segment of the pile. Since a stiffness per m<sup>2</sup> needs to be obtained the pile 1m diameter pile is considered as a 1m wide plate [Kn/m<sup>2</sup>/m]. In Figure 31, the estimations of the initial tangent modulus per depth is shown.

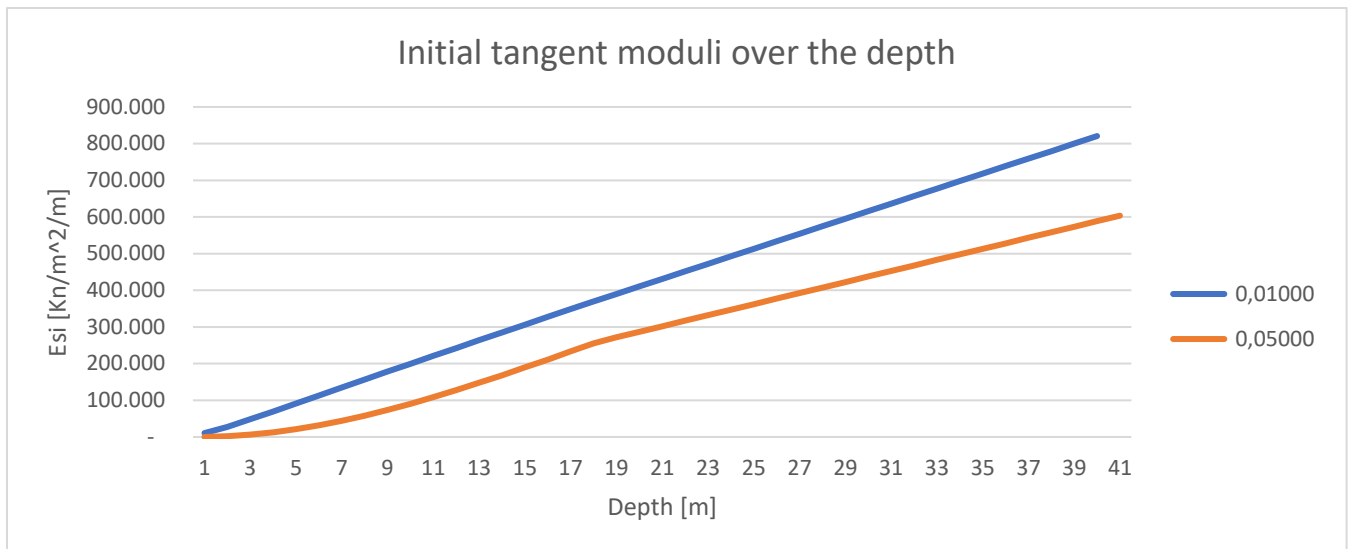


Figure 31 Initial tangent Moduli over the depth

Using these values in the proposed model could be considered inaccurate however this does give a proper first approximation of the spring stiffness over the depth.

DNV also states that *“The nonlinear p-y curves are meant primarily for analysis of piles for evaluation of lateral pile capacity in the ULS. These p-y curves have been calibrated for long slender jacket piles with diameters of up to 1.0 m. They have not been calibrated for monopiles with larger diameters and are in general not valid for such monopiles. P-y curves to be used for monopile design should be validated for such use, e.g. by FE analysis”.*(DNV, 2014)

Since the stiffness of the soil needs to be determined for an 8m diameter pile this statement states that it is probably not accurate for our purpose.

Furthermore a dynamic analysis is considered and the p-y curve is primarily meant for lateral pile capacity in the ULS. DNV stated the following: *“For dynamic analysis of the system of wind turbine, support structure and foundation, realistic stiffness values for the soil support of the foundation structure shall be applied. For example – in the case of pile foundations – p-y curves representative of the true physics of the pile-soil interaction, including realistic initial p-y stiffness, shall be applied. These requirements to realistic representation of stiffness also apply to assessment of the natural frequency of the system of wind turbine, support structure and foundation.* (DNV, 2014)

As a final view on the p-y curve since also liquefaction of the soil can be used to reduce the soil resistance it is interesting to note the p-y curve in liquefied sand. A main difference that can be seen in is that the slope of p-y curves for non-liquefied sand typically decreases with continued deflection, the slope of the back calculated p-y curves for liquefied sand increases with deflection as can be seen in Figure 32. (Rollins, Gerber, Lane, & Ashford, 2005) & (Franke & Rollins, 2013)&(Wang & Reese, 1998)

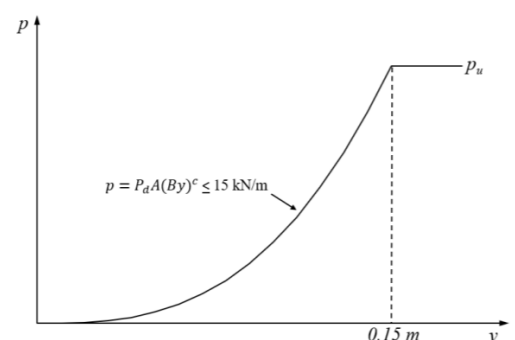


Figure 32 p-y cure for liquefied sand (Rollins et al., 2005)

### 6.2.4.2 Dynamic Soil Stiffness

To account for the fact that the p-y method is not calibrated for “vibrating” larger monopiles, further research has been done to find a fitting method of defining the soil stiffness. In research done by Versteijlen, de Oliveira Barbosa, van Dalen, & Metrikine (2018) a MATLAB model was developed to determine the dynamic soil stiffness and damping for large diameter pile. A modification on this MATLAB model was used to determine the spring stiffness of the soil for this thesis. This model will be referred to as the 1D effective model. It determines the stiffness of soil over the depth per discretization length at the varying requested frequencies.

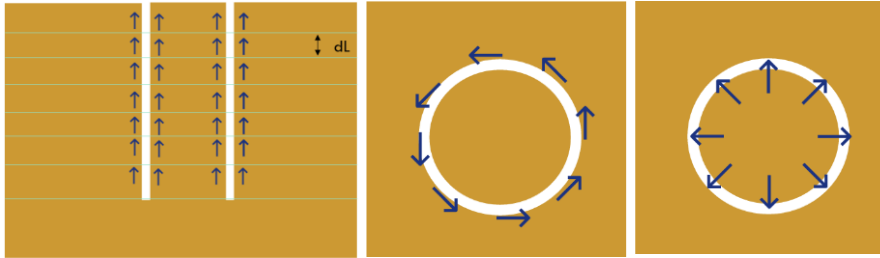


Figure 34 longitudinal, torsional and radial force applied to determine stiffness

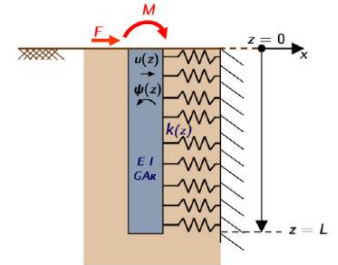


Figure 33 Graphical representation of the local 1d beam model (Versteijlen et al., 2018)

The stiffness is determined for each of the longitudinal, torsional and radial direction (Figure 34). For example, for the radial direction, the stiffness is calculated in the following manner: at each discretization level, the radial displacement at the outer edge and at that specific level induced by an unit radial distributed force applied also at the outer edge and at the same level is computed; the same is done for the inner edge; the inverse of the resulting displacements gives the radial stiffnesses at the outer and inner edges; if the stiffnesses are to be assumed equal at the outer and inner edges, the mean value between the two is considered.

An input for the MATLAB model to determine the soil stiffness is the Shear modulus. To correctly determine the shear modulus, research has been done which can be found in appendix A1. A choice was made to use a discretization length  $dL=0,1$  and shear modulus  $G=90\text{MPa}$  for all depths. The spring stiffnesses were determined for all 3 directions for different frequencies. As a result the stiffnesses varied severely per layer and per frequency, but did fluctuate around a mean value.

The research provided by Versteijlen, de Oliveira Barbosa, van Dalen, & Metrikine (2018) was performed on low frequencies (0,3Hz). It was thought that the accuracy could not be guaranteed for the higher order frequency excitations that are being used in this research. A choice was made to determine the mean value over the depth of the calculated stiffnesses at 0Hz and use this mean value as an input for the model for this research at all depths.

The choice to not implement the different stiffnesses resulting from the different frequencies lies in the fact that it was desired to first determine the results when the stiffness is kept the same at each excitation frequency. It was thought not to be desired to give certain frequencies an advantage or disadvantage due to the implementation of these stiffness values at that frequency. In future research this could however be applied.

In the model used in this thesis the spring stiffness are implemented uniformly over the depth. However, the Effective pressure  $F_{\sigma',h}$  acting on the radial stiffness  $K_r$  does increase with depth in the model. The stiffness values that will be used in the implementation of the model will be considered uniform over the depth:

<b>Radial stiffness;</b>	$k_r = 3,61E+08 \text{ [N/m/m}^2\text{]}$
<b>Transverse stiffness;</b>	$k_z \& K_\theta = 1,31E+08 \text{ [N/m/m}^2\text{]}$

### 6.2.5 Damping

Research shows that in simple models described by Wolf(1995) and Dobry and Gazetas(1986) the damping can be estimated:

$$C_y = \rho * V_s * A$$

$$C_z = \frac{3.4}{\pi(1 - \nu)} \rho * V_s * A$$

For the model the damping per unit area is desired:

$$\frac{c}{A} = \rho * V_s \quad (5)$$

Where A is the contact area with the soil. This was first introduced by Lysmer (1965) as the area of the rigid circular footing. More on this in the appendix A2.

The input parameters considered for this thesis are:

$$\rho = 1930 \frac{kg}{m^3} \text{ (for saturated sand) and } G = 90Mpa ; V_s = \sqrt{\frac{G}{\rho}} = 215,9 \left[ \frac{m}{s} \right]$$

Determination of the G modulus can be found in Appendix A1.

This value is lower compared to the lowest  $\frac{c}{A}$  value from the matlab model which was 1,08E+06. From calculation 5 the following damping values per unit area were determined:

$$\frac{C_y}{A} = 416.773,32$$

$$\frac{C_z}{A} = 751.757,39$$

When applying the damping values in the model and applying the different forcing values determined in 6.3.2 no penetration is recorded. The excitation for this test was at the bottom with the varying forcing amplitudes at 26,66Hz. When multiplying the damping derived from Dobry and Gazetas by a factor 0.1 and performing the runs the pile did penetrate the soil.

Another option to secure penetration would be to increase the Forcing amplitude however this is was not decided here. A more elegant option would be to increase the forcing amplitude, considering the assumption that the fact that exciting the system with a harmonic force amplitude at a magnitude determined statically is wrong. If statically the bearing capacity is reached does not per definition say that this force will also be enough to ensure penetration in a dynamic case as the damping counteracts the motion of penetration. In hindsight implementing a factor of 0.1 for the found damping is not an optimal solution, for now provides us with the necessary values in which penetration occurs. In this research the aim is not to perfectly simulate the soil but to find a relative difference. This is essential for the sensitivity study described in section 7.

Translated to the FEMAP model the naming convention of the parameters from Dobry and Gazetas are:  
 $C_y = C_\theta$  &  $C_z$ ;  $C_z = C_r$

<b>Radial damping;</b>	$C_r$	=75,2E+03 [Ns/m/m <sup>2</sup> ]
<b>Transverse damping;</b>	$C_z$ & $C_\theta$	=41,7+03 [Ns/m/m <sup>2</sup> ]

## 6.2.6 Choices and motivations

Recollection of the soil input values used in the model:

Element	Models	unit	Outside shaft	Inside shaft
$F_{\sigma'_h}$	The horizontal effective force (per surface area)	N /m <sup>2</sup>	7990*z	7990*z
$\mu_z$	frictional resistance to vibratory driving in z	-	0,364	0,364
$\mu_y$	frictional resistance to vibratory driving in y	-	0,364	0,364
K <sub>x</sub>	Soil stiffness in radial direction	N/m /m <sup>2</sup>	3,61E+8	3,61E+8
K <sub>y</sub>	Soil stiffness in transverse direction	N/m /m <sup>2</sup>	1,31E+8	1,31E+8
K <sub>z</sub>	Soil stiffness in transverse direction	N/m /m <sup>2</sup>	1,31E+8	1,31E+8
C <sub>x</sub>	Soil Damping ratio in radial direction	Ns/m /m <sup>2</sup>	7,52E+4	7,52E+4
C <sub>y</sub>	Soil Damping ratio in transverse direction	Ns/m /m <sup>2</sup>	4,17E+4	4,17E+4
C <sub>z</sub>	Soil Damping ratio in transverse direction	Ns/m /m <sup>2</sup>	4,17E+4	4,17E+4

Table 4 Soil Values

For implementation in the FEMAP model these values are all multiplied by the area the node that each node represents:

Node representation:

$$A_{node} = dl * dr = dl * \left( \frac{\pi * D_{pile}}{\#nodes} \right) = 0.8 * \left( \frac{\pi * 8}{36} \right) = 0.559 [m^2]$$

Element	Models	unit	Outside shaft	Inside shaft
$F_{\sigma'_h}$	The horizontal effective force (per surface area)	N /m <sup>2</sup>	4462,5*z	4462,5*z
$\mu_z$	frictional resistance to vibratory driving in z	-	0,364	0,364
$\mu_y$	frictional resistance to vibratory driving in y	-	0,364	0,364
K <sub>x</sub>	Soil stiffness in radial direction	N/m /m <sup>2</sup>	2,02E+8	2,02E+8
K <sub>y</sub>	Soil stiffness in transverse direction	N/m /m <sup>2</sup>	7,32E+7	7,32E+7
K <sub>z</sub>	Soil stiffness in transverse direction	N/m /m <sup>2</sup>	7,32E+7	7,32E+7
C <sub>x</sub>	Soil Damping ratio in radial direction	Ns/m /m <sup>2</sup>	4,20E+4	4,20E+4
C <sub>y</sub>	Soil Damping ratio in transverse direction	Ns/m /m <sup>2</sup>	2,33E+4	2,33E+4
C <sub>z</sub>	Soil Damping ratio in transverse direction	Ns/m /m <sup>2</sup>	2,33E+4	2,33E+4

Table 5 Soil values per node

Recollection of choices and assumptions made:

- Static frictional resistance: conservative approach
- Uniform stiffness and damping over the frequencies: decided to not actively influence the model with assumed varying stiffness and damping which would have an effect on the system.
- Uniform stiffness and damping over depth: first approach, in a future research it could be implemented to run the tests with varying parameters.
- A lower damping value then estimated from literature is implemented to ensure pile penetration. This is essential to be able to make comparisons for this thesis.
- Values for the inside of the shaft assumed to be equal.

### 6.3 Force excitation values

As described in section 5.3 the force that will be applied to the system will be harmonic in different directions with a certain force amplitude (A) and frequency ( $\omega$ ) as described in the following equation .

$$F_{ecc} = A * \sin(\omega t)$$

In this section the determination of the values used in the model are explained

#### 6.3.1 Forcing direction

The directions of interest are longitudinal and torsional and a combination of these two directions with a 90 degree phase shift to simulate the force excitation created by a rotating eccentric mass. The model tests will be performed using a harmonic force in these 3 different directions:

- Longitudinal
- Torsional
- Longitudinal & torsional (with a 90 degree phase shift)

#### 6.3.2 Forcing amplitude

Amplitude is determined by calculating the static resistance from the pile load capacity as determined by Wrana (2016). In this research the static resistance  $R_s$  is determined by multiplying the surface of the pile A by the unit skin resistance  $q_s$ :

$$R_s = A * q_s$$

the unit skin resistance is determined by the horizontal effective pressure and the friction coefficient which were determined in section 6.2.2

$$q_s = \mu * \sigma'_h(z) \text{ (wrana)}$$

By applying these determined values the total resistance is calculated as follows:

$$\sigma'_h(z) = 7990 * z$$

$$A = d * \pi * l ; l = 40; d_{out} = 8 ; d_{in} = 7.84 ; \mu = 0.364$$

$$R_{s(outside)} = \mu * d_{out} * \pi * 7990 * \int_0^{40} z dz$$

$$R_{s(outside)} = \mu * d_{out} * \pi * 7990 * \int_0^{40} z dz = 0.364 * 8 * \pi * 7990 * \left(\frac{1}{2} 40^2 - \frac{1}{2} 0\right)$$

$$R_{s(in)} = \mu * d_{in} * \pi * 7990 * \int_0^{40} z dz = 0.364 * 7.84 * \pi * 7990 * \left(\frac{1}{2} 40^2 - \frac{1}{2} 0\right)$$

$$R_s = R_{s(outside)} + R_{s(inside)} = 115,8 + E6 [N]$$

To ensure the value is more than the pile load capacity it is decided to implement 116N as the harmonic excitation amplitude. This force will be assumed as the medium case value. In the sensitivity analysis the force will be varied -20% and +20% . This forcing amplitude (in longitudinal direction) is considered to be high enough to ensure penetration when not considering damping. As described in section 6.2.5 this method is not considered ideal.

<b>Low case force amplitude;</b>	<b>92,8 [MN]</b>
<b>Medium case force amplitude;</b>	<b>116 [MN]</b>
<b>High case force amplitude;</b>	<b>139,2 [MN]</b>

### 6.3.3 Harmonic force frequency

The harmonic force frequencies are aimed to be on the resonance frequency as determined in FEMAP by performing a modal analysis on the full linear system.

#### 6.3.3.1 Modal analysis:

With the implemented soil values as described in Table 5, a modal analysis was performed in FEMAP. As a result for the longitudinal direction the 1<sup>st</sup> natural frequency with predominantly longitudinal waves was found at 26,6Hz. This will be referred to as the 1<sup>st</sup> natural frequency. In the torsional direction this frequency lies at 17,63Hz.

In the 1<sup>st</sup> longitudinal mode shape as can be seen in Figure 35 there is very little modal displacement at the bottom of the pile. The bottom of the pile also attached to the spring system like the rest of the soil. As the pile does not seem to behave like a rigid body the support given by soil can be considered to be very stiff. Realistically it would be expected to behave more like a rigid body. In Figure 36 the 1<sup>st</sup> symmetric mode of the pile without the soil system is shown. When these values are calculated using the wave equation approximately the same value was determined.

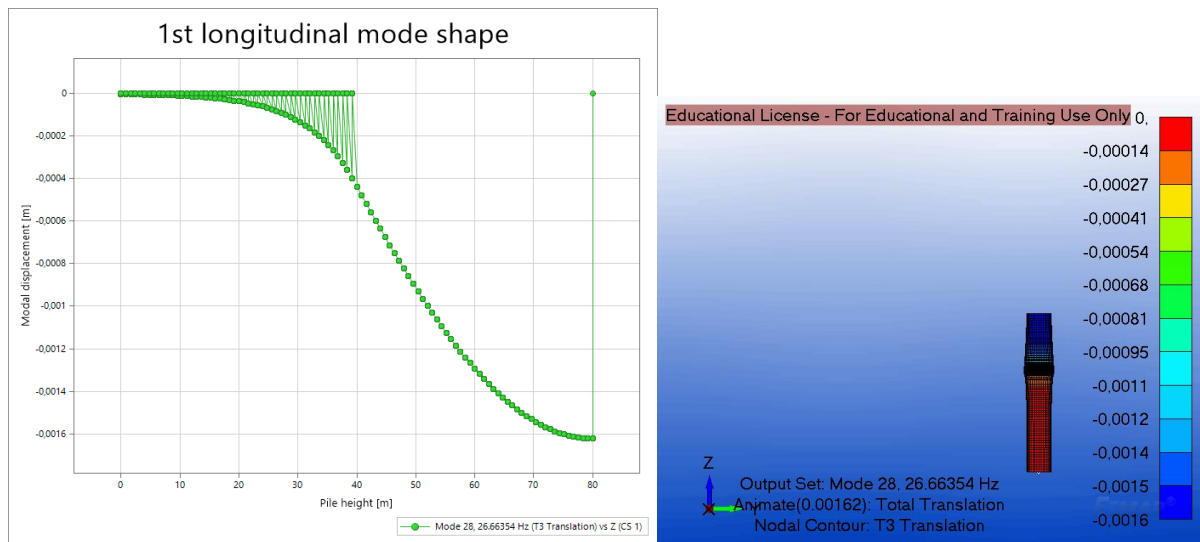


Figure 35 first longitudinal mode shape in soil system

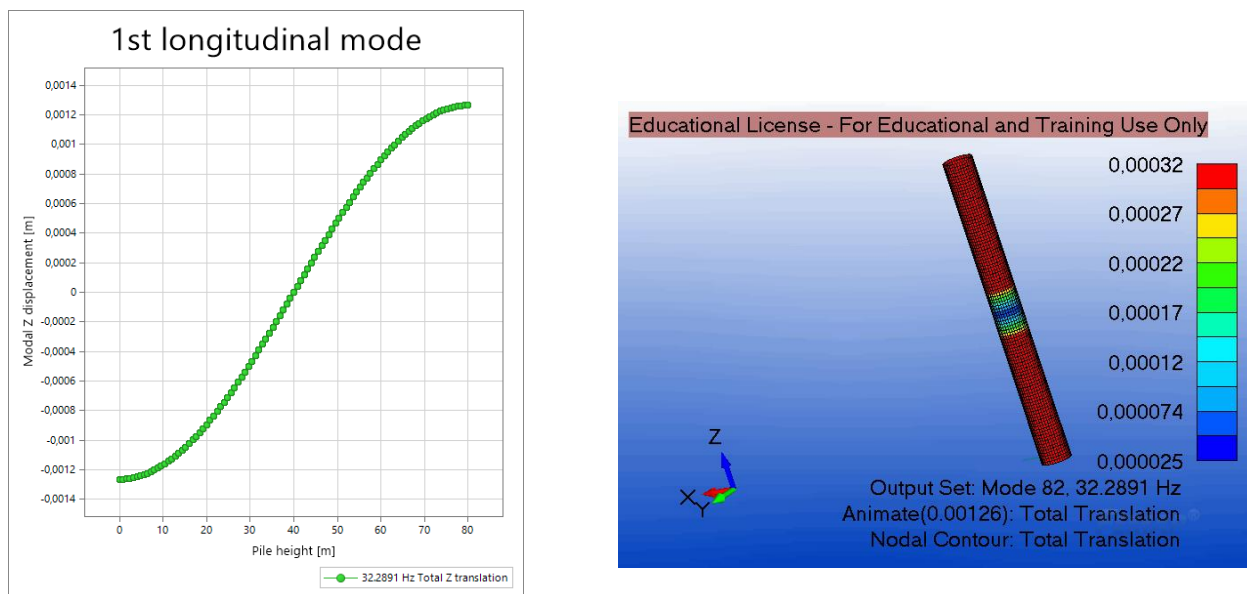


Figure 36 first longitudinal (symmetric) mode shape in vacuum

The 1<sup>st</sup> Torsional mode shape as can be seen in Figure 37 also has is very little modal displacement at the bottom of the pile. In Figure 38 the 1<sup>st</sup> symmetric mode of the pile without the soil system is shown.

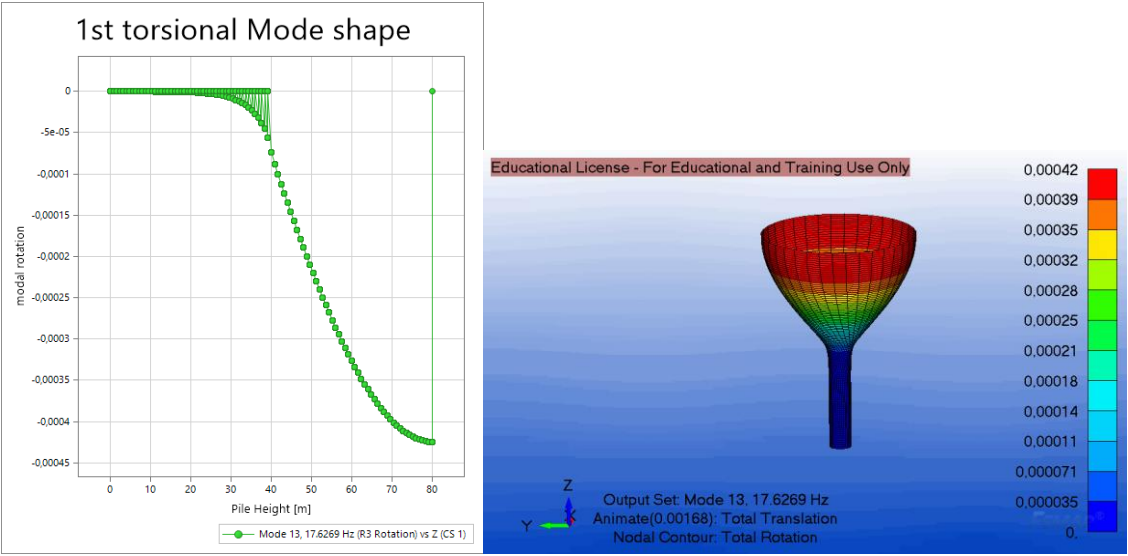


Figure 37 First torsional mode shape in soil system

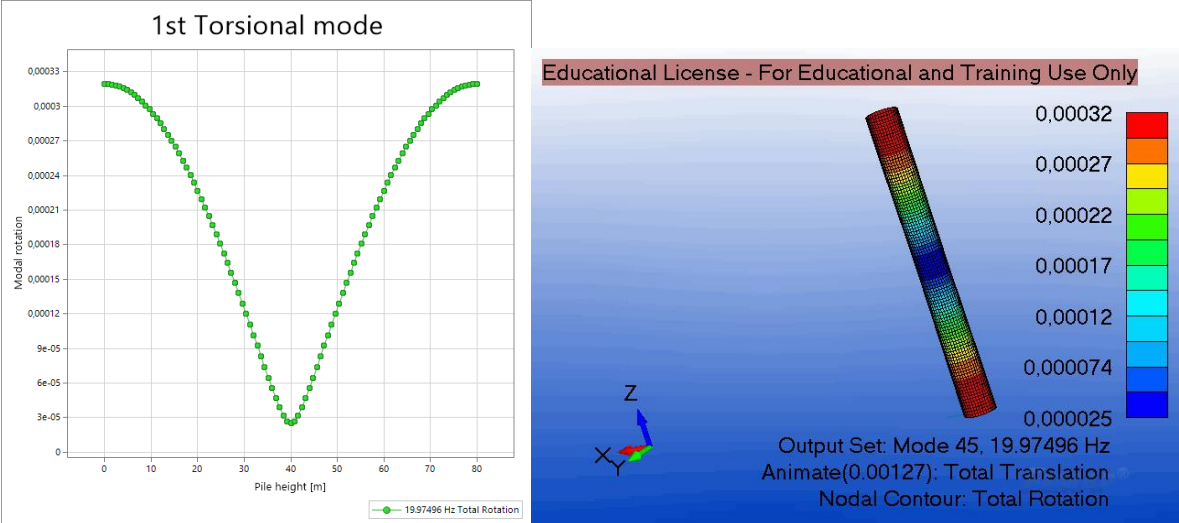


Figure 38 First torsional mode shape in vacuum

	Longitudinal	Torsional
Pile-soil	26.6 Hz	17.6 Hz
Pile only	32.3 Hz	20 Hz

Table 6 modal analysis results

A decision was made to use 24Hz, 26.66Hz and 29.33Hz as the first frequencies to simulate in the model. For the torsional direction 15.8, 17.6 Hz and 24Hz are determined for the initial simulations.

### 6.3.4 Chosen values

The choice was made to continue with the initially set parameters for which the values are described in Table 7. It must be noted that the force amplitude used at the defined frequencies are higher compared to the largest existing vibratory hammers.

Force Direction (z; $\Theta$ ;z& $\Theta$ )	z	$\Theta$	z& $\Theta$
Force Amplitude A (static friction +0% ;+20% +40%) [MN]	92,8	116	139.2
Force Frequency $\omega$ Modal analysis from model (in soil) (-50% ; 0 ;+50%) longitudinal	24Hz	26,66Hz	29.33Hz
Force Frequency $\omega$ torsional	15,8Hz	17,63Hz	24Hz

Table 7 Various force value input values

## 7 Model application & results

The purpose of the model is to simulate the penetration behavior at a certain depth when exciting it in various manners. The model must be able to determine the penetration displacement from where the penetration speed will be derived. The purpose is to determine the contribution to the penetration speed of the different excitations.

As described in previous sections the model consist of a pile partly embedded in a soil. This model was developed in FEMAP software, the exact implementation of the FEMAP elements can be found in appendix A4: Using FEMAP. The parameters for this system were determined from literature and the system will be excited by a harmonic force in the different force amplitudes, frequencies, directions and locations to determine their influence to the penetration speed in the model. The soils system parameters are kept the same throughout all tests.

### 7.1 Hypotheses

For the different harmonic force applications, hypotheses are made to predict what is expected to happen. The hypotheses and the force input variation values are described here: the results for these cases are described in the rest of his chapter.

#### Amplitude

- 1) Increasing the amplitude of the harmonic force at the bottom with a certain factor will result in an increase of penetration speed with a lower factor

#### Direction:

- 2a) torsional excitation will have an increased the penetration speed compared to longitudinal.
- 2b) longitudinal and torsional direction will have an increased penetration speed compared to longitudinal or torsional

#### Frequency;

Compared to off resonance frequencies an increase in penetration speed will occur when exciting the system at;

- 3a) The natural frequencies which are related to predominantly longitudinal vibrations
- 3b) The natural frequencies which are related to predominantly torsional vibrations

#### Excitation location:

- 4) Harmonically exciting the system in longitudinal and torsional direction at the bottom of the pile will increase the penetration speed compared to the exciting from the top.

In Table 8, the input values are summarized. The values that are kept equal in this test are represented by a black x and the values that are varied are represented by a red R1 (Run1), R2 and R3. I.e., for the amplitude sensitivity test, the values that are varied are 92,8MN, 116MN and 139MN while the rest is kept the same In this case the different runs (R1,R2,R3) are all excited in longitudinal direction at 26.66Hz from the bottom.

Sensitivity test:	Force amplitude			Direction			Frequency					Location	
	92.8MN	116MN	139MN	Torsional	Longitudinal	Combined	15.8Hz	17.63Hz	24Hz	26.66Hz	29.33Hz	Top	Bottom
1: Amplitude	R1	R2	R3		x					x			x
2a: Direction		x		R1	R2				x				x
2b: Direction		x		R1	R2	R3			x				x
3a:Frequency		x			x				R1	R2	R3		x
3b:Frequency		x		x			R1	R2	R3				x
4: Location		x			x				x			R1	R2

Table 8 input variations per hypotheses while keeping the rest the same

## 7.2 Approach & Results

For every test simulation performed with the input parameters described in Table 8 the displacement of the bottom node of the pile was calculated and represented in a graph as an output. In these graphs the displacement of a bottom node of the pile is displayed over time. To each displacement graph a trendline was added to show the averaged displacement of penetration. From this line the penetration speed was determined. The different penetration speeds are compared with the other penetration speeds in that set.

### 7.2.1 Force amplitude sensitivity

#### Hypotheses:

1) Increasing the amplitude of the harmonic force at the bottom with a certain factor will result in an increase of penetration speed with a lower factor

#### Approach:

Harmonically excite the system from the bottom at 26.66Hz with 92.8MN , 116MN and 139MN

Sensitivity test:	Force amplitude			Direction			Frequency					Location	
	92.8MN	116MN	139MN	Torsional	Longitudinal	Combined	15.8Hz	17.63Hz	24Hz	26.66Hz	29.33Hz	Top	Bottom
1: Amplitude	R1	R2	R3		x					x			x

Table 9 Force amplitude sensitivity input parameters

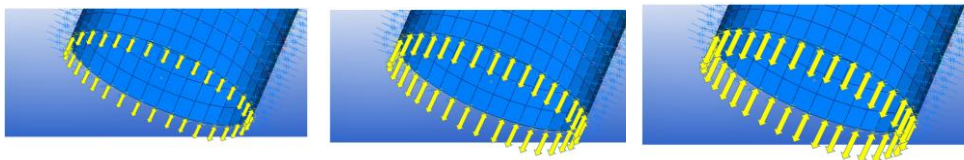


Figure 39 Visualization of the different force amplitudes

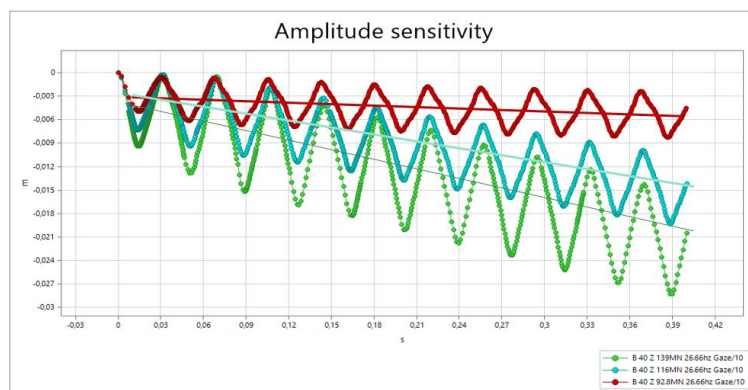


Figure 41 Amplitude sensitivity, node displacement

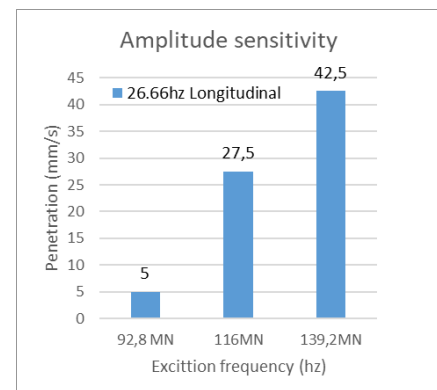


Figure 40 Amplitude sensitivity results

#### Result:

As can be seen in Figure 41 & Figure 40, the penetration speed increases with an increase in force amplitude. This is to be expected as the force is simply higher resulting in larger displacements per cycle.

The triangular motion of the displacement was not expected. Although it does not perfectly overlap with the applied sinusoidal force, this motion is thought to be acceptable for the nonlinear situation. In further simulations, especially at higher amplitudes, this phenomenon is less seen.

## 7.2.2 Excitation direction sensitivity

### Hypotheses:

2a) torsional excitation will have an increased penetration speed compared to longitudinal.

### Approach:

Harmonically excite the system from the bottom at a given frequency and force amplitude in the longitudinal and torsional direction.

Sensitivity test:	Force amplitude			Direction			Frequency					Location	
	92.8MN	116MN	139MN	Torsional	Longitudinal	Combined	15.8Hz	17.63Hz	24Hz	26.66Hz	29.33Hz	Top	Bottom
2a: Direction		x		R1	R2				x				x

Table 10 Excitation direction sensitivity input parameters

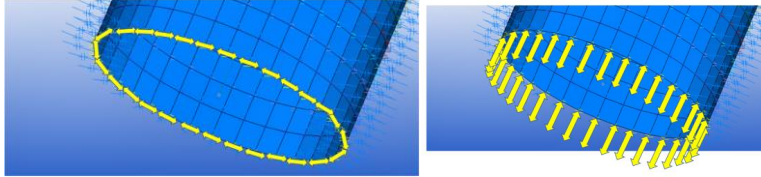


Figure 42 Visualization of the different excitation directions

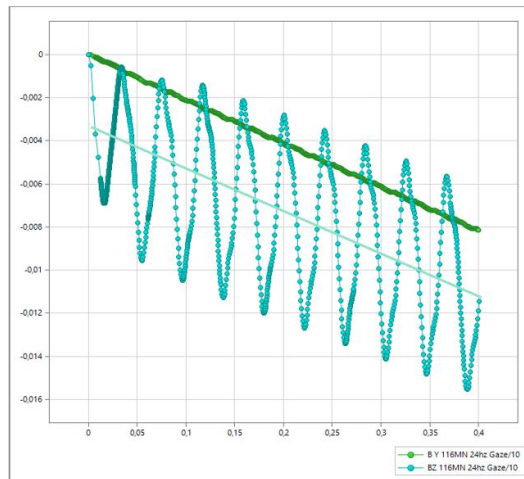


Figure 44 excitation direction sensitivity node displacement

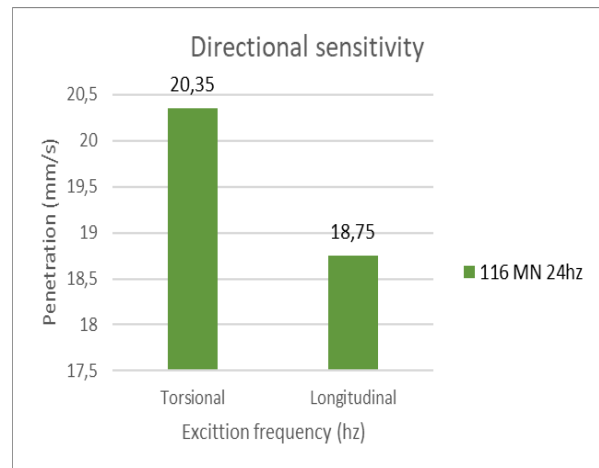


Figure 43 excitation direction sensitivity results graph

### Result:

As can be seen in Figure 44 & Figure 43, exciting in the Torsional direction resulted in a (slightly) higher penetration speed. This is to be expected as the force is simply higher resulting in larger displacements per cycle.

A possible explanation could be that the mode shapes at the bottom can be more dominant in the torsional direction compared to the longitudinal direction. Based on observation the motion is more abrupt in the longitudinal motion and when exciting in torsional direction the penetration in the result is more smooth.

**Hypotheses:**

2b) longitudinal and torsional direction will have an increased penetration speed compared to longitudinal or torsional.

**Approach:**

Harmonically excite the system from the bottom at a given frequency and force amplitude in the longitudinal, torsional and a combination of the two directions with a 90 degree phase shift.

Sensitivity test:	Force amplitude			Direction			Frequency					Location	
	92.8MN	116MN	139MN	Torsional	Longitudinal	Combined	15.8Hz	17.63Hz	24Hz	26.66Hz	29.33Hz	Top	Bottom
2b: Direction		x		R1	R2	R3			x				x

Table 11 Excitation direction sensitivity input parameters 2b

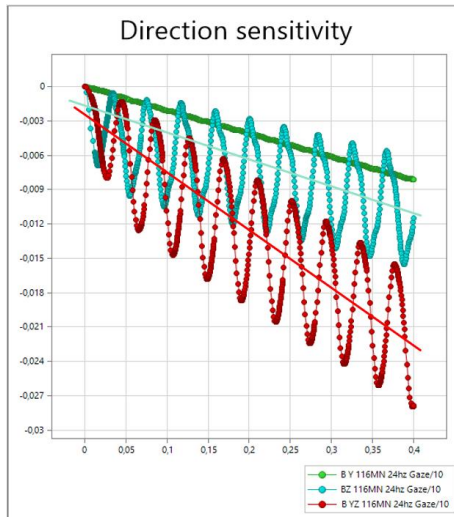


Figure 46 Excitation direction sensitivity, displacement (2b)

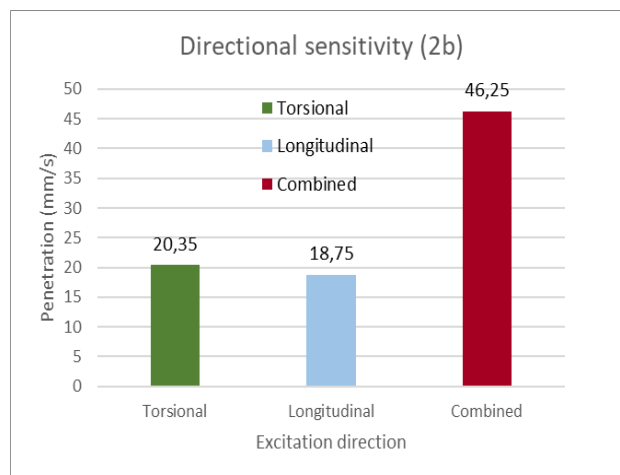


Figure 45 Excitation direction results

Node

**Result:**

As can be seen in Figure 46 & Figure 45 the combined excitation penetration has a faster penetration speed than torsional. In this current case it is more than double of either the torsional or the longitudinal excitation.

### 7.2.3 Frequency sensitivity

#### Hypotheses:

Compared to off resonance frequencies an increase in penetration speed will occur when exciting the system at;

3a) the natural frequencies which are related to predominantly longitudinal vibrations

3b) the natural frequencies which are related to predominantly torsional vibrations

#### Approach:

Harmonically excite the system from the bottom at varying frequencies at a given harmonic force amplitude in the longitudinal direction (3a) & torsional direction (3b)

Sensitivity test:	Force amplitude			Direction			Frequency					Location	
	92.8MN	116MN	139MN	Torsional	Longitudinal	Combined	15.8Hz	17.63Hz	24Hz	26.66Hz	29.33Hz	Top	Bottom
3a:Frequency		x			x				R1	R2	R3		x
3b:Frequency		x		x			R1	R2	R3				x

Table 12 Frequency sensitivity input parameters

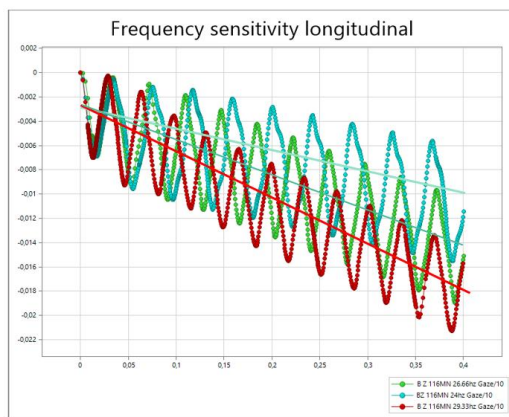


Figure 48 Frequency sensitivity (3a) node displacement

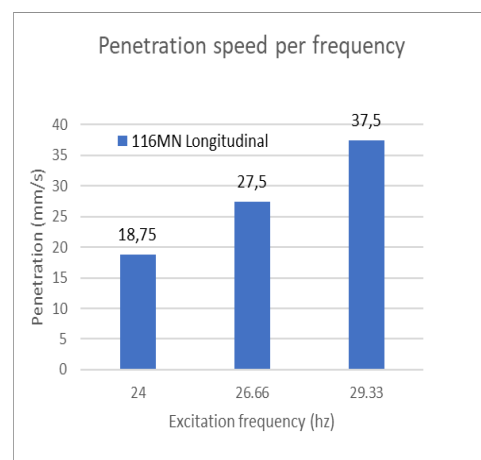


Figure 47 Frequency sensitivity (3a) results

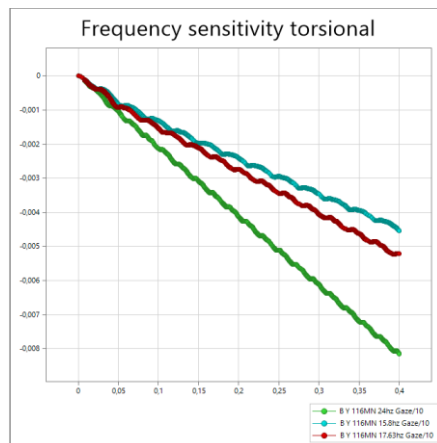


Figure 50 Frequency sensitivity (3b) node displacement

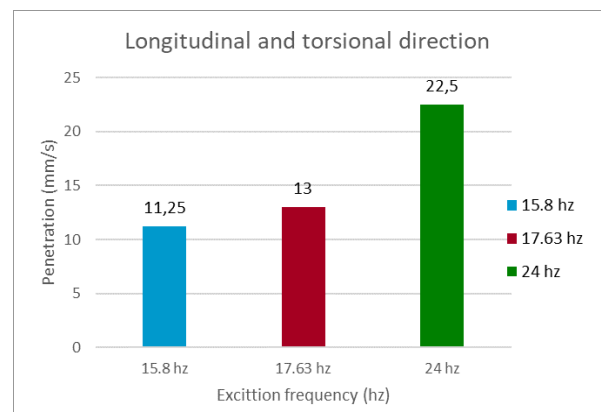


Figure 49 Frequency sensitivity (3b) results

#### Result:

As can be seen in Figure 48 & Figure 47, for the longitudinal direction a higher frequency has a faster penetration. This result was not expected. This observation was also made for the torsional direction as can be seen in Figure 50 & Figure 49. It would be expected that exciting the system in the frequency equal to the 1<sup>st</sup> natural frequency with predominantly longitudinal waves would have a higher penetration speed. Possible explanation is that the natural frequency was not accurately determined. Another thing to note is that for this test it can be said that a low variation in frequencies was applied. A follow up study has been performed in section 7.3 where a larger variation of frequencies was tested.

## 7.2.4 Excitation location sensitivity

### Hypotheses:

4) Harmonically exciting the system in longitudinal and torsional direction at the bottom of the pile will increase the penetration speed compared to the exciting from the top.

### Approach:

Harmonically excite the system from the bottom at varying frequencies at a given harmonic force amplitude in the longitudinal direction (3a) & torsional direction (3b)

Sensitivity test:	Force amplitude			Direction			Frequency					Location	
	92.8MN	116MN	139MN	Torsional	Longitudinal	Combined	15.8Hz	17.63Hz	24Hz	26.66Hz	29.33Hz	Top	Bottom
4: Location		x			x				x			R1	R2

Table 13 Location sensitivity input parameters

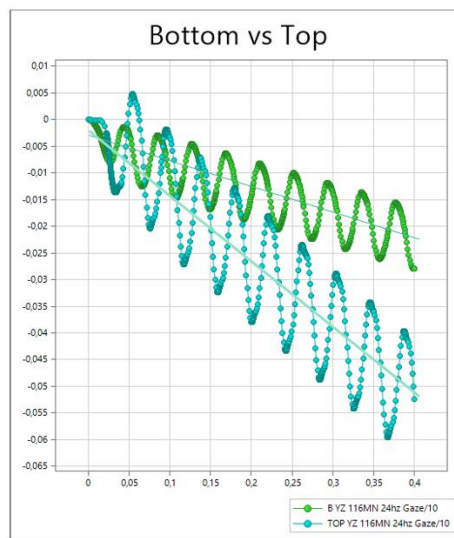


Figure 52 Location sensitivity node displacement

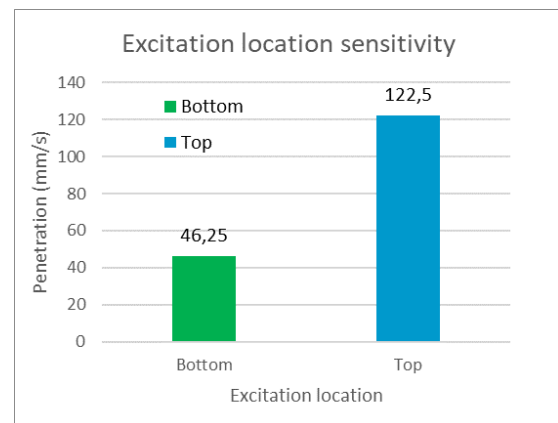


Figure 51 Location sensitivity results

### Result:

As can be seen in Figure 52 & Figure 51, exciting the system from the top results in a higher penetration speed compared to exciting from the bottom. A possible explanation is the fact that it is not optimal to add energy in a system where the system is constraint the most.

### 7.3 Frequency sensitivity 2.0

Due to the fact that in test 1 an increase in penetration speed was found instead of a maximum penetration speed at the natural frequency further research is done. For the modelled system it is expected that there is a frequency where the system is in resonance and that at this frequency the penetration speed would be higher compared to other neighboring (off resonance) frequencies.

The modal analysis performed in FEMAP determines the modes in the linear situation without sliding. To perform a broader analysis a sweep was performed to find the reactions to the system at different frequencies by simply performing the simulations. For the sweep of the longitudinal excitation scenario, simulation were performed for different frequencies up to 160 Hz. For the higher frequencies the time increment for the simulation was decreased so that there would always be at least 8 time steps per cycle.

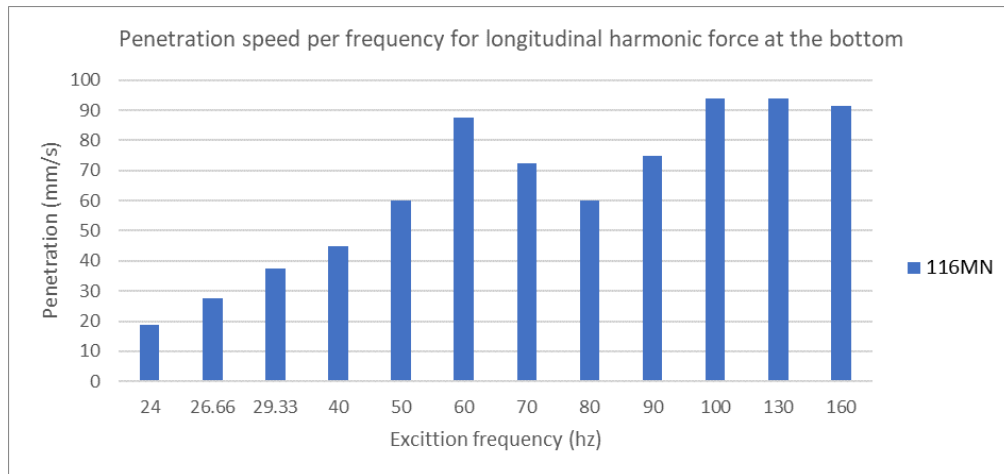


Figure 53 Penetration speed per frequency for longitudinal excitation

#### Results for frequency sensitivity with a longitudinal excitation (up to 160Hz):

In Figure 53 a clear “peak” can be observed at 60 Hz. This observation is different from the modal analysis. As described in the modal analysis the sliding was not taken into account. Therefore, a possible explanation for the observations is that this difference in expected effective frequency is due to the contribution of the sliding. This identified peak could be dependent to the force amplitude. A more extensive sweep was performed in longitudinal direction where the same sweep was performed with different force amplitudes. The results for this sweep are shown in Figure 54.

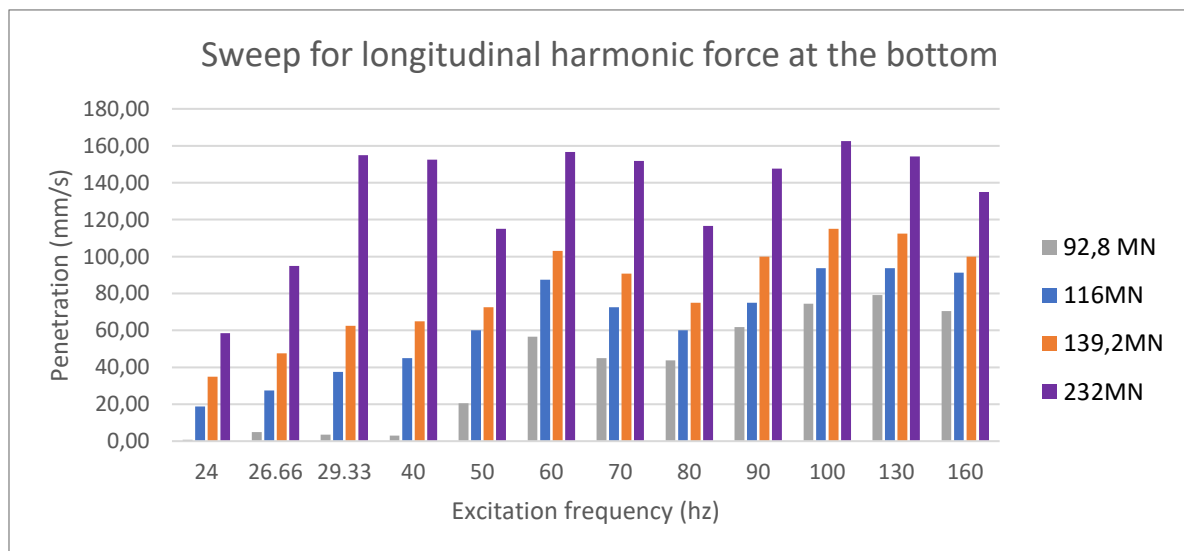


Figure 54 Sweep for longitudinal harmonic force at the bottom

From the results shown in figure Figure 54 the observation is made that for this model for an amplitude up to 139,2 MN the first peak in penetration speed is found at 60Hz. However when the harmonic force amplitude applied at the bottom of the pile is increased to 232MN a shift is seen. With a doubling of the force amplitude a shift in the first optimal frequency can be observed.

**Results frequency sensitivity for torsional excitation (up to 80Hz):**

Also for torsional excitation a sweep (up to 80Hz) was performed. In Figure 55 the results of this sweep can be observed.

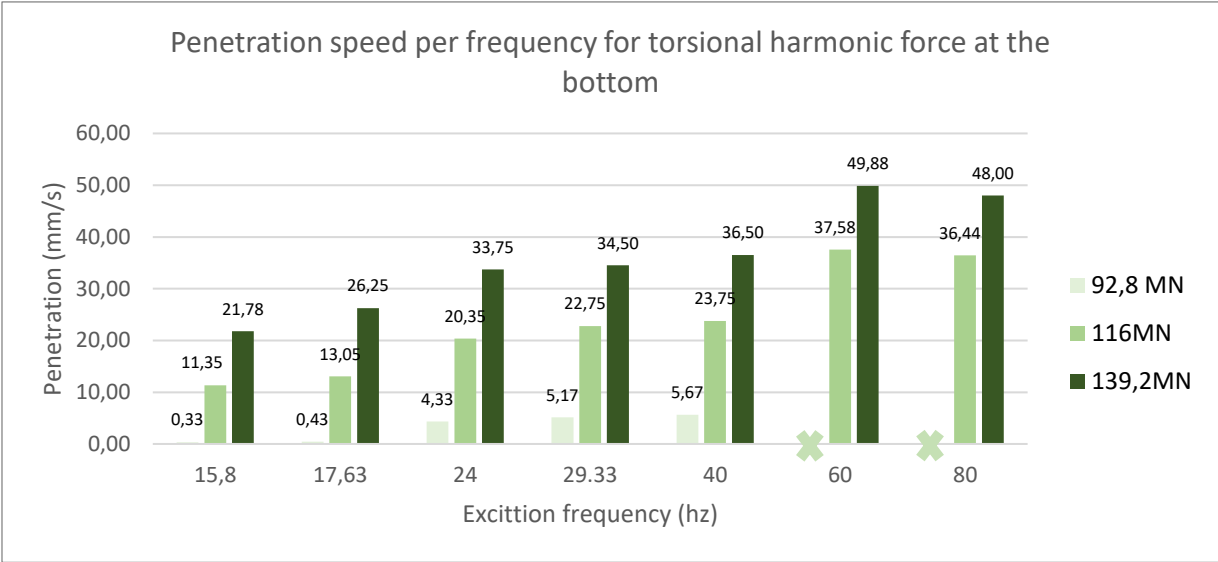


Figure 55 Sweep for torsional harmonic force at the bottom

Although less obvious than for the longitudinal sweep, like in the longitudinal case, a peak at 60Hz is observed.

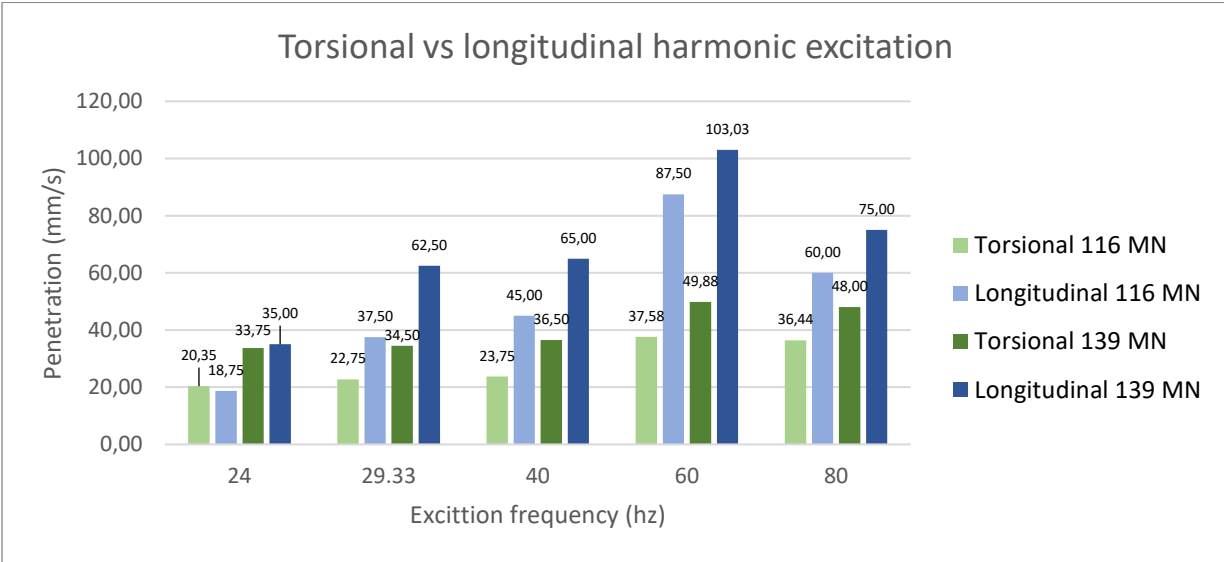


Figure 56 Torsional vs Longitudinal harmonic excitation

When comparing the increase in penetration speed between the longitudinal and torsional situation in Figure 56, it can be observed that the longitudinal has a higher increase in penetration speed when increasing the excitation frequency to 60Hz.

## 7.4 Analysis of the motion

### 7.4.1 Visualization of slip displacement vs node displacement

To display the motion of the node in comparison to the sliding displacement in Figure 57 these two are compared. Since the node can displace before sliding occurs it is observed that the node displacement “leads” the sliding displacement. Considering that there is a relatively high stiffness implemented, the slider follows the node almost perfectly.

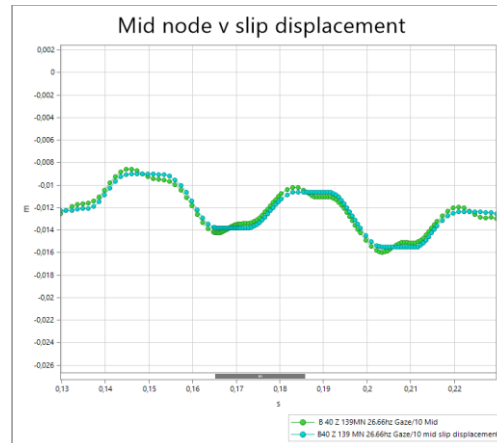


Figure 57 middle node, nodal displacement vs sliding displacement

### 7.4.2 Depth dependent node displacement

To better understand the motion of the pile an analysis was performed on the displacement of nodes at different height of the pile during penetration.

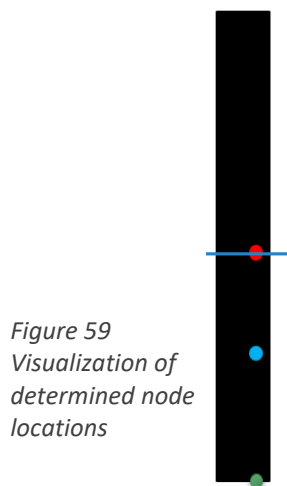


Figure 59  
Visualization of  
determined node  
locations

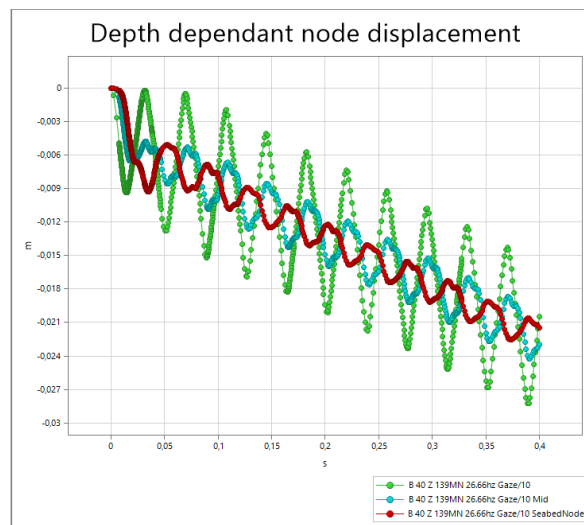


Figure 58 Depth dependent node displacement

In the case that was analyzed the pile is excited longitudinally from the bottom. In Figure 58 & Figure 59 it is observed that at the bottom the node displacement is much higher than the nodes in the middle and at the seabed. This seems logical since this is where the force excitation is located. It is also observed that the different node displacements are not in phase. This is considered to be due to the elasticity of the pile. The displacement and phase per node vary over depth therefore the pile does not seem to behave like a rigid body. This was also observed in the modal analysis.



## 8 Conclusions

---

The aim of this thesis is to determine the factors of influence on the shaft resistance and their relative contribution to the penetration performance for monopile installation using the Vibrodrill. This is done by identifying factors of influence with respect to forcing and identifying relative differences in the influence on the penetration speed by performing various tests on a developed pile-soil model.

### **Factors of influence**

Factors of influence were determined for the vibratory pile installation. They can be categorized into 3 categories, the pile, the soil and the force. For the pile the factor of influence consist of the material properties, geometry and dimensions of the pile. For the soil there are many factors that can influence the penetration performance in vibratory driving of a pile. For instance the frictional reduction due to fluidization and liquefactions are still to be further investigated. The main focus for this thesis is on the factors of influence of the forced excitation. The factors of influence on a harmonic excitation are; force amplitude, frequency, direction and excitation location.

### **Existing models**

Existing models were researched to determine if an existing model could contribute to the aim of this thesis on gaining insight on pile penetration by exciting it in various manners. The penetration models should be capable to describe the penetration performance of the pile when exciting the system at the bottom with the varying harmonic excitations in longitudinal and torsional direction on a flexible pile. From this study it is concluded that, currently, no available models with these specifications were found.

### **Developed model**

For this thesis a new penetration model was developed. The purpose of this model is to describe the penetration speed at different harmonic force parameters. The developed model is based on finite elements by using the FEMAP software. This model consists of a simple pile-soil interaction system, which is not yet validated with test data. More realistic models would be more complex and include more calculation time or have test data to validate it.

The soil structure interaction elements are uncoupled and composed of a gap element with an elastic perfectly plastic sliding component in the directions parallel to the pile axis. Also damping elements are applied in all 3 directions of the cylindrical coordinate system. The parameters, related to the soil structure interaction that are attached to a node on the pile, do not change as the pile moves downward. The sliding displacement is calculated with constant parameters for a pile embedded into 40m of soil. In this way a calculation could be performed without much calculation time, determining the penetration speed at an embedded depth of 40m or any other depth.

The model was not validated as no real life tests have been performed since the method is still in development. No conclusions on accuracy of the model can be made. From the different test results relative differences can be found.

## Penetration speed results

Results show that the model is able to describe the penetration speed at a certain depth as reasonably expected. The results fairly match the hypotheses that were made. The exact values of the results are due to the properties implemented into the system for this specific case. To the results no definite conclusions can be taken on penetration speed in a real-life environment as no validation with test is performed. A conclusion can be made in the fact that sensitivities were found for the excitation input parameters of the model. From the observations it can be stated that there is a sensitivity in harmonic force amplitude, as an increase in force amplitude resulted in an increase of penetration speed. The penetration speed in this model is amplitude dependent.

From the varying result in the frequency sensitivity analysis it can be concluded that the penetration speed is also frequency dependent. In the simulations an interesting observation occurs at 60Hz. In the case where a total harmonic force amplitude up to 139,2 MN was applied at the bottom, an increase in penetration speed was observed when increasing the excitation frequency up to 60Hz. At 60Hz a peak is observed, and increasing the frequency up to 60 Hz, the penetration speed reduces. At 60z the penetration is evidently higher than the neighboring frequencies. At an increased force amplitude of 232MN a first peak was found at 29.33Hz instead of at 60Hz. From this it can be concluded the optimum frequency is amplitude dependent.

The exact values described here are considering the specific set of values for this case representing the soils and pile. It must be noted that the harmonic excitation for which the highest penetration speed can be achieved is highly dependent on the medium which surrounds the pile. The sensitivity of the soil parameters on penetration speed was not examined in this thesis. The excitation input parameters to achieve this "optimal" penetration are interdependent as a change in amplitude changes the first optimal frequency to excite the system in. For each amplitude there is a possibly different optimum frequency.

The resulting penetration speeds, due to varying the direction of the harmonic force excitation, is dependent on frequency and amplitude. From the observations the excitation in longitudinal direction results in a higher increase in penetration speed when the excitation frequency is increased compared to exciting the system in torsional direction. From the observations a higher penetration speed was observed when exciting the system from the top instead of at the bottom for the specific case examined.

From analyzing the displacement of the nodes at different embedment depths when exciting the system, it was found that the displacement and phase per node vary over depth. It can be concluded that, when excited, the pile does not behave like a rigid body. This flexible motion is also seen in the modal analysis. From these results it can be stated that it matters how the system is excited and that an optimum can be found. The system is amplitude-, frequency, direction and location dependent.

## 9 Recommendations

---

With this research a step is taken towards understanding the penetration behavior of a flexible pile when exciting harmonically at the bottom. This research provides a first step towards understanding of the Vibro-drill system performance. For future research recommendations have been made.

### **Coupled soil system**

One important recommendation is to improve the soil reaction in the model to a coupled soil system. In the model now the different elements representing the soil are uncoupled. If the model would be desired to be more realistic to the behavior of soil the implementation of coupling the soils elements is recommended.

### **Depth dependent spring stiffness**

In this research a uniform spring stiffness over the depth was assumed to represent the soil stiffness as described in section 6.2.4.2. It is recommended to increase the stiffness over the depth to obtain a more realistically accurate model.

### **Increased resistance during penetration**

Currently the model can only determine the penetration speed at a given depth. Since the parameters representing the soil do not change when penetrating the pile. The pile will penetrate with a certain speed and motion without taking the increased depth into account. To be able to determine a refusal depth it is recommended to implement an increasing horizontal effective pressure during penetration. If a depth dependent spring stiffness is implemented this should also be dependent to the penetration displacement in the model.

### **Damping value**

For this thesis the damping value that was determined from research was decreased by a factor of 10 to ensure penetration. This method of changing inner parameters of the system to ensure penetration is not advised. It is recommended to perform the analysis with leaving the damping values found from literature unchanged.

### **Dynamic friction**

In the current model the frictional resistance of the slider element is constant. The element is linearly elastic perfectly plastic. In this case the dynamic friction is equal to the (critical) static friction. However, when conforming more to reality, the dynamic friction is lower than the static friction. Since the dynamic friction is lower, the results from the analysis are expected to be different from what was determined in this thesis.

### **Test result analysis**

From the results of this thesis more analysis can be performed. To increase the resolution of the sweep analysis more tests should be performed with a smaller step in frequency. The energy dissipation due to the sliding and dampers can be calculated. In the analysis performed, the efficiency is determined by penetration speed. The efficiency for penetration per cycle should also be determined as well as the total implemented energy vs penetration speed.

### **Field tests**

Field tests need to be performed to better understand the soil-effects of vibratory driving large diameter piles and to validate the model. For validation purposes it is recommended to perform these tests at a test location with homogeneous soil since in the model a homogeneous soil is assumed. CPT tests should be performed to determine the soil conditions. The friction along the shaft should be measured while penetrating the pile under different circumstances. To gain more insight in the friction fatigue of penetrating a large diameter pile in a fluidized soil. The friction measurements should be at both the inside and the outside of the pile. In the current model no decrease in resistance due to liquefaction is implemented. Research should be performed on a (frequency dependent) decrease in resistance due to liquefaction of large diameter piles.

For the validation of the model the motion of the pile at different locations along the length of the pile should be measured. Also the rotational velocity of the eccentric rotating masses should be measured to determine the total harmonic force they excite. For the guidance of the pile the upward force should be measured to determine the total downward facing force.

# Bibliography

---

- Allnamics Pile Testing Experts. (2019). Allnamics.
- B Arntz. (2018). *Developing the Vibro-drill; A feasibility study into an improved installation method for offshore foundation piles.*
- Barman, U. (2019). *Soil texture classification using multi class support vector machine.*
- Berghe, J. F. van den. (2001). *Sand Strength Degradation within the Framework of Vibratory Pile Driving.*, PhD thesis presented to the Faculty of Applied Science, Université catholique de Louvain., Belgium.
- Berghe, J. F. van den, & Holeyman, A. (1997). *Comparison of two models to evaluate the behaviour of a vibratory driven sheet pile.*, Submitted to the XIth Young Geotechnical Engineers Conference., *Geotechnical Engineers and Computers.*, September 24 - 27, 1997, Madrid, Spain, pp. 60 - 72.
- BNEF. (2017). *2H 2017 Offshore Wind Market Outlook.* Retrieved from <https://about.bnef.com/blog/global-offshore-wind-market-set-to-grow-sixfold-by-2030/>
- Brennan, A. J. (2005). Evaluation of Shear Modulus and Damping in Dynamic Centrifuge Tests. *Journal of Geotechnical and Geoenvironmental Engineering*, 131(December), 987–1003. [https://doi.org/10.1061/\(ASCE\)1090-0241\(2005\)131](https://doi.org/10.1061/(ASCE)1090-0241(2005)131)
- Dierssen, G. (1994). *Ein bodenmechanisches Modell zur Beschreibung des Vibrations- rammens in körnigen Böden.*, Doctoral Thesis, University of Karlsruhe, GERMANY.
- DNV. (2014). *Offshore standard DNV-OS-J101, Design of offshore wind turbine structures.*
- Edward P. Heerema. (1979). *Relationsihp between wall friction, displacement velocity and horizontal stress in clay and in sand, for pile driveability analysis.*
- Ekanayake, S. D., Liyanapathirana, D. S., & Leo, C. J. (2013). Influence zone around a closed-ended pile during vibratory driving. *Soil Dynamics and Earthquake Engineering*, 53, 26–36. <https://doi.org/10.1016/j.soildyn.2013.06.005>
- Franke, K. W., & Rollins, K. M. (2013). *Simplified Hybrid p-y Spring Model for Liquefied Soils.* *Journal of Geotechnical and Geoenvironmental Engineering*, ASCE, Vol. 139, No. 4, pp. 564-576.
- Gazetas, G., & Dobry, R. (1984). *Simple radiation damping model for piles and footings.*
- Grabe, M. &. (2006). *Numerical prediction of settlements and vibrations due to vibratory pile driving using a continuum model.* *Proceedings of TRANSVIB 2006, Paris 21-22 September*, pp. 243-252.
- Harpoth, M. H. (2017). *Development of driveability model for piles for offshore wind turbines.*
- Henke, S., & Grabe, J. (2006). Simulation of pile driving by 3-dimensional Finite-Element analysis. *Proc. of the 17th EYGEC.--Zagreb*, (August 2016), 215–233.
- Henke, S., & Grabe, J. (2007). *Simulation of pile installation by three- dimensional Finite Element analyses.* *Darmstadt Geotechnics*, No. 15, Ed.: Prof. Dr.-Ing. Rolf Katzenbach. pp. 179-192.
- Henke, S., & Grabe, J. (2009). Numerical modeling of pile installation. *Proceedings of the 17th International Conference on Soil Mechanics and Geotechnical Engineering: The Academia and Practice of Geotechnical Engineering*, 2, 1321–1324. <https://doi.org/10.3233/978-1-60750-031-5-1321>
- Henke, S., & Hügel, H. M. (2007). *Räumliche Analysen zur quasi-statischen und dynamischen Penetration von Bauteilen in den Untergrund. Tagungsband zur 19. Deutsche Abaqus-Benutzerkonferenz in Baden-Baden. Artikel 2.13.*
- Holeyman & Legrand. (1994). Soil modelling for pile vibratory driving. *Int. Conf. on Design and Construction of Deep Foundation, Orlando*, Pp. 1165-1178.
- Holeyman, A. (1993). *HYPERVIB1, An analytical model-based computer program to evaluate the penetration speed of vibratory driven sheet piles.*, Research report prepared for BBRI, June -93, 23 pp.

- Holeyman, A. (1996). *A method to predict the driveability of vibratory driven piles.*, Proc. of 5th Int. Conf. On the application of Stress-Wave theory to piles., September 11-13, Orlando FL., pp. 1101-1112.
- Holeyman, A. (2000). KEynote lecture: vibratory driving analysis. In Balkema (Ed.), *Application of Stress-wave Theory to piles.*
- Johnson, R. M., Parsons, R. L., Dapp, S. D., & Brown, D. A. (2006). *Soil Characterization and p-y Curve Development for Loess,* Kansas Department of Transportation, Bureau of Materials and Research, July.
- Jonker, G. (1987). *Vibratory Pile Driving Hammers for Oile Installation and Soil Improvement Projects.*, Proc. of Nineteenth Annual Offshore Technology Conf., Dallas, Texas, OTC 5422, pp. 549-560.
- Kastelein, R. A. (2014). *Effect pile driving on porpoise hearing.* (September), 1–17.
- Lenart, S. (2008). The response of saturated soils to a dynamic load. *Acta Geotechnica Slovenica*, 5(1), 37–49.
- Lo, K. F., Ni, S. H., Huang, Y. H., & Lehmann, L. (2012). Free field vibrations due to pile driving using a coupled fem with SBFEM method. *Journal of GeoEngineering*, 7(2), 69–73.  
[https://doi.org/10.6310/jog.2012.7\(2\).4](https://doi.org/10.6310/jog.2012.7(2).4)
- Lysmer, J. (1965). Vertical motion of rigid footing. *Universtity of Michigan.*
- Masoumi, H. R., & Degrande, G. (2008). Numerical modeling of free field vibrations due to pile driving using a dynamic soil-structure interaction formulation. *Journal of Computational and Applied Mathematics*, 215(2), 503–511. <https://doi.org/10.1016/j.cam.2006.03.051>
- Massarch, K. R. (2002). Effects of Vibratory Compaction. . . *TransVib 2002 – Intl. Conf. on Vibratory Pile Driving and Deep Soil Compaction.* Louvain-La-Neuve. Keynote Lecture, 2002, Pp. 33–42.
- Massarsch, K. R., Fellenius, B. H., & Bodare, A. (2017). Fundamentals of the vibratory driving of piles and sheet piles. *Geotechnik*, 40(2), 126–141. <https://doi.org/10.1002/gete.201600018>
- MSC Nastran. (2012). *MSC Nastran 2012 Dynamic Analysis Users Guide.*
- Muni Budhu. (2015). *Soil Mechanics Fundamentals Budhu.* Retrieved from <https://www.mathalino.com/reviewer/geotechnical-engineering/unit-weights-and-densities-soil>
- Nastran, M. (2012). *MSC Nastran 2012 Dynamic Analysis User's Guide.*
- Nikishkov, G. P. (2004). INTRODUCTION TO THE FINITE ELEMENT METHOD. *University of Aizu, Aizu-Wakamatsu 965-8580.*, <https://doi.org/10.7142/igakutoshokan.55.211>
- Noorany. (1985). SIDE FRICTION OF PILES IN CALCAREOUS SANDS. *THE ELEVENTH INTERNATIONAL CONFERENCE ON SOIL MECHANICS AND FOUNDATION ENGINEERING, SAN FRANCISCO.*
- OECD, & IEA. (2018). *Global Energy & CO2 Status Report 2017.* (March), 1–14. Retrieved from <https://www.iea.org/geco/%0Ahttps://www.iea.org/publications/freepublications/publication/GECO2017.pdf>
- Powrie, W. (1997). *Soil mechanics, concepts and application.*
- Prof. John Atkinson. (2019). GeotechniCAL. Retrieved from UWE University of the west of england Bristol website: <http://environment.uwe.ac.uk/geocal/SoilMech/stresses/stresses.htm>
- Qi, L. (2006). Grounding Performance Analysis of the Substation Grounding Grids by Finite Element Method in Frequency Domain. *IEEE Transactions on Magnetics.*
- Ramshaw, C. (2000). Computation of ground waves due to piling. i: Application of stress-wave theroy to piles. *Rotterdam: Niyama & Neim (Eds) Balkema, Pp. 495-502. Richart,*.
- Randolph, M. F., Dolwin, J., & Beck, R. (1994). Design of driven piles in sand. *Geotechnique*, 44(3), 427–448.  
<https://doi.org/10.1680/geot.1994.44.3.427>
- Rocscience. (2018). *Laterally Loaded Piles.*
- Rodger, A. A., & Littlejohn, G. (1980). *A study of vibratory driving in granular soils.*, *Geotechnique*, Vol. 30, No. 3, pp. 269-293.
- Rollins, K. M., Gerber, T. M., Lane, J. D., & Ashford, S. A. (2005). Lateral resistance of a full-scale pile group in

- liquefied sand. *Journal of Geotechnical and Geoenvironmental Engineering*, 131(1), 115–125.  
[https://doi.org/10.1061/\(ASCE\)1090-0241\(2005\)131:1\(115\)](https://doi.org/10.1061/(ASCE)1090-0241(2005)131:1(115))
- Schmid, W. E. (1969). *Driving resistance and bearing capacity of vibro-driven model piles*. (American Society of Testing and Materials, ASTM STP 444, pp. 362–375).
- Shahraini, V. (2019). Soil dilatation.
- SMITH, E. A. L. (1960). *Pile-driving analysis by the wave equation.*, *Journal of the Soil Mechanics and Foundations Divisions, ASCE, Vol. 86, August*.
- Spagnoli, G. (2014). *Theoretical Evaluations of Liquefaction*. (September 2008).
- Subramanian, N. (2016). *Design of Steel Structures*. Retrieved from  
<https://www.scribd.com/document/83249264/Appc-Soil-Properties-718>
- T. W. Lambe & R.W. Whitman. (1969). *Soil Mechanics*. New York: John Wiley & Sons,.
- tpub. (2002). Coastal Engineering Manual. Retrieved from coastalengineeringmanual website:  
[http://coastalengineeringmanual.tpub.com/Part\\_III-Chap\\_1/Part\\_III-Chap\\_10034.htm](http://coastalengineeringmanual.tpub.com/Part_III-Chap_1/Part_III-Chap_10034.htm)
- V. Adams and A. Askenazi. (1999). Building Better Products with Finite Element Analysis. In *OnWord Press, Santa Fe*,.
- Vanden Berghe, J. F., & Holeyman, A. (2014). *Comparison of impact versus vibratory driven piles : with a focus on soil - structure interaction*. 76.
- Verruijt, A. (1987). *Soil Dynamics and*. 8544. <https://doi.org/10.1016/B978-0-444-98958-1.50002-9>
- Versteijlen, W. G., de Oliveira Barbosa, J. M., van Dalen, K. N., & Metrikine, A. V. (2018). Dynamic soil stiffness for foundation piles: Capturing 3D continuum effects in an effective, non-local 1D model. *International Journal of Solids and Structures*, 134, 272–282. <https://doi.org/10.1016/j.ijsolstr.2017.11.007>
- Viking, K. (2002). Vibro-Drivability. *Department of Civil and Architectural Engineering Stockholm, Sweden*, (May).
- Wang, S. T., & Reese, L. C. (1998). *Design of Piles Foundations in Liquefied Soils. Geotechnical and Earthquake Engineering and Soil Dynamics III, Geotechnical Special Publication No. 75, ASCE, pp. 1331-1343*.
- Warrington. (1989). *Drivability Of Piles By Vibration*.
- Wrana, B. (2016). Pile Load Capacity – Calculation Methods. *Studia Geotechnica et Mechanica*, 37(4), 83–93.  
<https://doi.org/10.1515/sgem-2015-0048>
- Youn, J.-U., Choo, Y.-W., & Kim, D.-S. (2008). Measurement of small-strain shear modulus G max of dry and saturated sands by bender element, resonant column, and torsional shear tests . *Canadian Geotechnical Journal*, 45(10), 1426–1438. <https://doi.org/10.1139/t08-069>
- Zheng., Y.-P. H. and Y.-P. (2015). *Measurement of Soft Tissue Elasticity in Vivo: Techniques and Applications. CRC Press*,.

## ii. List of Figures

Figure 1 Vibrodrill concept .....	8
Figure 2 Functions of the Vibrodrill system .....	10
<i>Figure 3 New improved mechanics of the vibrodrill system</i> .....	12
Figure 5 Soil in motion.....	17
Figure 6 outward movement of soil.....	17
Figure 7 movement of the pile.....	17
Figure 8 Soil Mechanics: Concepts and Applications (Powrie, 1997).....	18
Figure 9 Dilatation(Shahraini, 2019) .....	18
<i>Figure 10 changes in the soil skeleton caused by cyclic loading results in excess pore-water pressure</i> .....	18
Figure 11 difference in waves (Zheng., 2015) .....	19
Figure 12 USCS fine grained soils (ASTM D-2487-98).....	20
Figure 13 USCS Course grained soils (ASTM D-2487-98).....	20
Figure 14 USDA Classification system (Barman, 2019) .....	20
Figure 15 soil classification in particle size.....	21
Figure 15 Values of the empirical factors of shaft resistance(Viking, 2002) .....	23
Figure 16 Values of soil resistance (After Warrington 1989) .....	24
Figure 18 Discription of principle behind the modified one dimensional model (gardner, 1987).....	27
Figure 19 axisymmetric model for pile jacking (Ekanayake et al. 2013) .....	30
Figure 20 Model of the pile without soil .....	32
Figure 21 Pile in soil with depth dependent force and soil stiffness.....	32
Figure 21 Schematic view of the proposed model.....	33
Figure 22 Visualization of applied axial and torsional forcing at the bottom of the pile.....	34
Figure 24 CGAP element (linear elastic perfect plastic) (MSC Nastran, 2012).....	34
Figure 25 Variation of skin friction (Randolph & Beck 1994) .....	37
Figure 26 Pore water pressure (Prof. John Atkinson, 2019) .....	38
Figure 27 effective pressure (Prof. John Atkinson, 2019) .....	38
Figure 27 Driving unit resistance reduction .....	39
Figure 29 Laterally Loaded Pile Theory (Rocscience, 2018) .....	40
Figure 30 Generic p-y curve defining soil reaction modulus (Rocscience, 2018).....	40
Figure 30 Initial tangent modulus .....	40
Figure 31 Initial tangent Moduli over the depth.....	41
Figure 32 p-y cure for liquefied sand (Rollins et al., 2005).....	41
Figure 34 Graphical representation of the local 1d beam model (Versteijlen et al., 2018).....	42
Figure 34 longitudinal, torsional and radial force applied to determine stiffness.....	42
Figure 35 first longitudinal mode shape in soil system.....	46
Figure 36 first longitudinal (symmetric) mode shape in vacuum.....	46
Figure 37 First torsional mode shape in soil system .....	47
Figure 38 First torsional mode shape in vacuum .....	47
Figure 40 Visualization of the different force amplitudes.....	50
Figure 40 Amplitude sensitivity results .....	50
Figure 41 Amplitude sensitivity, node displacement .....	50
Figure 42 Visualization of the different excitation directions.....	51
Figure 43 excitation direction sensitivity results graph .....	51
Figure 44 excitation direction sensitivity node displacement.....	51
Figure 45 Excitation direction results.....	52
Figure 46 Excitation direction sensitivity, Node displacement (2b).....	52
Figure 47 Frequency sensitivity (3a) results.....	53

Figure 48 Frequency sensitivity (3a) node displacement.....	53
Figure 49 Frequency sensitivity (3b) results.....	53
Figure 50 Frequency sensitivity (3b) node displacement.....	53
Figure 51 Location sensitivity results .....	54
Figure 52 Location sensitivity node displacement .....	54
Figure 53 Penetration speed per frequency for longitudinal excitation .....	55
Figure 54 Sweep for longitudinal harmonic force at the bottom .....	55
Figure 55 Sweep for torsional harmonic force at the bottom .....	56
Figure 56 Torsional vs Longitudinal harmonic excitation.....	56
Figure 58 middle node, nodal displacement vs sliding displacement.....	57
Figure 59 Depth dependent node displacement .....	57
Figure 60 Visualization of determined node locations.....	57
Figure 60 Gmax vs Effective stress researches.....	69
Figure 61 Gmax per effective pressure ( Yoon, choo & kim 2008).....	70
Figure 62 horizontal effective stress over the depth .....	70
Figure 63 Initial aim of graduation chart.....	81
Figure 64 Initial plate model in FEMAP .....	83
Figure 65 Harmonic force scaled and plotted over the nodal displacement showing the sawtooth motion .....	85

### iii. List of Tables

---

Table 1 factors of influence summarized (non-accounted factors of influence on friction between soil and steel : Surface Roughness, Rate of deformation (Suba Rao)) .....	21
Table 2 Model element description .....	33
Table 3 Soil elements .....	37
Table 4 Soil Values.....	44
Table 5 Soil values per node.....	44
Table 6 modal analysis results.....	47
Table 7 Various force value input values .....	48
Table 8 input variations per hypotheses while keeping the rest the same .....	49
Table 9 Force amplitude sensitivity input parameters.....	50
Table 10 Excitation direction sensitivity input parameters.....	51
Table 11 Excitation direction sensitivity input parameters 2b.....	52
Table 12 Frequency sensitivity input parameters .....	53
Table 13 Location sensitivity input parameters .....	54
Table 14 1st natural frequency comparison in different methods .....	83

## iv. List of Definitions

---

*Liquefaction* = Loss of soil strength by and stiffness due to increased pore water pressure in response to an applied stress in example caused by earthquake vibrations.

*Fluidization* = soil converted to a fluid dynamic state due to the upward flow of additional fluid (or gas) through the soil.

*Vibro-driving* = Installation due to inducing vibrations at the top of the (sheet) pile

Vibro-drilling= Installation due to inducing vibrations at the bottom of the (sheet) pile

*Jetting* = process of using jets of liquid under high pressure to create a guided bore through soils

*Penetration* = downward movement of the pile relative to the soil

*Longitudinal resonance frequency*: “The natural frequencies which are related to predominantly longitudinal vibrations.”

*Off-resonance frequency*: a frequency that does not coincide with the natural frequencies of the dynamics system. Dynamic magnification compared to static response is close to 1 (<1.1)

Optimal penetration = highest penetration speed determined by the model

CPT = cone penetration test

SSI = Soil structure interaction

FEM = Finite Element Method

DEM = Discrete element method

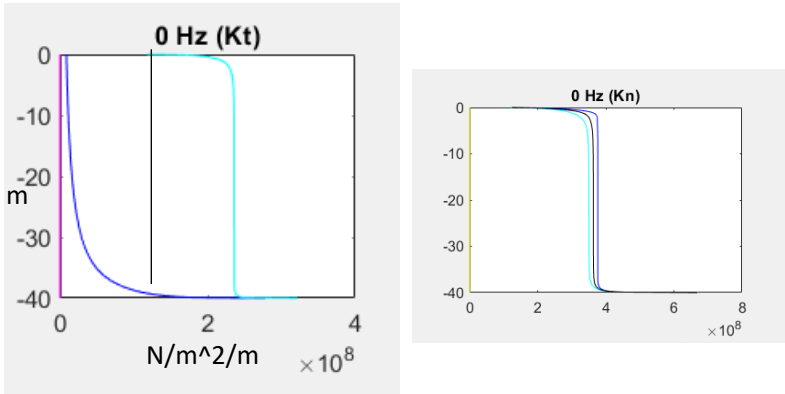
PPV = peak particle velocity

Slip displacement = sliding displacement

# Appendices

## A1: Implementation of the 1D effective model

The model was tested at different discretization lengths. A discretization length of 0,1 was decided for the further research. With a discretization length of 0,1 at 0Hz the stiffness was constant at 361MN/M<sup>2</sup>/m, which could be acceptable in terms of size.



An input for the MATLAB model to determine the soil stiffness is the Shear modulus. To correctly determine the shear modulus research has been done.

Different researches show close correlations when it comes to the shear modulus. Also note that the shear modulus can change with increasing effective stress acting upon the soil. Research shows the following relation between effective stress and Shear modulus Gmax:

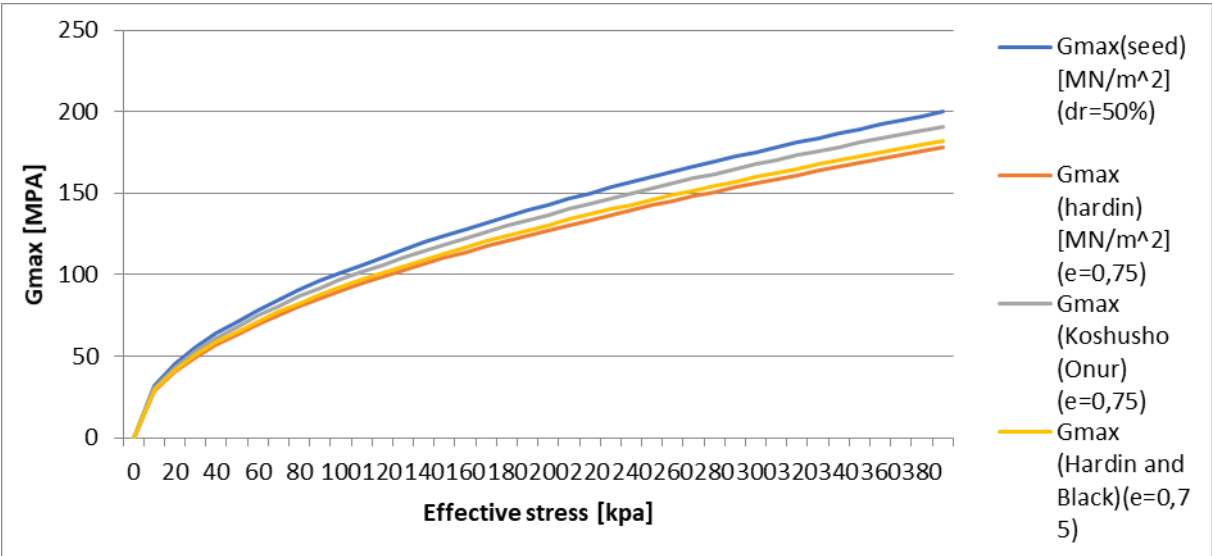


Figure 60 Gmax vs Effective stress researches

Separate Research done by Youn on the Small strain shear modulus shows the following graph in saturated sand: (Youn, Choo, & Kim, 2008)

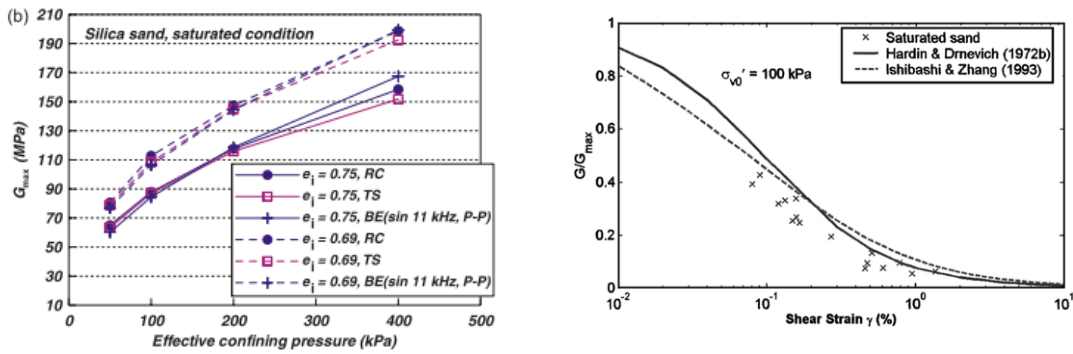


Figure 61  $G_{max}$  per effective pressure (Yoon, choo & kim 2008)

As described in previous chapters, the pressure increases over the depth. Since in the matlab model only one shear modulus  $G$  can be implemented a choice must be made. For this research a shear modulus of 90MPa was decided for. Since the small strain stiffness needs to be determined the  $G_{max}$  is considered as the shear modulus. A  $G_{max}$  of 90MPa is at about 100 Kpa effective pressure as can be seen in figure 56 and 57 . 100 Kpa is about 12 m depth In our case as can be seen in figure 57.

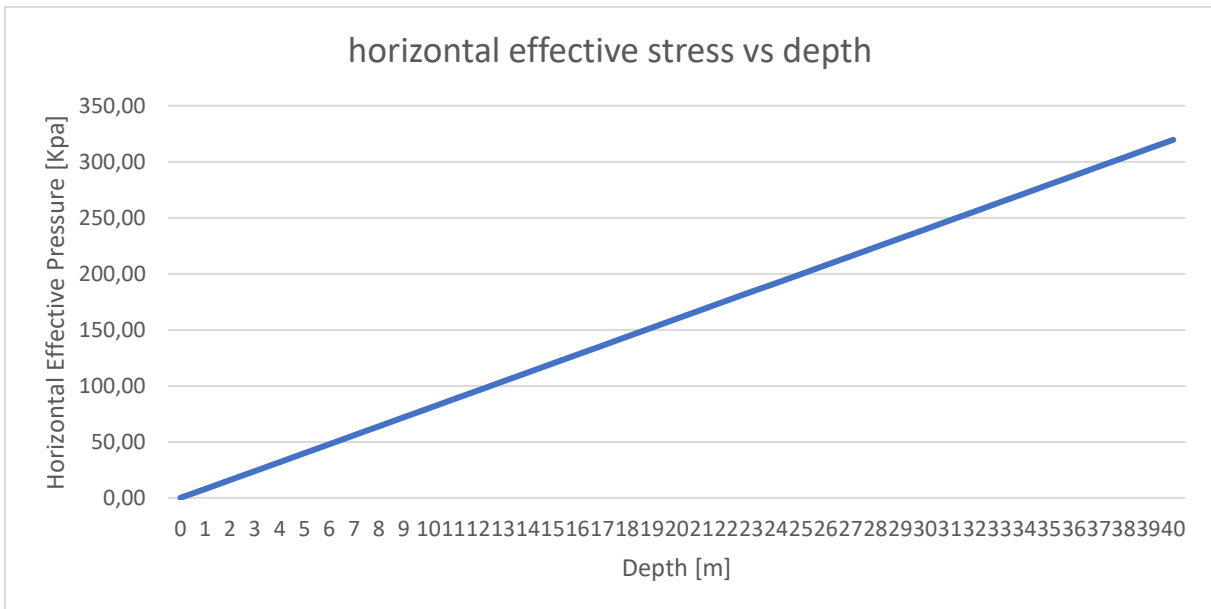


Figure 62 horizontal effective stress over the depth

Effectively the soil stiffness as it would be estimated at 12 meters depth is used for all depths along the pile.

On the Matlab model run with G=90MPa of dl=0,1 0,2 and 0,8: Plots are also included as figures).

**dl= 0,1 run:**

The following parameters were used the matlab program

```
L = 40;           % Embedment depth
dL = 0.1;        % Disretization size
R = 4;           % Inner radius of pile
Thick = 0.08;    % Thickness of pile wall
H = inf;         % Thickness of layer
G = 9e7;         % Shear modulus of soil
Pois = 0.40;     % Poisson's ratio of soil
Rho = 1930;     % Density of soil
Damp = 0.01;    % Material damping of soil
Freq = 0:10:100; % Frequency range (Hz)
```

Per frequency I Calculated the average (of inner and outer together)stiffness K, Damping value C and  $\alpha =$

$$\frac{C}{K} = \frac{Im}{K} \text{ ( in Versteijlen } \alpha = 2,08 * 10^{-2} \text{ )}$$

dl=0,1 KN	Frequency	alpha	Mean K	Mean C
	0	NaN	3,61E+08	-
	10	0,01430	3,34E+08	4,77E+06
	20	0,01248	3,50E+08	4,37E+06
	30	0,01312	3,74E+08	4,91E+06
	40	0,00896	4,04E+08	3,62E+06
	50	0,01069	3,96E+08	4,24E+06
	60	0,00804	4,48E+08	3,60E+06
	70	0,00689	4,61E+08	3,18E+06
	80	0,00613	4,73E+08	2,90E+06
	90	0,00546	4,87E+08	2,66E+06
	100	0,00492	4,93E+08	2,43E+06
	Mean	9,10E-03	4,22E+08	3,67E+06

dl=0,1 Kt	Frequency	alpha	Mean K	Mean C
	0	NaN	1,31E+08	-
	10	0,07828	1,18E+08	9,27E+06
	20	0,03002	1,67E+08	5,01E+06
	30	0,01064	2,15E+08	2,29E+06
	40	0,00669	2,26E+08	1,51E+06
	50	0,00939	2,38E+08	2,23E+06
	60	0,00636	2,50E+08	1,59E+06
	70	0,00486	2,39E+08	1,16E+06
	80	0,00586	2,60E+08	1,52E+06
	90	0,00454	2,68E+08	1,22E+06
	100	0,00483	2,32E+08	1,12E+06
	Mean	1,61E-02	2,21E+08	2,69E+06

dl=0,1 Kv	Frequency	alpha	Mean K	Mean C
	0	NaN	1,83E+08	-
	10	0,03843	2,80E+08	1,08E+06
	20	0,01180	4,02E+08	4,74E+06
	30	0,01033	3,28E+08	3,39E+06
	40	0,01108	4,27E+08	4,73E+06
	50	0,00675	4,47E+08	3,02E+06
	60	0,00803	3,50E+08	2,81E+06
	70	0,00682	4,80E+08	3,28E+06
	80	0,00482	4,74E+08	2,29E+06
	90	0,00750	4,16E+08	3,12E+06
	100	0,00495	5,10E+08	2,52E+06
	Mean	1,11E-02	4,11E+08	3,10E+06

For 0 Hz the mean of the Kt/ Mean of Kn = **0.3616**

(KtValues(1,3)/KnValues(1,3)) = **0.3616**

this value could be expected since:

$$G = \frac{E}{2(1 + \nu)} \rightarrow \nu = 0,4 \rightarrow G = 0,357 * E$$

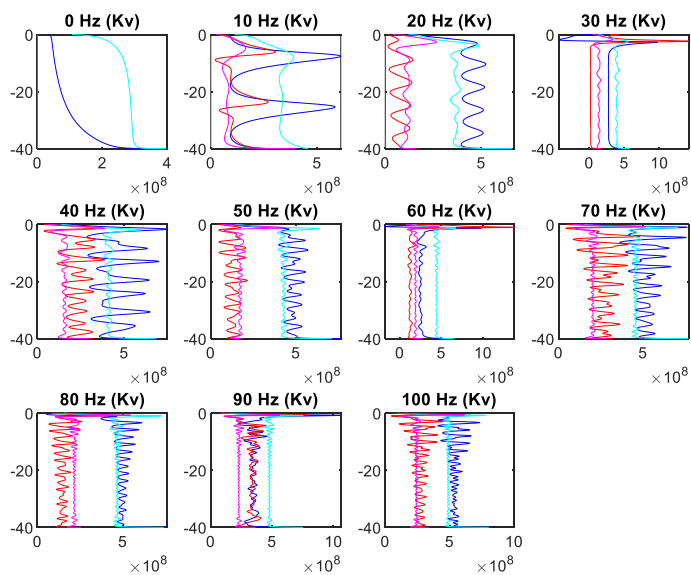
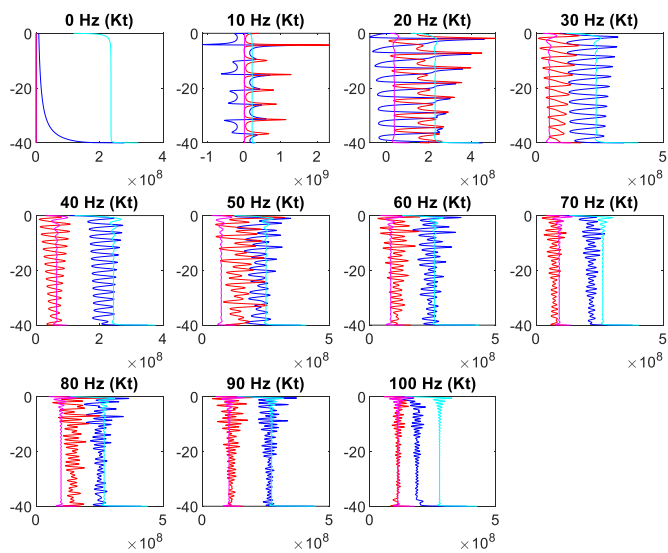
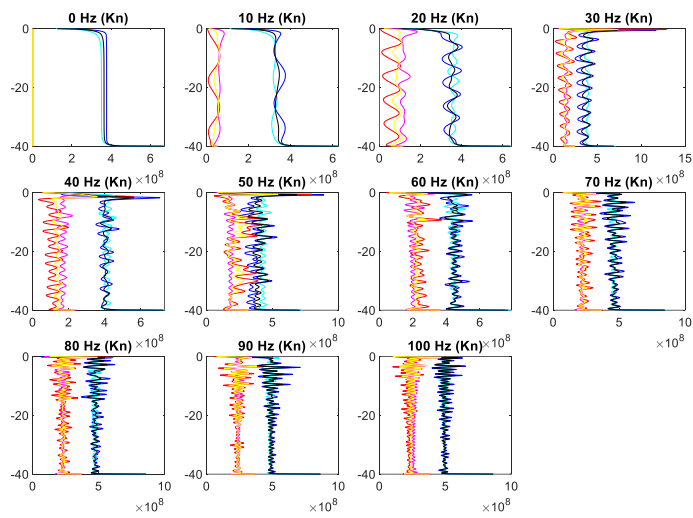
The kt/kn ratio's on the other frequencies are close. For the kv/kn ratio's however this was not the case where it varies more around 1.

Hz	Kt/Kn ratio	Kv/Kn ratio
0	0,3616	0,5064
10	0,3552	0,8390
20	0,4759	1,1464
30	0,5758	0,8765
40	0,5598	1,0580
50	0,6005	1,1295
60	0,5571	0,7811
70	0,5186	1,0417
80	0,5488	1,0013
90	0,5499	0,8534
100	0,4705	1,0340

From the Matlab model a  $K_{\theta}/K_r$  ratio of 0,36 is calculated.

This value could be expected since:  $G = \frac{E}{2(1+\nu)} \rightarrow \nu = 0,4 \rightarrow G = 0,357 * E$  (not sure if I can make this comparison)

### Output plots from Matlab analysis:



For the determination of the damping different methods have been compared with each other in terms of resulting values. the different values are described in this section

#### 9.1.1.1 Damping from 1D effective model;

From the modified MATLAB model the damping C was determined from the Imaginary part of output.

$$C = \frac{Im}{\omega}$$

The value determined with this method was compared with a value obtained from Versteijlen (2018). The value that was used by Versteijlen (2018) in determining the soil damping is described in a  $\alpha$  value:

$$c(z) = \alpha * K_{eff}(z) ; \text{ where } \alpha = 2,08 * 10^{-2}$$

To compare with the  $\alpha$  value from Versteijlen the Damping value obtained from the medified MATLAB model was rewritten to an  $\alpha$  value by the stiffness value K and damping value C:

$$\alpha = \frac{C}{K} = \frac{Im}{K}$$

From the modified MATLAB model a highly varying  $\alpha$  value was found using the damping coefficient and decreasing on higher excitation frequencies. A decision was made to keep the damping the same over all frequencies to not actively influencing the system by adding an assumed damping . A higher damping is expected to result in a lower efficiency of penetration.

**Cn** ( $C_r$  in picture) =  $3,61E+08 * 2,08E-02 = 7,5088+E6$ [Ns/m/m<sup>2</sup>] (uniform over all depths)

**Ct** ( $C_z$  &  $C_\theta$  in picture) =  $1,31E+08 * 2,08E-02 = 2,7248+E6$ [Ns/m/m<sup>2</sup>] (uniform over all depths)

When implementing the proposed damping into the FEMAP model it seems like the damping values are too high. The static resistance was calculated (section 6.3.2) and the force needed to overcome the resistance was applied as a harmonic force (26.6Hz). In the model the forcing damps out so much that penetration does not occur, a follow-up test for  $\alpha = 0$  was performed where it did penetrate as expected and at  $\alpha = 0,005$  where again It did not penetrate. It seems like the material damping of 0.01 entered in the MATLAB model might be too high.

## A2: Damping value determination

In 1965, Lysmer (22), utilizing the results of an "exact" solution to the vertical rigid circular disk problem, suggested the use of the following frequency-independent "dashpot" coefficient to model vertical radiation damping in an elastic halfspace:

$$c_v = \rho A \cdot \left[ \frac{3.4}{\pi(1-\nu)} V_s \right] \dots \dots \dots (1)$$

in which  $A = \pi R^2$  = the area of the circular disk and  $\rho$ ,  $\nu$  and  $V_s$  = the mass density, Poisson's ratio and shear (S) wave velocity, respectively, of the homogeneous halfspace. Richart and Whitman (30) extended Lysmer's idea and presented frequency-independent approximations ("analog") for the radiation "dashpot" coefficients pertaining to horizontal

In Gazetas & Dobry (1984) the area A is described as the area of the circular disk like in the problem defined by Lysmer (1965)

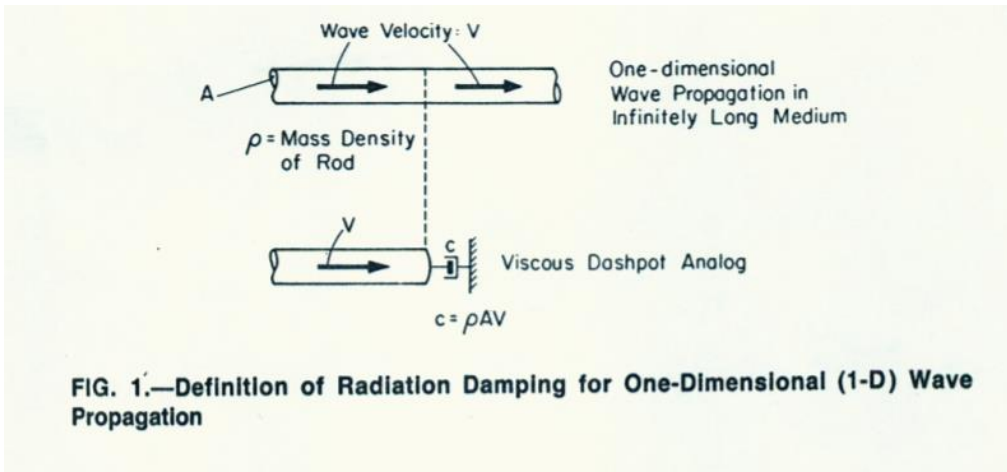


FIG. 1.—Definition of Radiation Damping for One-Dimensional (1-D) Wave Propagation

(Gazetas & Dobry, 1984)

### Rigid Circular Footing

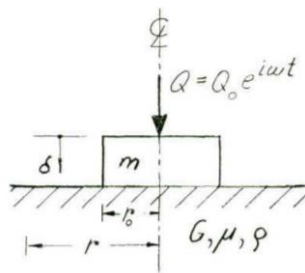


Fig. 10 Footing-Soil System

We now turn to the key matter of the present work, the idealized half-space model for the footing-soil system. This system, which is shown in Fig.10, consists of a circular rigid footing of mass  $m$  which rests upon a homogeneous, isotropic and perfectly elastic half space with the physical constants  $G$ ,  $\mu$  and  $\phi$ .

It was shown on page 7 that one can find the steady-state

From Lysmer(1965), it can be seen that A is indeed the surface contact to the ground. In this case the area of the circular disk on the ground

# A3: Appendix P-Y method parameters

## Appendix p-y method calculation

Used angle of internal friction 35 degrees; 18kn/m<sup>3</sup>; A=0,9

Values used	value	unit
A	0,9	-
kinch (@40')	75	lb/inch <sup>3</sup>
k	20851,0335	kN/m <sup>3</sup>
H	0-40	m
y	0-0,01	m
Pu(H) determination:		kN/m
C1	3	
C2	3,5	
C3	55	
Angle of internal friction	35	
D	1	m
gamma	18,9333	KN/m <sup>3</sup>

### 6.8.6 Lateral Bearing Capacity for Sand

The ultimate lateral bearing capacity for sand has been found to vary from a value at shallow depths determined by Eq. 6.8.6-1 to a value at deep depths determined by Eq. 6.8.6-2. At a given depth the equation giving the smallest value of  $p_u$  should be used as the ultimate bearing capacity.

$$p_{us} = (C_1 \times H + C_2 \times D) \times \gamma \times H \quad (6.8.6-1)$$

$$p_{ud} = C_3 \times D \times \gamma \times H \quad (6.8.6-2)$$

where

$p_u$  = ultimate resistance (force/unit length), lbs/in. (kN/m) (s = shallow, d = deep),

$\gamma$  = effective soil weight, lb/in.<sup>3</sup> (KN/m<sup>3</sup>),

$H$  = depth, in. (m),

$\phi'$  = angle of internal friction of sand, deg.,

$C_1, C_2, C_3$  = Coefficients determined from Figure 6.8.6-1 as function of  $\phi'$ ,

$D$  = average pile diameter from surface to depth, in. (m).

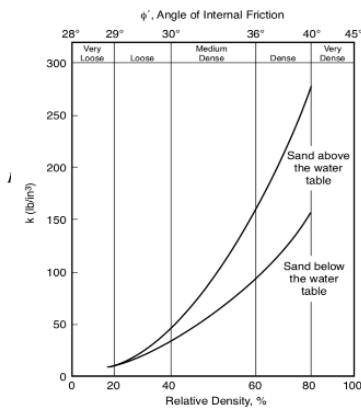
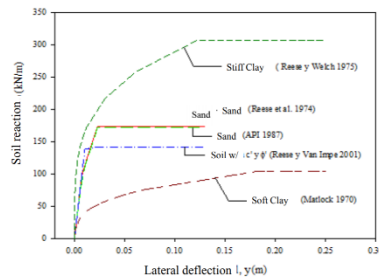


Figure 6.8.7-1—Relative Density, %

### P-Y Curves for Different Soil Types



### 6.8.7 Load-Deflection (p-y) Curves for Sand

The lateral soil resistance-deflection (p-y) relationships for sand are also non-linear and in the absence of more definitive information may be approximated at any specific depth  $H$ , by the following expression:

$$P = A \times p_u \times \tanh \left[ \frac{k \times H}{A \times p_u} \times y \right] \quad (6.8.7-1)$$

where

$A$  = factor to account for cyclic or static loading condition. Evaluated by:

$A = 0.9$  for cyclic loading.

$A = \left( 3.0 - 0.8 \frac{H}{D} \right) \geq 0.9$  for static loading.

$p_u$  = ultimate bearing capacity at depth  $H$ , lbs/in. (kN/m),

$k$  = initial modulus of subgrade reaction, lb/in.<sup>3</sup> (kN/m<sup>3</sup>). Determine from Figure 6.8.7-1 as function of angle of internal friction,  $\phi'$ .

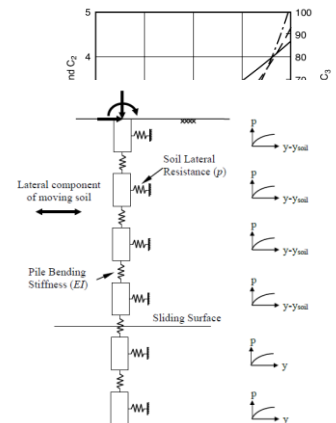
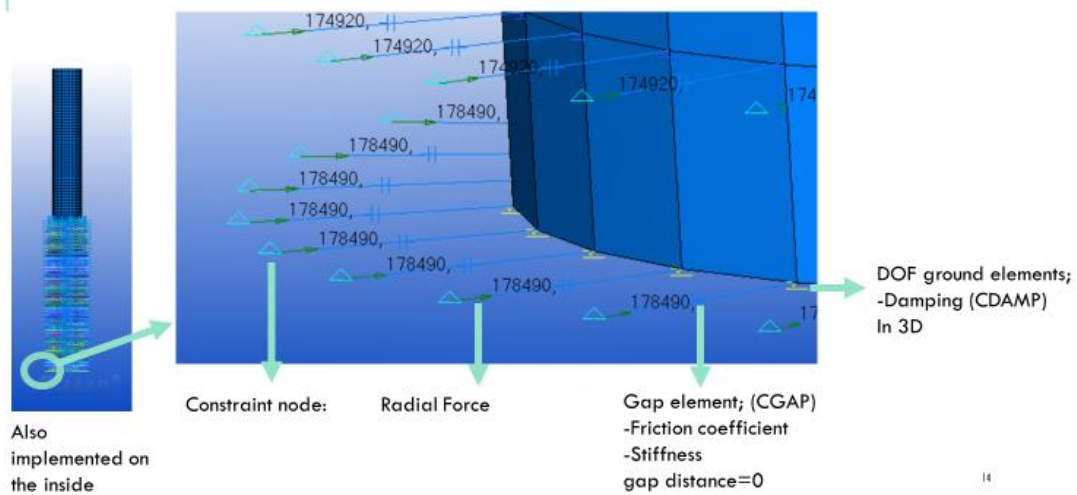


Figure 2-1: Spring mass model used to compute lateral response of loaded piles

### Typical Values of Unit Weight for Soils

Type of soil	$\gamma_{sat}$ (kN/m <sup>3</sup> )	$\gamma_d$ (kN/m <sup>3</sup> )
Gravel	20 - 22	15 - 17
Sand	18 - 20	13 - 16
Silt	18 - 20	14 - 18
Clay	16 - 22	14 - 21

# A4: Using FEMAP



## Pile Shell elements

The pile was modelled as a cylindrical surface in FEMAP with the set dimensions. This surface was modelled as a Plate element with the give thickness and material properties. The surface of the cylinder was “meshed” into 36 nodes along the circumference of the pile and into 100 nodes longitudinally.

## Constraints

To attach the elements a fixed constraint was placed at 1m from the pile in radial direction. On both the inside and the outside of the pile, this is the case for all the elements.

## Radial Force

On each gap element a radial force is applies with the determined depth dependent magnitude

## Gap elements

On the bottom half of the pile, up to 40m, Gap elements (Nastran CGAP).

## DOF ground elements

For the damping elements to the ground DOF ground elements were attached to each node. (Nastran CDAMP)

## Applied forcing

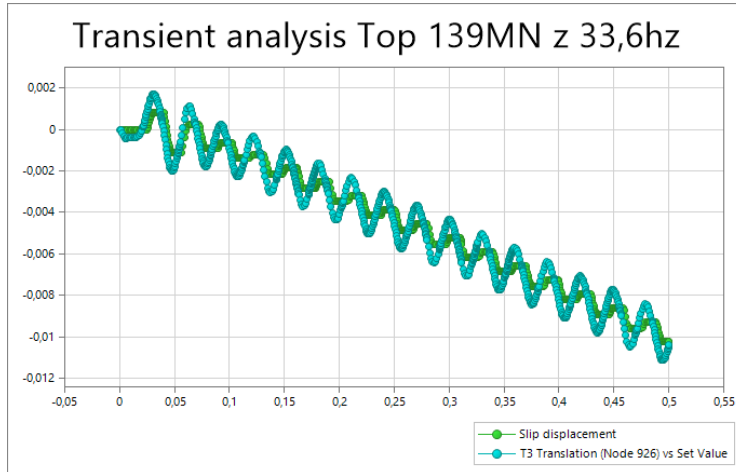
In Applying the harmonic force values in the FEMAP model, the total value is divided by the number of radial nodes to determine the force per node. This force is multiplied by a harmonic function with the desired frequency.

$$F_{node} = \frac{F_{total}}{\#nodes}$$

	Total Force	Per node (/36)
Force Amplitude A[N] 92,8MN	9,28E+07	2,90E+06
Force Amplitude A[N] 116MN	1,16E+08	3,63E+06
Force Amplitude A[N] 139MN	1,39E+08	4,35E+06

### Non-linear transient analysis

From the transient analysis the slip displacement can be plotted and the slip displacement of the element. It can be seen that these are the same, for the rest of the thesis we will use the translation in T3 (z) direction. We can also see that the displacement of the node nicely proceeds the slip displacement like we would expect.



### Limitations

This model is not considered a general penetration model, because there is no increase in pressure ( and spring and damping coefficients) as the pile penetrates into the soil.

The model is made out of linear springs and not a complete (half)space of soil elements modelling the soil characteristics the soil is not representative to reality. It is considered a mathematical exercise on pile penetration speed in a simple model. The model is de-coupled while in reality the system would be coupled.

### Pile values:

Pile		
Young's Modulus	2,10E+11	[MPa]
Mass Density	7850	[kg/m <sup>3</sup> ]
Poissons ratio	0,3	[-]
Overall structural Damping coeff(G =2 * (critical damping ratio)),	0,04	[-]
Diameter	8	[m]
DL nodes	0,8	[m]
#radial nodes	36	[-]
Area per node	0,558505361	[m <sup>2</sup> ]

## Screen shots for reconfiguration purposes

In this section a few screen shots of the implementation of the FEMAP model are shown to ensure the reader can rebuild using the same parameters used.

The screenshots show the following configurations:

- Define Property - GAP Element Type:** ID 1, Title GAP outer, Material, Color 110, Layer 1. Property Values: Initial Gap 0, Compression Stiffness 201620435, Tension Stiffness 0, Transverse Stiffness 73164202, Y Friction Coefficient 0,364, Z Friction Coefficient 0,364, Preload Force 0. Additional NASTRAN Options: Adaptive checked, Max Penetration 0, Max Adjustment Ratio 0, Min Penetration Ratio 0, Y Friction = Static, Z Friction = Kinetic. Interface Element Options: Normal X 0, Y 0, Z 0, Width or Area 0.
- NASTRAN Dynamic Analysis:** Frequency ID 3. Options for Dynamic Analysis: Equivalent Viscous Damping Overall Structural Damping Coeff (G) 0,04. Limit Response Based on Modes: Number of Modes 0, Lowest Freq (Hz) 0, Highest Freq (Hz) 0. Equivalent Viscous Damping Conversion: Rigid Body Zero Modes (FZERO) 1,E-4. Frequency Response: Freq for System Damping (W3 - Hz) 0, Freq for Element Damping (W4 - Hz) 0.
- Function Definition:** ID 12, Title excitation\_17.63Hz, Type 1..vs..Time. X-Time vs Y-Factor plot showing a sinusoidal wave. Data Entry: Single Value selected.
- Editing Load Definition:** Load Set 8, Bottom Y 116MN 2Hz, Title Harmonic forcing, Coord Sys 1..Global Cylindrical. Force: Direction Constant selected. Load: FX 2,3283E-10, FY -3222222, FZ 0. Time/Freq Dependence 14..Copy of excitation\_17.63Hz.
- Define Material - ISOTROPIC:** ID 1, Title ISOTROPIC Material, Color 55, Layer 1. Stiffness: Young's Modulus, E 2,1E+11; Shear Modulus, G 0; Poisson's Ratio, nu 0,3. Thermal: Expansion Coeff, a 0; Conductivity, k 0; Specific Heat, Cp 0; Heat Generation Factor 0. Limit Stress: Tension 0, Compression 0, Shear 0. Mass Density 7850, Damping, 2C/Co 0, Reference Temp 0.
- Analysis Set:** Title Trans Analysis Set 132MN 33hz k0 c7518416/10 Gaze. Analysis Program 36..NX Nastran. Analysis Type 12..Nonlinear Transient Response. Solve Using Integrated Solver selected, License Type 0..Desktop.

NASTRAN Modal Analysis

Method ID: 1

Skip EIGx

**Real Solution Methods**

- Lanczos
- Auto (HOU/MHOU)
- Subspace

**Legacy Real Solution Methods**

- Givens
- Modified Givens
- Inverse Power
- Inverse Power/Sturm
- Householder
- Modified Householder

**Complex Solution Methods**

- Hessenberg
- Complex Inverse Power
- Complex Lanczos

**Solution Type**

- Direct
- Modal

**Range of Interest**

Real      Imaginary

From (Hz)    0,      0,

To (Hz)      0,      0,

**Eigenvalues and Eigenvectors**

Number Estimated: 0

Number Desired: 10

**Normalization Method**

- Mass    Node ID: 0
- Max
- Point    DOF: 0

**Mass**

- Default
- Lumped
- Coupled

**Complex Solution Options**

Convergence: 0,

Region Width: 0,

Overall Damping (G): 0,

Prev... Next... OK Cancel

NASTRAN Dynamic Analysis

Frequency ID: 3

Use Load Set Options

**Options for Dynamic Analysis**    **Solution Frequencies**

**Equivalent Viscous Damping**

Overall Structural Damping Coeff (G): 0,04

Modal Damping Table: 0..None

As Structural (KDAMP)

**Limit Response Based on Modes**

Number of Modes: 0

Lowest Freq (Hz): 0,

Highest Freq (Hz): 0,

**Equivalent Viscous Damping Conversion**

Convert using Solution Freq (WMDAL)

Rigid Body Zero Modes (FZERO): 1,E-4

Freq for System Damping (W3 - Hz): 0,

Freq for Element Damping (W4 - Hz): 0,

**Frequency Response**

Frequencies: 0..None

Modal Freq...

**Transient Time Step Intervals**

Number of Steps: 0

Time per Step: 0,

Output Interval: 0

**Response/Shock Spectrum**

Damping/Freq Correlation: 0..None

Prev... Next... OK Cancel

NASTRAN Nonlinear Analysis

Use Load Set Options

**Control Options**    **Advanced Options**

Skip NLPARM     Creep

**Basic**

Increments or Time Steps: 200

Time Increment: 0,0025

Max Iterations / Step:

**Stiffness Updates**

Method: 0..Default

Iterations Before Update: 5

**Output Control**

Intermediate: 1..YES

Output Every Nth Step: 1

**Convergence Tolerances**

- Displacement: 0,001
- Load: 0,001
- Work: 1,E-7
- Vector
- Length

**Solution Strategy Overrides**

- Arc-Length Method
- None or Advanced Overrides
- Full Newton-Raphson
- Modified Newton-Raphson
- Line Search
- Quasi-Newton
- Bisection

Prev... Next... Defaults OK Cancel

Boundary Conditions

**Primary Sets**

Constraints: 1..Untitled

Loads: 7..test pressure

Temperatures: 0..From Load Set

Initial Conditions: 0..None

Constraint Equations: 0..From Constraint Set

Bolt Preloads: 0..From Load Set

**Other DOF Sets**

Master (ASET): 0..None

Kinematic (SUPPORT): 0..None

SUPPORT1: 0..None

OMIT: 0..None

QSET: 0..None

CSET: 0..None

BSET: 0..None

Prev... Next... OK Cancel

## A5: Plate model

In this section visuals are presented to give a feel on the initial objective. A python model was also written however the code will not be presented here. The main function of this section is to give a small insight in what was worked on. Mainly this was a lot of testing at the Maasvlakte.

### Aim of thesis

The final aim of this thesis is to research the dynamic properties of the Vibrodrill system and create a model in which the flipper interactions caused by vibrations through the plate can be predicted.

#### **Aim: Model vibrations of a cylinder and multiple vibrodrill flippers in free air**

AIM: BUILD AND VALIDATE A MODEL THAT CAN PREDICT VIBRATIONS OF A PLATE AND MULTIPLE VIBRODRILL FLIPPERS IN FREE AIR.

*CREATE AN ADDITION TO THE MODEL; ESTIMATING PLATE AND FLIPPER VIBRATIONS FOR A CILINDER IN STEAD OF A PLATE*

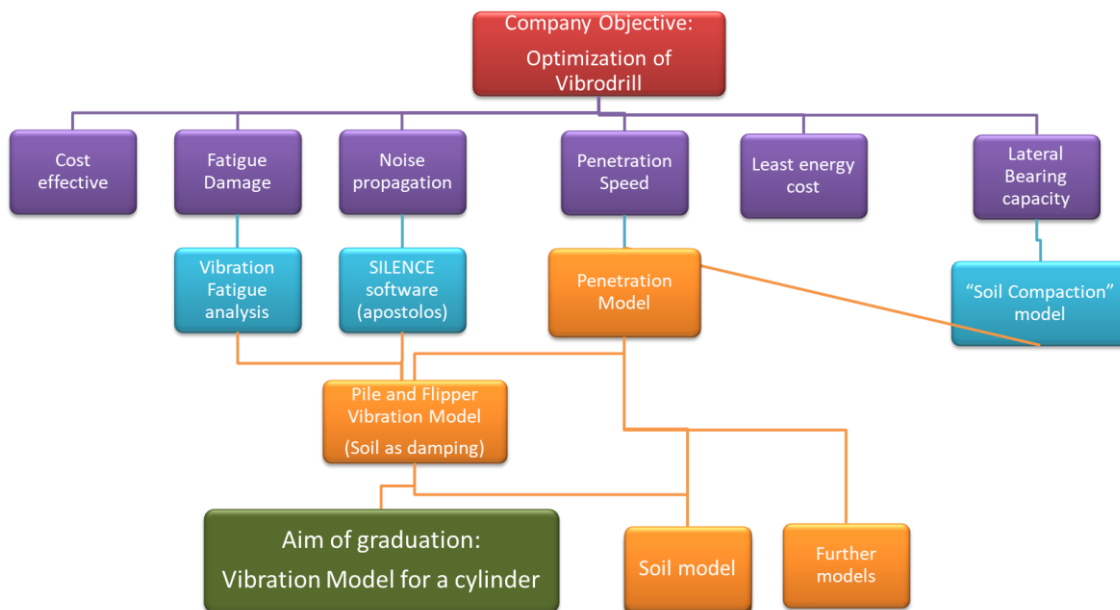


Figure 63 Initial aim of graduation chart

## Testing:

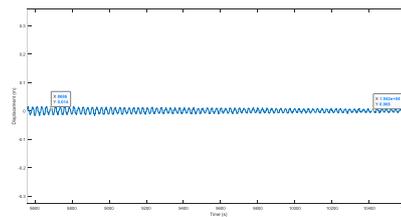
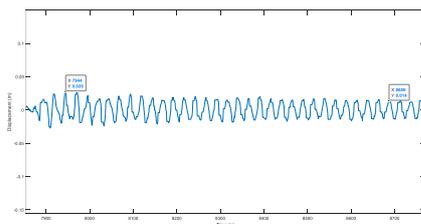
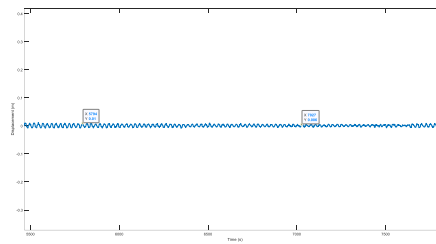
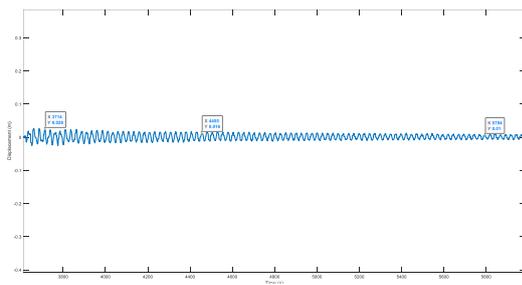
Internal damping: from decay line van accelerometer test on plate

$$\text{logarithmic decrement: } \delta = (1/n) * LN\left(\frac{x(t)}{x(t+nT)}\right)$$

$$\text{Damping ratio: } \zeta = \frac{1}{\sqrt{\left(1 + \left(\frac{2\pi}{\delta}\right)^2\right)}}$$

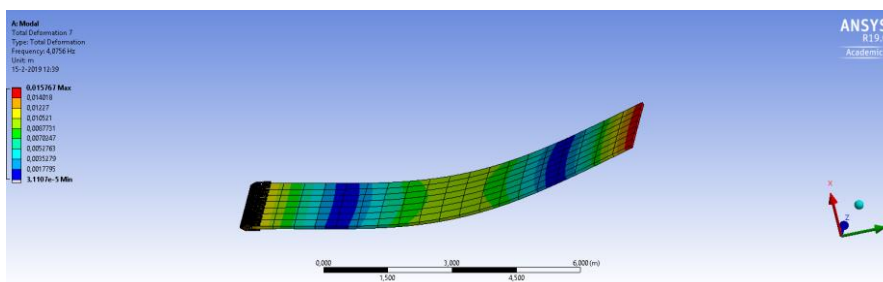
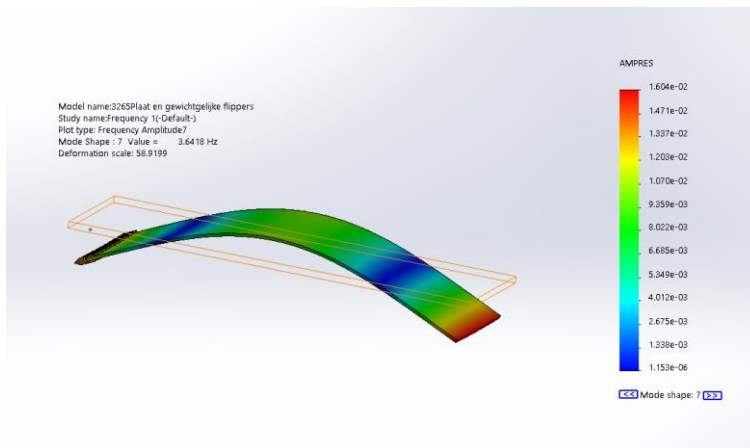
x1	0,28	0,28	0,28	0,28
xn	0,016	0,01	0,006	0,008
n	30	80	130	100
logarithmic decrement	0,095407	0,041653	0,029562	0,035553
damping ratio	0,015183	0,006629	0,004705	0,005658

This is the modal damping of the first mode



30 cycles in 7.45 sec = 4,026846 hz Natural frequency

# Comparison 1<sup>st</sup> natural frequency of a plate



	$\omega_n$ [Hz]
Test	4,02684564
Solidworks	3,64
Ansys	4,0756

Table 14 1st natural frequency comparison in different methods

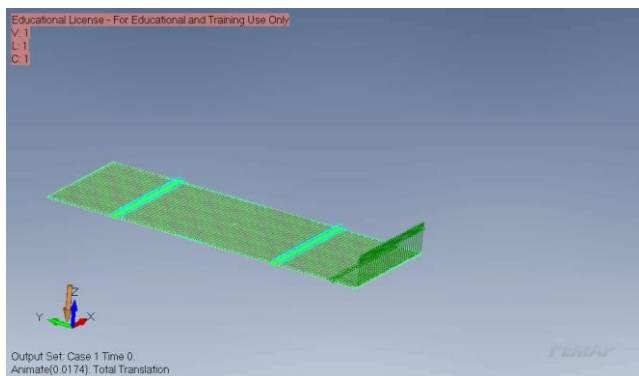


Figure 64 Initial plate model in FEMAP

# Chosen Software: FEMAP

	Available to student	3D Stucture dynamics	3D Pile-Soil interaction	Stick/slip	Excited at any location
GRLWEAP (Pile Dynamics)			Semi-empirical	Semi-empirical	
Allwave (Allnamics)			Semi-empirical	Semi-empirical	
Joao model (MATLAB)					
Plaxis (FEM)					
Abaqus (CEL/MPM)	Limited		Springs as soil	?	
<b>FEMAP (FEM)</b>			Springs as soil	Gap element	
ANSYS (FEM)	Limited		Springs as soil	CONTA178	
COMSOL (FEM)			Springs as soil	?	

CEL = Coupled Eulerian-Lagrangian  
 MPM= material point method  
 Other interesting Software: ANURA3D(MPM), LPILE, TZPILE, SAP2000

Advantage FEMAP: able to use elements from other software like ANSYS, ABAQUS and NASTRAN  
And company communication with external engineering company

*Since this information does not directly contribute to the revised objective of this thesis it was decided to delete the additional information in this section to prevent intellectual property violations.*

# A:6 0D vs FEM sawtooth

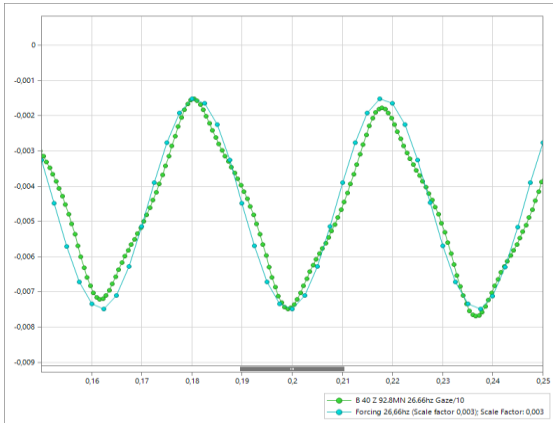
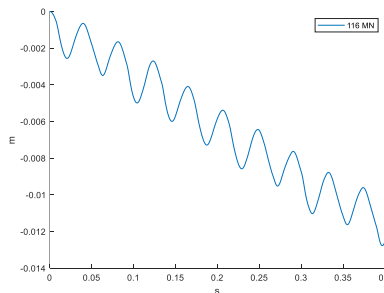
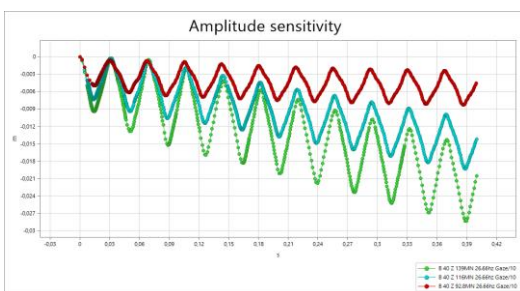
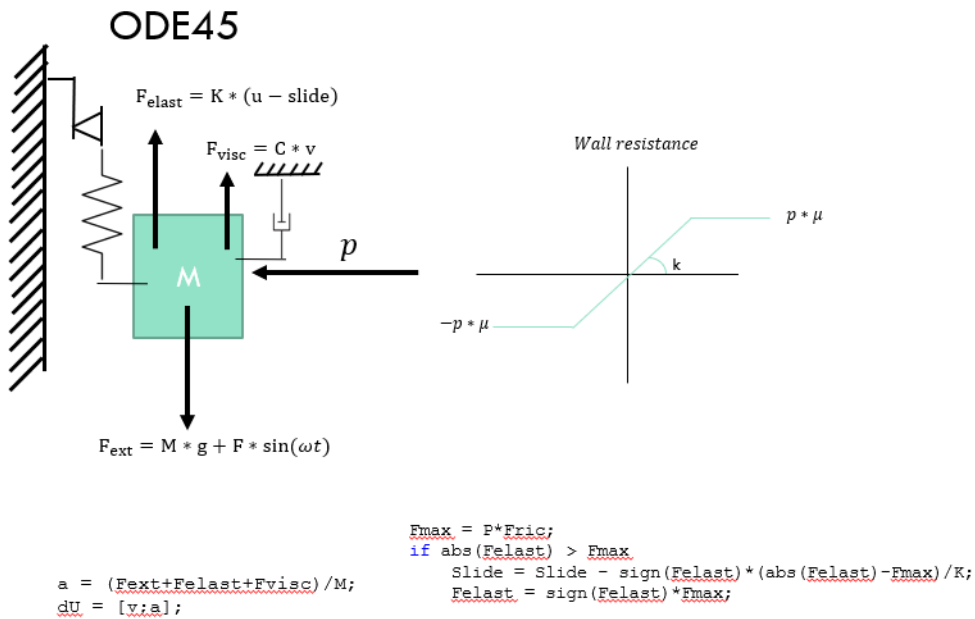


Figure 65 Harmonic force scaled and plotted over the nodal displacement showing the sawtooth motion

To determine if the sawtooth motion also appears in a 1d model this 1d model was built in MATLAB.

From the graphs it can be observed that a sharp but not sawtooth-like motion is determined by the 1d model



## A7: Output values

Test Name	mm/s	Test Name	mm/s
B40Z92.8MN26.66Hz	5	B40Z139,2MN29.33Hz	62,5
B40Z116MN26.66Hz	27,5	B40Z232MN26,66Hz	95
B40Z139MN26.66Hz	42,5	B40Z232MN29,33Hz	155
B40Y116MN24Hz	20,35	B40Z232MN40Hz	152,5
B40Z116MN24Hz	20	B40Z232MN50Hz	115
T40Z92.8MN24Hz	125	B40Z232MN60Hz	156,66
B40Z92.8MN24Hz	0,75	B40Z232MN70Hz	151,85
B40ZY116MN24Hz	46,25	B40Z232MN80Hz	116,66
T40ZY116MN24Hz	122,5	B40Z232MN90Hz	147,61
B40Z116MN29.33Hz	37,5	B40Z232MN100Hz	162,5
B40Y116MN15.8Hz	11,25	B40Z232MN130Hz	154,16
B40Y116MN17.63Hz	13	B40Z232MN160Hz	135
B40Z116MN50Hz	60	B40Y116MN15,8Hz	11,35
B40Z116MN60Hz	87,5	B40Y116MN15,8Hz	13,05
B40Z116MN80Hz	60	B40Z116MN24Hz	20,35
B40Z116MN100Hz	93,75	B40Y116MN29,33Hz	22,75
B40Z116MN90Hz	75	B40Y116MN40Hz	23,75
B40Z116MN160Hz	91,25	B40Y116MN60Hz	37,57
B40Z116MN70Hz	72,5	B40Y116MN80Hz	36,44
B40Z116MN130Hz	93,75	B40Y139,2MN15,8Hz	21,77
B40Z92.8MN40Hz	3	B40Y139,2MN17,63Hz	26,25
B40Z92.8MN50Hz	20,5	B40Y139,2MN24Hz	33,75
B40Z92.8MN60Hz	56,66	B40Y139,2MN29.33Hz	34,5
B40Z92.8MN70Hz	45	B40Y139,2MN40Hz	36,5
B40Z92.8MN80Hz	43,75	B40Y139,2MN60Hz	49,87
B40Z92.8MN90Hz	61,81	B40Y139,2MN80Hz	48
B40Z92.8MN100Hz	74,5	B40Y92,8MN15,8Hz	0,33
B40Z92.8MN130Hz	79,16	B40Y92,8MN17,63Hz	0,43
B40Z92.8MN160Hz	70,5	B40Y92,8MN24Hz	4,33
B40Z139,2MN40Hz	65	B40Y92,8MN29.33Hz	5,16
B40Z139,2MN50Hz	72,5	B40Y92,8MN40Hz	5,66
B40Z139,2MN60Hz	103,03		
B40Z139,2MN70Hz	90,74		
B40Z139,2MN80Hz	75		
B40Z139,2MN90Hz	100		
B40Z139,2MN100Hz	115		
B40Z139,2MN130Hz	112,5		
B40Z139,2MN160Hz	100		
B40Z232MN160Hz	58,57		
B40Z116MN40Hz	45		
B40Z92.8MN29.33Hz	3,66		
B40Z139,2MN24Hz	35		
B40Z139,2MN26.66Hz	47,5		